In presenting the dissertation as a partial fulfillment of the requirements for an advanced degree from the Georgia Institute of Technology, I agree that the Library of the Institute shall make it available for inspection and circulation in accordance with its regulations governing materials of this type. I agree that permission to copy from, or to publish from, this dissertation may be granted by the professor under whose direction it was written, or, in his absence, by the Dean of the Graduate Division when such copying or publication is solely for scholarly purposes and does not involve potential financial gain. It is understood that any copying from, or publication of, this dissertation which involves potential financial gain will not be allowed without written permission.

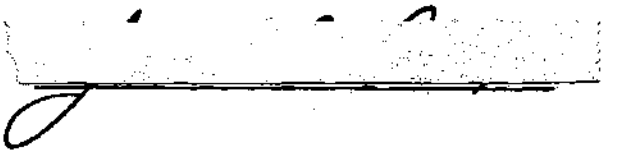

3/17/65
b

THE ANALYSIS OF DIELECTRIC-LOADED FERRITE PHASE SHIFTERS INCLUDING THE EFFECTS OF LOSSES

A THESIS

Presented to
the Faculty of the Graduate Division
by
James Lamar Allen

In Partial Fulfillment
of the Requirements for the Degree
Doctor of Philosophy in the School
of Electrical Engineering

Georgia Institute of Technology
May, 1966

THE ANALYSIS OF DIELECTRIC-LOADED FERRITE PHASE SHIFTERS INCLUDING THE EFFECTS OF LOSSES

Approved: _____

_____

Chairman

_____

Date approved by Chairman: May 24, 1966

ACKNOWLEDGEMENTS

The work reported here could not have been accomplished without the assistance, cooperation, and encouragement of many individuals and groups, and it is with pleasure that I take this opportunity to acknowledge that fact.

Particular thanks go to my advisor, Dr. F. K. Hurd, for his suggestions, constructive criticism, and encouragement during this investigation. The critical discussions held with him were especially valuable. I also wish to express my thanks to Dr. D. C. Fielder and Dr. A. L. Stanford for their suggestions in the preparation of the manuscript.

A special debt of gratitude is owed to the Sperry Microwave Electronics Company of Clearwater, Florida for financial support through a research contract with the Georgia Institute of Technology and to a number of employees of the company for their cooperation and assistance. In particular, I wish to thank Mr. B. J. Duncan and Dr. G. R. Harrison for arranging the financial support and suggesting that I look for a problem related to ferrite latching phase shifters. The many suggestions obtained from stimulating discussions with Dr. G. P. Rodrigue are gratefully acknowledged. Sincere thanks go to Mr. D. R. Taft, who performed the experimental measurements presented in the thesis, which add so much to the impact of the theoretical work. The professional help of Mrs. Frances Silverman, Mrs. Janice Witherspoon, Mrs. Margaret Cort, and Mr. David Powell, all of the Sperry Publications Department, who took my rough draft and transformed it into a finished product, is gratefully acknowledged.

To my wife, Lou Ann, goes heartfelt gratitude for her patience, understanding and encouragement through difficult times of intensive work.

TABLE OF CONTENTS

TABLE OF CONTENTS (Continued)

o

LIST OF ILLUSTRATIONS

LIST OF ILLUSTRATIONS (Continued)

LIST OF ILLUSTRATIONS (Continued)

LIST OF ILLUSTRATIONS (Continued)

SUMMARY

Ferrite devices have traditionally been designed by "cut-and-try" experimental methods supplemented by general guidelines provided by qualitative theoretical results. Numerous reasons exist for the lack of precise analytical design procedures. Ferrite devices are, in general, very complex structures and the analysis techniques required are corresponding complex. The analysis of ferrite loaded structures typically leads to lengthy transcendental equations involving functions of complex arguments. Such equations can be solved only by numerical techniques. In addition to the computational difficulties, a more fundamental difficulty has been the absence of an adequate mathematical model for magnetic losses in ferrites. Recently, the stringent demands imposed on the operating characteristics of ferrite components for phased array applications have strongly emphasized the need for analytical design procedures which can provide accurate quantitative predictions of both loss and phase characteristics of ferrite devices.

The purpose of this investigation is to develop the necessary mathematical models for magnetic losses in ferrites and to use those models in the development of techniques for analytical design of practical ferrite devices. Phase shifters are selected as the particular type of ferrite device to concentrate attention upon in so far as design is concerned, one reason being that the problems encountered in ferrite phase shifter design are typical of those encountered in most other ferrite device design. In addition, because of the current intensive interest in ferrite phase shifters for application as beam steering elements in phased array radar systems, analytical design procedures developed for phase shifters will find immediate useful application.

A new type of phase shifter has been developed experimentally for the phased array applications. This device, which is commonly referred to as a

"digital" or "latching" ferrite phase shifter, consists of a transmission structure loaded by a "square hysteresis loop" ferrite physically arranged to form a closed magnetic path. The two remanent magnetization states then correspond to the stable operating states of the phase shifter. The device can be switched from one state to the other by a pulse of magnetic energy. No bias power is required to maintain operation at either of the stable operating states. Such phase shifters are particularly attractive, because they are markedly smaller in physical size and require considerably less switching power than more conventional ferrite devices. The important point to be made here, however, is that this device operates with the ferrite in a partially magnetized state. Other devices, such as circulators and Faraday rotators, also utilize partially magnetized ferrites. Still others, such as resonance isolators and some conventional phase shifters, operate with the ferrite magnetically saturated. It is, thus, important to have accurate loss representations for saturated and partially magnetized ferrites.

The loss representation desired in both cases is one which is simple in physical concept, quantitatively accurate, and whose mathematical formulation requires only measurable or calculable intrinsic parameters of the material. For magnetically saturated ferrites the traditional Landau-Lifshitz phenomenological loss representation certainly satisfies the first and third of the desired conditions. However, general opinion in the past has been that this representation is not quantitatively accurate in the region far from resonance, particularly for polycrystalline materials.

By a combination of analytical and experimental results, it is shown in this thesis that the Landau-Lifshitz loss representation does in fact yield good quantitative loss prediction for saturated polycrystalline ferrites even in the region far from resonance. The validity of this loss representation is investigated by solving the exact boundary value problem for a dielectric-loaded analog phase shifter, whose phase shift element is a single magnetically saturated ferrite slab. The theoretical operating characteristics obtained in this manner are

examined as a function of applied bias field and for a variety of material and dimensional parameter combinations.

The representation of losses in partially magnetized ferrites is complicated by the existence of a multiplicity of magnetic domains of various shapes and orientations. The only technique available in the literature for representing magnetic losses in such materials is the "bulk" loss representation normally associated with totally unmagnetized samples. This type of loss representation is undesirable for partially magnetized materials for several reasons, the principal two being its failure to provide an explicit relationship between overall losses and fundamental material parameters such as saturation magnetization and resonance linewidth, and its failure to provide accurate quantitative prediction of magnetic losses observed in ferrite devices.

Because of the inherent disadvantages of the "bulk" representation of magnetic losses, an alternate way of representing losses in partially magnetized ferrites is developed in this thesis. The new representation meets the three desired conditions mentioned above. It is based on an extension of the Landau-Lifshitz tensor representation of losses in saturated samples (or single domains) to multi-domain (partially magnetized) samples. Analytical expressions for the components of the new "lossy" small signal permeability tensor for partially magnetized ferrites are derived using a spatial averaging technique on the permeability tensors for combinations of "single" domains whose effective fields and saturation magnetizations are oriented at different angles. In its complete form, the new "average" tensor is considerably more complex than the Landau-Lifshitz tensor, but it reduces to the latter if the material is assumed to be saturated. The real (phase shift) parts of the average permeability components are found to be proportional to the net magnetization of the sample. The imaginary (loss) parts of the components are related to resonance linewidth and to an effective magnetization. The effective magnetization in the loss term is always greater than the net magnetization but less than the saturation magnetization for the material. The validity of the derived "average" permeability tensor for the

prediction of losses in partially magnetized ferrites is demonstrated by a comparison of the theoretically predicted characteristics of several devices with experimental results. The devices examined are remanence ("latching") phase shifters, whose phase shift elements are ferrite toroids. The theoretical characteristics are obtained by solving the exact boundary value problem for each structure.

One of the more interesting results of the theoretical analysis of latching phase shifters is a prediction of an unexpected strong dependence of loss in the partially magnetized ferrite on resonance linewidth. Experimental results are presented which verify this surprising prediction, convincingly demonstrating the validity of the "average" tensor representation of losses in partially magnetized materials. A brief discussion of various damping mechanisms contributing to the broadening of the resonance line is given, along with a discussion of a possible change in interpretation of the linewidth parameter required in the mathematical representation of losses for some materials of types not examined in detail in this thesis.

A number of alternate procedures for the exact analysis of ferrite loaded structures are examined. The exact propagation constant equation for at least one phase shifter configuration is established by each method. The exact propagation constant equations are solved numerically. A "small loss" computational technique, which has been used extensively in the past to predict losses in dielectrics and more recently in ferrites, is shown to be unsatisfactory for the quantitative prediction of magnetic or dielectric losses.

As a prelude to the derivation of the "average" permeability tensor, various equations of motion for the magnetization in magnetically saturated ferrites are examined. All of the equations, with phenomenological damping terms included, are shown to be obtainable from a single equation. The various forms of the one general phenomenological equation simply highlight specific aspects of the problem.

The practicability of precise analytical design of latching and applied field ferrite devices, including the prediction of insertion loss, is demonstrated. Quantitative relationships are provided relating device transfer characteristics to the intrinsic material and dimensional parameters for a number of phase shifter configurations. These relationships, when programmed for digital computer solution, allow a very wide variety of parameter combinations to be examined in a short time (typically more than one hundred configurations per minute). Extensive design data for waveguide latching and analog phase shifters are presented in the form of families of normalized curves.

CHAPTER I

INTRODUCTION

Intensive experimental and theoretical effort has been devoted in recent years to the exploitation of the unique properties of ferrites*. These efforts have been rewarded by the development of a host of new devices, many of which display transmission properties previously unattainable in passive devices.

It was the demonstration of the gyromagnetic nature of ferrites at microwave frequencies by Polder (1), Beljers (2), and Roberts (3) that first made it apparent that nonreciprocal passive devices could be constructed. Among the earliest to demonstrate the practical importance of ferrites was Hogan (4), who utilized the microwave Faraday rotation phenomena to build a 180^{o} nonreciprocal phase shifter. It soon became apparent that not only do ferrites exhibit Faraday rotation but ferrite devices can also manifest nonreciprocal properties in a variety of other ways such as nonreciprocal attenuation, nonreciprocal birefringence, nonreciprocal coupling through apertures, nonreciprocal field displacement, and nonreciprocal phase shift (5). Ferrite devices may also exhibit reciprocal phase shift, attenuation, coupling through apertures and other useful reciprocal properties. An important feature of both the reciprocal and the nonreciprocal properties is that they can be varied in a controlled fashion by changing an applied magnetic bias field.

Some interesting ferrite devices which have found wide application in the microwave industry are load isolators, circulators, phase shifters, polarization rotators, tunable filters, switches and power limiters. Lax and Button (6) give an excellent review of most of the important properties of ferrites as well as descriptions and typical operating characteristics of many of the devices mentioned above.

*The word "ferrite" is used here to represent any ferrimagnetic material.

Both the nonreciprocal and the reciprocal phase shift characteristics of ferrite-loaded transmission structures have been used in practical devices. As an example, nonreciprocal phase shift sections are crucial parts of ferrite duplexers (7) and of some types of ferrite switches (8). In addition, reciprocal and nonreciprocal phase shifters have been constructed to perform all of the usual functions of variable phase shifters in communication and measurement systems.

The development of ferrite phase shifters as practical devices began with the initial observations of nonreciprocal phase shift in rectangular waveguide made by Kales, Chait, and Sakiotis (9). Rowen (10) published a set of measurements of phase shift and differential phase shift as a function of the position of a transversely-magnetized ferrite slab in a rectangular waveguide. Lax, Button, and Roth (11) obtained a quantitative solution for ferrite phase shifters consisting of either one or two transversely-magnetized ferrite slabs in an otherwise empty rectangular waveguide as shown in Figure 1. Their solution, which neglected all losses, was worked out numerically for variable applied magnetic field, ferrite-slab thickness and slab location. The nonreciprocal distrotion of the rf field patterns was plotted for the fundamental TE mode. Crowe (12) carried out a theoretical investigation of the propagation constant for the TE modes of a simple structure shown in Figure 2, which is composed of a single transversely-magnetized ferrite slab against the side wall of a rectangular waveguide. Crowe's analysis, which was principally concerned with mode behavior in the vicinity of magnetic resonance, included the effects of magnetic losses but neglected dielectric and waveguide losses.

Rectangular waveguide phase shifters utilizing transversely-magnetized ferrite slabs proved to require large dc bias fields (typically 1000 oersteds for 45^{o} of differential phase shift per inch) and hence required considerable power for switching and holding. Placing a large diameter ferrite rod at the center of a rectangular waveguide and applying a dc magnetizing field along the direction of propagation resulted in a reciprocal phase shifter of the type shown in

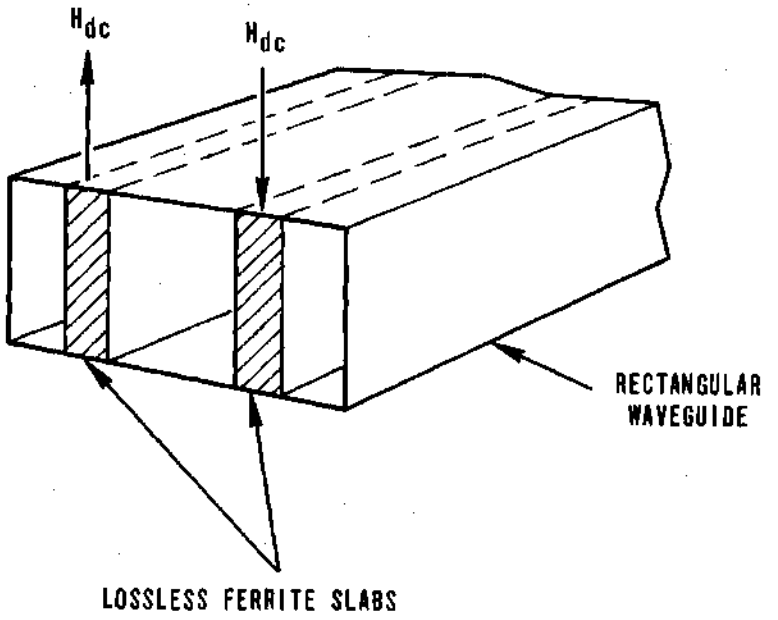

Figure 1. Twin-Slab Nonreciprocal Phase Shifter Analyzed by Lax, Button, and Roth

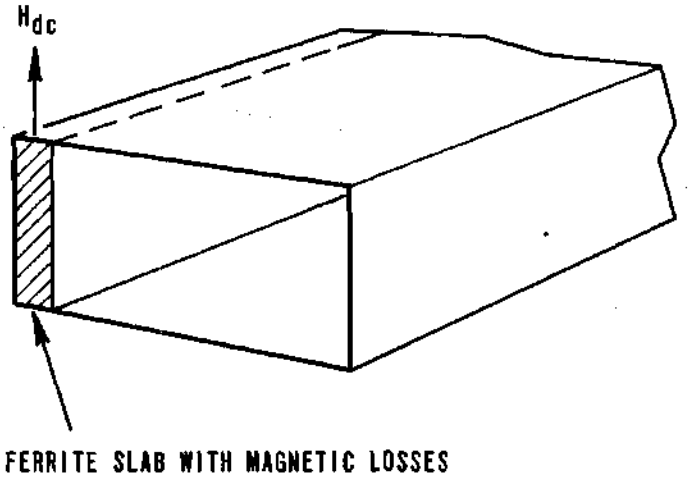

Figure 2. Single-Slab Waveguide Structure Analyzed by Crowe

Figure 3, which required a very low bias field (typically 50 oersteds for 45^{o} of reciprocal phase shift per inch) and a correspondingly small switching and holding power (13) (14) (15) (16) (17). Unfortunately, this device is very frequency sensitive. Button and Lax (18) analyzed a model of this type of phase shifter by first-order perturbational theory.

A most significant advance in phase shifters for rapid switching applications was the experimental development of ferrite "latching" devices (19) (20) (21) (22) (23) (24) (25) (26). The ferrite latching phase shifter, one form of which is shown in Figure 4a, consists of a transmission structure loaded by a "square hysteresis loop" ferrite physically arranged to form a closed magnetic path. The two remanent magnetization states shown in Figure 4b correspond to the stable operating states of the phase shifter. Switching power is thus required only in transferring from one state to the other. Such devices are particularly attractive because they are markedly smaller in physical size and require considerably less switching power than more conventional ferrite devices which use externally applied dc bias fields supplied by electromagnets. Latching phase shifters have been constructed in waveguide, helical, coaxial, and stripline structures. Very little analytical work has been done on any of these configurations. Exceptions are the work by Schloemann (27) and by Ince and Stern (28) (29). Schloemann solved the parallel-plane model of a latching phase shifter shown in Figure 5. He examined the relation of differential phase shift to various parameters of the device. Magnetic losses were computed but only for the case of zero spacing between ferrite slabs. Ince and Stern have analyzed a waveguide nonreciprocal latching phase shifter of the form shown in Figure 6 with the effects of losses included as a perturbation of the lossless solution. Differential phase shift and losses were computed for various combinations of the device parameters. Both Schloemann and Ince and Stern treated magnetic losses as "bulk" losses which they computed from a magnetic loss tangent. This scheme provides no insight into the relationship between total loss in the

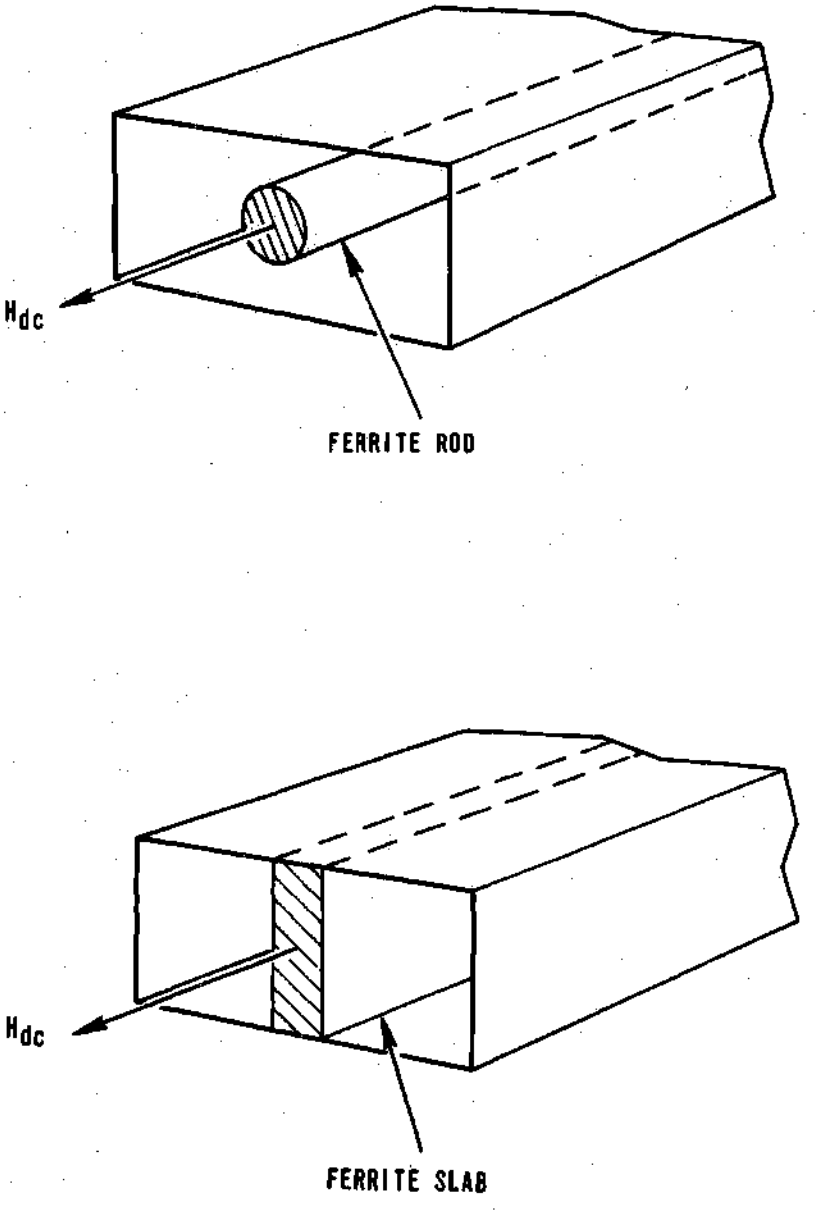

Figure 3. Two Reciprocal Phase Shifter Configurations

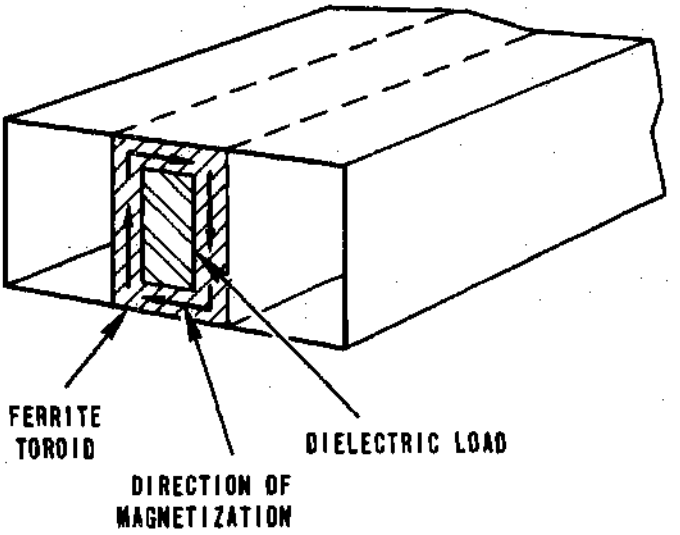

Figure 4a. A Waveguide Nonreciprocal Latching Phase Shifter

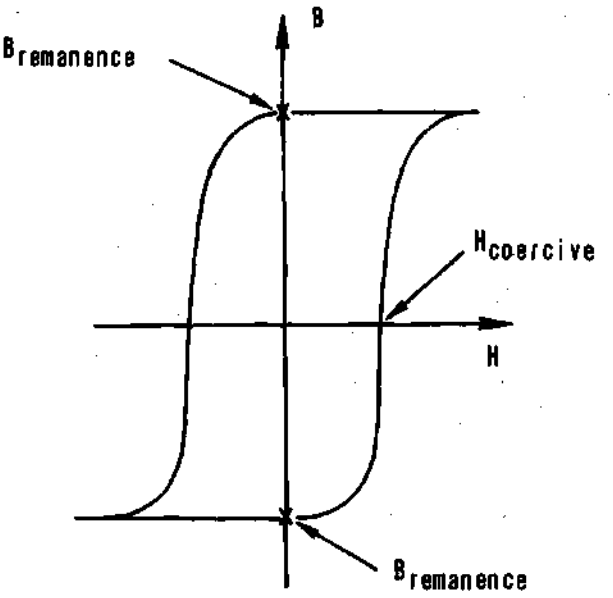

Figure 4b. Hysteresis Loop of a High Remanence
(i.e., "Square-Loop") Ferrite

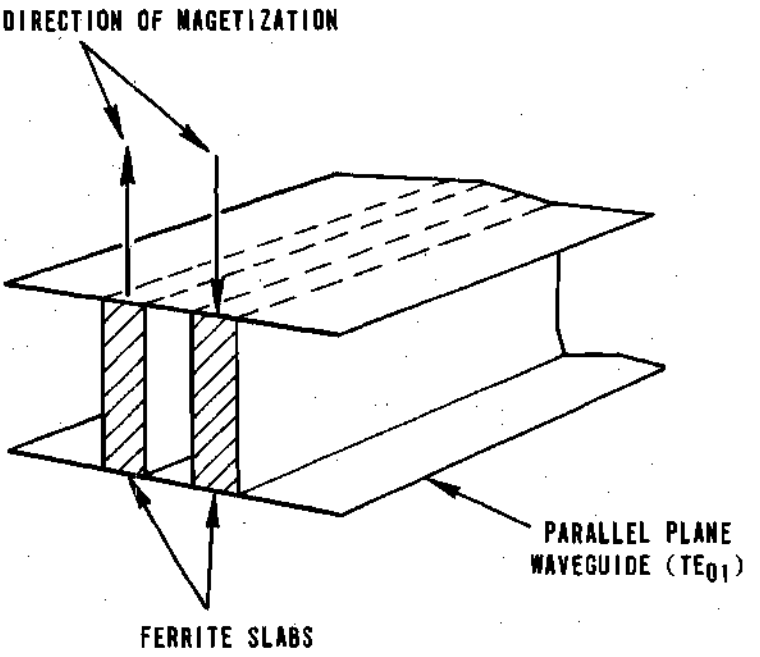

Figure 5. Phase Shifter Configuration Analyzed by Schloemann

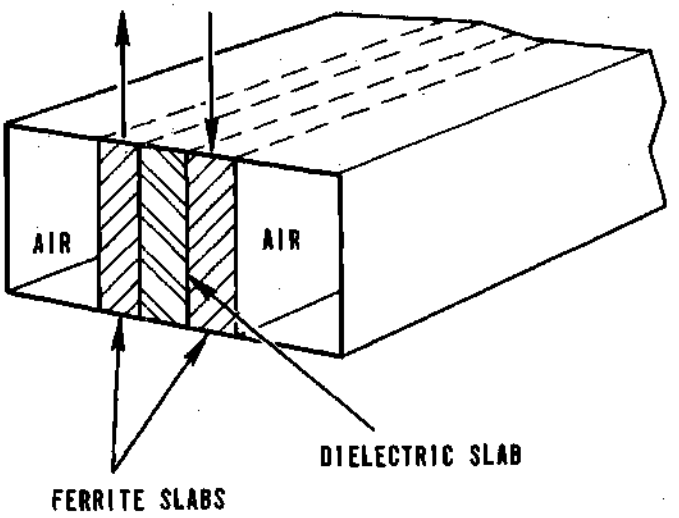

Figure 6. Phase Shifter Configuration Analyzed by Ince and Stern

device and the intrinsic parameters of the ferrite and furthermore does not yield accurate loss predictions. Neither Schloemann nor Ince and Stern considered operation in the external bias field mode (i.e., $H_{dc} \neq 0$).

The analytical work reviewed above, much of which is in the form of perturbation solutions, has provided a qualitative understanding of the behavior of ferrite devices and has been extremely useful in establishing design guidelines. Currently, there is widespread interest in ferrite phase shifters for use as beam steering elements in phased array radar systems. The state of the art in phased array systems is such that the demands placed on the performance characteristics of the phase shifters are so severe that the existing qualitative analysis is unable to provide satisfactory design information. A particularly serious deficiency in the available theoretical results is the absence of exact quantitative solutions which include the effects of losses. In an effort to help remedy that situation, this thesis presents an exact analysis of some important ferrite phase shifter configurations of both the latching and applied-field types with the effects of magnetic, dielectric, and waveguide losses included. Special attention is given to the problem of providing an accurate quantitative accounting of magnetic losses in unsaturated ferrite media and to relating the total magnetic loss in a phase shifter to the measurable intrinsic parameters of the material, such as its saturation magnetization and linewidth. The principal goal of the study was to establish material models and analysis procedures which could be used for quantitative prediction of loss and phase data for ferrite devices, and in particular for ferrite phase shifters, utilizing either saturated or unsaturated polycrystalline materials. In line with the general goal, a number of conclusions, which are important not only to ferrite phase shifter analysis but also to the analysis of ferrite devices per se, are inferred from the results of the study of loss representations in saturated and unsaturated ferrites. The validity of the theoretical predictions is checked by comparison with experimental results.

CHAPTER II

PRACTICAL FERRITE PHASE SHIFTERS AND THEIR MODELS

Introduction

Since the early 1950's, workers in microwave ferrimagnetics have, as illustrated in Chapter I, devoted considerable attention to the development of various types of ferrite phase shifters. A continuing goal of phase shifter research and development from that time until now has been to create ferrite phase shifters suitable for use as beam steering elements in phased array radar systems. Some of the desired electrical properties of phase shifters for this application are (a) controlled phase variation at high switching speeds, (b) phase shift independent of frequency over a wide range of frequencies, (c) high rf power capability, (d) low insertion loss, and (e) low switching and holding power. Simultaneous achievement of these characteristics has proven to be most difficult, but, recently, promising experimental results have been obtained.

Of the phase shifters thus far conceived, the ferrite latching type appears to hold the most promise of eventually meeting the stringent requirements of phased array applications. Considerable activity and interest is presently concentrated on improving the fundamental understanding of the operating characteristics, design techniques, and basic limitations of this device. For this reason, the major emphasis throughout this thesis is on latching phase shifters. However, a number of specific phase shifters of the applied field type are also analyzed and discussed. In addition, the general features of the procedures used are shown to be applicable in the analysis of other ferrite devices.

General Properties of the Models

Configurations

All of the phase shifters studied in this work can be represented by models whose configurations consist of a number of full-height vertical slabs of dielectric interleaved with full-height vertical slabs of transversely magnetized ferrite in a section of rectangular waveguide. As an example, Figure 7 illustrates a model configuration with one ferrite and three dielectric slabs. The normal operating transmission mode of the practical devices studied is the lowest order transverse electric mode the device structure will support. This fact is utilized as a simplifying assumption in the analysis of the models. For the purposes of analysis, it is also assumed that the model structures are infinitely long in the direction of propagation.

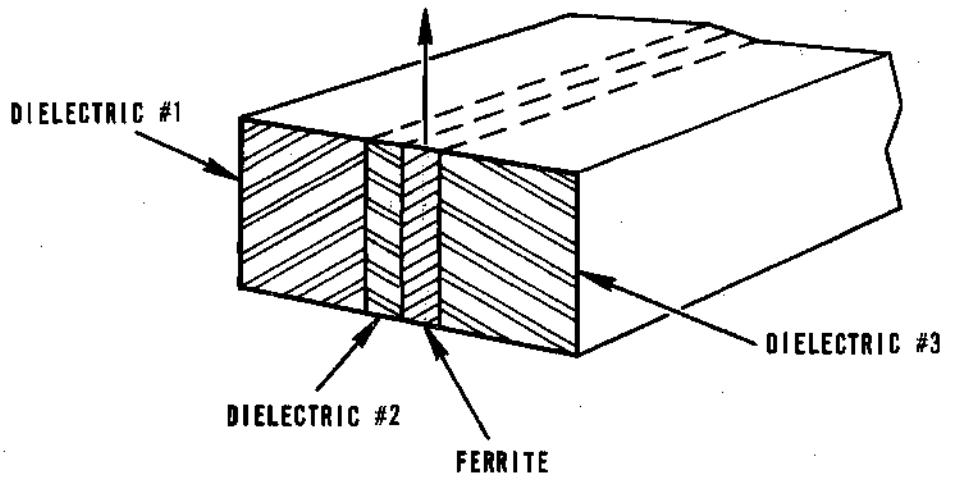

Figure 7. A Model Configuration With One Ferrite And Three Dielectric Slabs

Materials

Dielectrics. The macroscopic electromagnetic properties, including the effects of losses, of the dielectric regions in the phase shifter models are accounted for in the usual manner by a complex permittivity $\epsilon_d = \epsilon_o(\epsilon'_d - j\epsilon''_d)$ and by a permeability $\mu_d = \mu_o$ where ϵ_o and μ_o are the permittivity and permeability of free space.

Ferrites. The dielectric properties of the ferrite are accounted for by the complex permittivity $\epsilon_f = \epsilon_o(\epsilon'_f - j\epsilon''_f)$. The gross features of the magnetic properties of ferrites are very similar to those of iron and other ferromagnetic metals.* However, good microwave ferrites are distinguished from the magnetic metals by one outstanding characteristic. This characteristic, which is largely responsible for the unique microwave behavior of ferrites, is their extremely high resistivity (typically 10^6 to 10^8 ohm-cm for ferrites compared to 10^{-5} ohm-cm for iron). An rf wave incident on an iron sample "sees" an effective reflector, whereas the same wave incident on a ferrite sample can enter and travel through substantial amounts of the material without excessive reflection or attenuation. As it passes through the ferrite, the wave has an opportunity for strong interaction with the spinning electrons responsible for the magnetic properties of the material. Due to this interaction, under appropriate circumstances, Faraday rotation and other nonreciprocal properties may be manifested.

The vital property of ferrites which is responsible for their great utility in microwave applications is their unique permeability. The ferrites microwave permeability is due to the effects of certain electrons, which may be thought of as behaving en mass gyroscopically according to the classical picture of Figure 8. It is found that the effective charge, mass and spin of these electrons are associated with an angular momentum and a magnetic moment in the directions shown, which it may be noted are the same as those to be expected for a spinning positive mass and negative charge. Applying a dc magnetic

*The remainder of this paragraph and all of the next two paragraphs follow the excellent discussion of Fox, Miller, and Weiss (5).

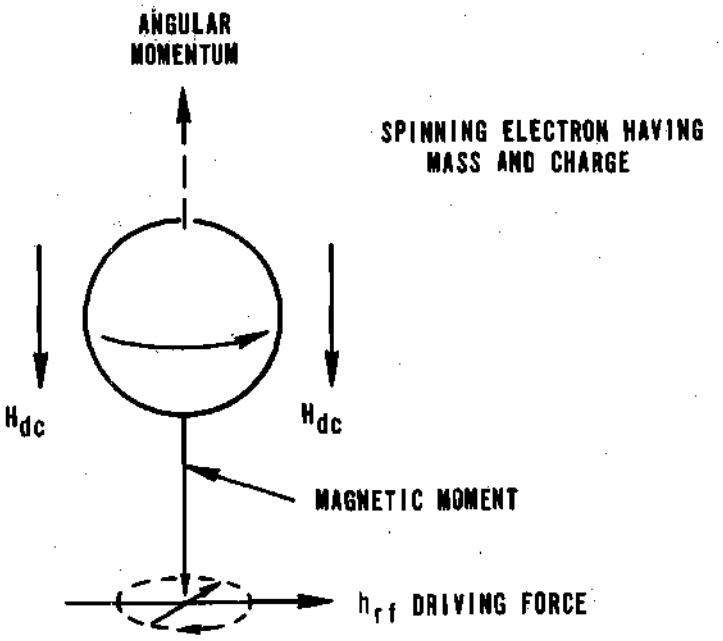

Figure 8. Schematic Representation of an Electron
[From Fox, Miller, and Weiss p.7.]

field H_{dc} will result in the axis of the electron spins becoming aligned with the dc field. If the spin axis is momentarily deflected from parallelism with the dc field, it will not immediately return to its initial orientation but will precess as a gyroscope about the dc field at its "natural" frequency which is proportional to the magnitude of H_{dc}. This frequency is called the gyromagnetic resonance frequency, and the behavior of ferrites in microwave devices is profoundly dependent on the relative magnitudes of the frequency of the applied rf wave and the gyromagnetic frequency. The precession which results when an rf magnetic field is applied perpendicular to H_{dc} causes the tip of the magnetic moment vector to describe an elliptical path as indicated by the dashed line in Figure 8. The direction of rotation around the ellipse will always be clockwise when viewed along H_{dc}. As a result of the precession of magnetic moment, it is seen that a component of magnetic flux is produced which is perpendicular to both H_{dc} and h_{rf}.

The description given above is obviously a much simplified explanation of ferrite behavior. Actually, most of the electrons in the ferrite may be grouped into pairs with the spins of the electrons of any pair pointing in opposite directions. These electrons do not contribute to any first order magnetic effects. By virture of certain forces between them, known as "exchange forces," some electrons line up with their spins mutually parallel and are easily oriented en mass by the application of a relatively small magnetic field. This is what makes the material appear "magnetic." Ever present thermal energy tends at the same time to create disorder in the alignment of the electron spins with the result that at any temperature greater than absolute zero the spins never all line up perfectly with the applied field. Nevertheless, it is a good assumption that, out of the total number of unpaired electron spins, a fraction do line up with the applied field and behave in accordance with the simple classical picture given above. From this simple model a very useful mathematical description of the dynamic behavior of the macroscopic magnetization can be formulated.

Tensor Permeability In Saturated Ferrites. If a sufficiently large dc magnetic field is applied to a ferrite sample, all the microscopic magnetic moments of the material will be aligned and the sample is said to be magnetically saturated. Based on the classical model discussed above, each microscopic magnetic moment is associated with a spinning positive mass having a negative charge. Adjacent microscopic spin moments are assumed to be so tightly bound (due to the exchange forces) that they maintain a common orientation as they precess. From classical dynamics, the equation of undamped motion for a spinning mass with angular momentum $\vec{J}$ when subjected to a net torque $\vec{T}$ is

$$\frac{d\vec{J}}{dt} = \vec{T} \qquad (1)$$

In the present problem $\vec{T}$ is the torque exerted on the microscopic dipole moment by the net magnetic field. Alternatively, if $\vec{M}$ represents the net magnetic

moment per unit volume, the torque $\vec{T}$ is the torque exerted on the macroscopic magnetization per unit volume $\vec{M}$, i.e., $\vec{T} = \vec{M} \times \vec{H}$. The angular momentum per unit volume is directly proportional to $\vec{M}$ (30). The constant of proportionality is called the gyromagnetic ratio γ. Thus, $\vec{J} = \vec{M}/\gamma$, and

$$\frac{d\vec{M}}{dt} = \gamma(\vec{M} \times \vec{H}) \tag{2}$$

Equation 2 can also be derived quantum mechanically from a spin-Hamiltonian that includes terms for the Zeeman, dipole-dipole and exchange interactions, as well as one for the crystalline anisotropy energy. The equations of motion are then obtained by the usual procedure of calculating the commutator of the spin-Hamiltonian and the spin angular momentum (31) (32) (33) (34).

The solutions of Equation 2 of major interest for the present study are the small signal solutions, i.e., the response of the magnetization to a small rf signal field superimposed on a large dc bias field. In this situation, the relationship between the rf magnetization $\vec{m}$ and the rf magnetic intensity $\vec{h}$ can be obtained by letting

$$\vec{M} = \vec{M}_s + \vec{m}e^{j\omega t} \qquad \vec{H} = \vec{H}_i + \vec{h}e^{j\omega t}$$

where $\vec{M}_s$ = saturation magnetization, $\vec{H}_i$ = internal static magnetic field

$\vec{m}e^{j\omega t}$ = rf magnetization $\vec{h}e^{j\omega t}$ = rf magnetic field

substituting into the equation of motion, equating terms of first order in ω and then solving for $\vec{m}$ in terms of $\vec{h}$. Performing these operations, it is discovered that the relationship between $\vec{m}$ and $\vec{h}$ is in the form of a tensor, i.e., $\vec{m} = \overleftrightarrow{X}\vec{h}$ where $\overleftrightarrow{X}$ is the small signal tensor susceptibility. Since $\vec{b} = \mu_o(\vec{h} + \vec{m})$, $\vec{b}$ is related to $\vec{h}$ by $\vec{b} = \mu_o(1 + \overleftrightarrow{X})\vec{h} = \overleftrightarrow{\mu}\vec{h}$ where $\overleftrightarrow{\mu}$ is the tensor permeability. The lossless tensor permeability, obtained in the indicated manner from Equation 2 is

$$\vec{\mu} = \mu_o \begin{bmatrix} \mu & -j\kappa & 0 \\ j\kappa & \mu & 0 \\ 0 & 0 & 1 \end{bmatrix} \tag{3}$$

where $\mu = 1 + \dfrac{\omega_o \omega_m}{\omega_o^2 - \omega^2}$ $\qquad \kappa = \dfrac{\omega \omega_m}{\omega_o^2 - \omega^2}$

ω = microwave radian frequency

$\omega_o = \gamma H_i$, $\omega_m = \gamma M_s$, H_i = internal static magnetic field,

M_s = saturation magnetization, γ = gyromagnetic ratio.

Obviously μ and κ have singularities when $\omega = \omega_o = \gamma H_i$. This is defined as the resonance condition.

In reality there must, of course, be a damping term in the equation of motion of $\vec{M}$ to account for losses. The details of the mechanisms contributing to this damping are just beginning to be understood and, as yet, there has been no derivation from first principles of an equation of motion which includes a damping term. As an alternative, the damping is usually represented phenomenologically. That is, a term having the proper dimensions and which appropriately represents the observed experimental results is added. Historically, there have been several suggested forms for the damping term but only the Landau-Lifshitz (35), the Bloch-Bloembergen (36) (37), and the Gilbert (38) forms have been widely used. There seems to be (or to have been) a tendency to interpret the equations of motion based on these three damping forms as being fundamentally different (39) (40). However, as the "derivation" below will show, it seems more reasonable and considerably less confusing to adopt the point of view that the phenomenological equations of motion are simply expansions of the vector time rate of change of $\vec{M}$ in terms of an arbitrary set of vectors. In general the expansion must contain at least three linearly independent vectors because the motion described takes place in three dimensional space. One of

the independent vectors will logically be the ($\vec{M}$ x $\vec{H}$) term of the lossless equation of motion. The coefficients in the expansion are adjusted empirically to insure that each term has the proper dimensions and that the net result adequately accounts for the observed experimental results. For example, a general expansion of $\frac{d\vec{M}}{dt}$ in terms of the three linearly independent vectors $\vec{M}$, ($\vec{M}$ x $\vec{H}$), and ($\vec{M}$ x ($\vec{M}$ x $\vec{H}$)) can be written as

$$\frac{d\vec{M}}{dt} = A\vec{M} + B(\vec{M} \times \vec{H}) + C\,\vec{M} \times (\vec{M} \times \vec{H}) \tag{4}$$

where A, B and C are undetermined coefficients. All three of the specific equations mentioned above are contained in this one equation. Landau and Lifshitz set A = 0 (justifiable on the assumption of a strong exchange field between adjacent spin moments), B = a positive constant = γ, C = a negative constant. Thus, the Landau-Lifshitz (LL) equation of motion is

$$\frac{d\vec{M}}{dt} = \gamma(\vec{M} \times \vec{H}) - |C|\,\vec{M} \times (\vec{M} \times \vec{H}) \tag{5}$$

Taking the dot product of $\vec{M}$ with $\frac{d\vec{M}}{dt}$ yields

$$\vec{M} \cdot \frac{d\vec{M}}{dt} = 1/2\ \frac{d|\vec{M}|^2}{dt} = \gamma\,\vec{M} \cdot (\vec{M} \times \vec{H}) - |C|\,\vec{M} \cdot \left[\vec{M} \times (\vec{M} \times \vec{H})\right] \equiv 0$$

Therefore $|\vec{M}|$ is a constant of the motion. The constant C may then be expressed as $C = -\lambda/|\vec{M}|^2$ where λ is a positive damping factor having the units of frequency. The LL equation in its more familiar form is then

$$\frac{d\vec{M}}{dt} = \gamma(\vec{M} \times \vec{H}) - \frac{\lambda}{|\vec{M}|^2}\left[\vec{M} \times (\vec{M} \times \vec{H})\right] \tag{6}$$

The Gilbert equation can be obtained from the LL equation by letting $\lambda = \alpha\gamma|\vec{M}|$, taking the cross product of $\vec{M}$ with Equation 6 and solving for $\vec{M} \times (\vec{M} \times \vec{H})$ in terms of $M \times \frac{d\vec{M}}{dt}$ and $(M \times H)$, and finally substituting the relation obtained for $\vec{M} \times (\vec{M} \times \vec{H})$ into Equation 6 to obtain

$$\frac{d\vec{M}}{dt} = \gamma_G (\vec{M} \times \vec{H}) - \frac{\alpha_G}{|\vec{M}|} \vec{M} \times \frac{d\vec{M}}{dt} \tag{7}$$

where $\gamma_G = \gamma(1 + \alpha^2)$, γ = gyromagnetic ratio

α_G = a dimensionless constant related to λ by $\alpha = \frac{\lambda}{\alpha|\vec{M}|}$

The Bloch-Bloembergen (BB) equation can be obtained by using the vector identity $\vec{A} \times (\vec{B} \times \vec{C}) = \vec{B}(\vec{A} \bullet \vec{B}) - \vec{C}(\vec{A} \bullet \vec{B})$ to write Equation 6 in the form

$$\frac{d\vec{M}}{dt} = \gamma(\vec{M} \times \vec{H}) - \frac{\lambda(\vec{H} \bullet \vec{M})\ \vec{M}}{|\vec{M}|^2} + \lambda\vec{H} \tag{8}$$

The Bloch-Bloembergen equation, as it was initially reported, omitted the third term of Equation 8 and was written in the form (36)

$$\frac{d\vec{M}}{dt} = \gamma(\vec{M} \times \vec{H}) - \frac{\lambda(\vec{H} \bullet \vec{M})}{|\vec{M}|^2} \vec{M} \tag{9}$$

Because Bloembergen was interested in investigating the individual relaxation processes, as opposed to simply accounting for the overall magnetic losses, he chose to write the damping term using two damping parameters which were to be related to two types of processes by which energy could be transferred out of the uniform mode of precession. The BB equation is, thus, often written as

$$\left(\frac{d\vec{M}}{dt}\right)_{x,y} = \gamma(\vec{M} \times \vec{H})_{x,y} - \frac{M_{x,y}}{T_2} \qquad (10)$$

$$\left(\frac{d\vec{M}}{dt}\right)_{z} = \gamma(\vec{M} \times \vec{H})_{z} - \frac{M_z - M_o}{T_1}$$

T_1 and T_2 are identified as the relaxation times for the longitudinal and transverse magnetization components, respectfully. M_o is the magnitude of the magnetization in the presence of the field $\vec{H}$. $\vec{M}$ is not a constant of the motion in this representation. As noted by various authors (41) (42) (43), the equation of motion as written in Equation 10 leads to negative losses under some circumstances. In a later paper (37), this difficulty was corrected by Bloembergen by "adding on" the third term of Equation 8 which he had previously neglected. The modified BB equation was written in terms of one time constant as

$$\frac{d\vec{M}}{dt} = \gamma(\vec{M} \times \vec{H}) - \frac{\vec{M} - \vec{M}_o}{\tau} + \frac{|\vec{M}|}{|\vec{H}|}\frac{\vec{H}}{\tau} \qquad (11)$$

The modified BB and the LL equations are equivalent in the small signal approximation if

$$\lambda \frac{|H_z|}{|M_z|} = \alpha\gamma|H_z| = \frac{1}{\tau}$$

From the preceeding discussion, it is apparent that the three forms of the equation of motion with losses examined are but different forms of a single phenomenological equation. The various forms simply highlight specific aspects of the general problem. The original LL form is mathematically convenient to use and adequately accounts for the overall magnetic losses. For this reason, a majority of the theoretical papers have used the LL damping form.

The Gilbert form, which can be written as

$$\frac{d\vec{M}}{dt} = \gamma_G \left| \vec{M} \times \left(\vec{H} - \frac{\alpha_G}{\gamma_G |\vec{M}|} \frac{d\vec{M}}{dt} \right) \right| \tag{12}$$

permits the interesting heuristic interpretation that the dissipation introduces an effective magnetic field opposite in direction and proportional in magnitude to $\frac{d\vec{M}}{dt}$ (44). The Bloch-Bloembergen form with two time constants can be useful in examining individual loss mechanisms. Yet all three are but special cases of Equation 4.

An unusual form of the equation of motion including losses which, although still phenomenological in nature, represents a step towards the desired derivation from first principles, was developed by Callen (45). In place of the LL parameter λ or the two relaxation times T_1 and T_2, Callen's equation contains three parameters which are defined in terms of definite quantum-mechanical transition probabilities, i.e., of creation and destruction of magnons. He justifies the form of his equation on the basis of various physical models related to the spin wave concept.

For the purposes of device analysis, where the desired end result is to accurately predict overall magnetic losses, separating the losses into pieces which can be attributed to different intrinsic mechanisms is unnecessary and a single damping parameter in the equation of motion is sufficient. It appears to be commonly accepted opinion (46) (47) that both the LL and BB damping forms adequately account for the overall magnetic loss in polycrystalline materials near resonance, but that neither form would yield good quantitative predictions in the region far from resonance where phase shifters normally operate. The latter contention, however, has not been borne out by the current study. In fact, as will be shown in Chapter IV, the LL damping form permits extremely accurate predictions of magnetic loss in phase shifters. The form of the

equation of motion which is used throughout this work is the modified LL equation given in Equation 7. Computing $\vec{\mu}$ in the small signal approximation using Equation 7 leads to

$$\vec{\mu} = \mu_o \begin{bmatrix} \mu & -j\kappa & 0 \\ j\kappa & \mu & 0 \\ 0 & 0 & 1 \end{bmatrix} \tag{13}$$

where $\mu = 1 + \dfrac{(\omega_o + j/\tau)\omega_m}{(\omega_o + j/\tau)^2 - \omega^2}$ $\qquad \kappa = \dfrac{\omega\ \omega_m}{(\omega_o + j/\tau)^2 - \omega^2}$ (14)

Or separating μ and κ into real and imaginary parts, $\mu = \mu' - j\mu''$, $\kappa = \kappa' - j\kappa''$

$$\mu' = 1 + \frac{\omega_m \tau \omega_o \tau \left[(\omega_o\tau)^2 - (\omega\tau)^2 + 1\right]}{\Delta} \tag{15}$$

$$\mu'' = \frac{\omega_m \tau \left[(\omega_o\tau)^2 + (\omega\tau)^2 + 1\right]}{\Delta}$$

$$\kappa' = \frac{\omega\tau\omega_m\tau \left[(\omega_o\tau)^2 - (\omega\tau)^2 - 1\right]}{\Delta}$$

$$\kappa'' = \frac{2\omega\tau\omega_o\tau\omega_m\tau}{\Delta}$$

$$\Delta = \left[(\omega_o\tau)^2 - (\omega\tau)^2 - 1\right]^2 + (2\omega_o\tau)^2$$

where ω = microwave radian frequency

$\omega_o = \gamma_G H_i$, $\omega_m = \gamma_G M_s$

H_i = internal static magnetic field

M_s = saturation magnetization

γ = gyromagnetic ratio

$$\gamma_G = \gamma(1+\alpha^2),\ \alpha = \frac{1}{\omega\tau}$$

τ = an "effective" damping time constant

The real and imaginary parts of μ and κ are shown in Figure 9 as functions of the static internal field H_i with τ as a parameter. The absorption linewidth ΔH is customarily defined as the width of the absorption (μ'' or κ'') curve at half-maximum absorption. The linewidth is easily shown to be related to τ by $\Delta H = \frac{2}{\gamma\tau}$ (48).

An interesting observation about the relative magnitudes of μ'' and κ'' can be made by imposing the physical requirement of nonnegative energy dissipation on the ferrite. Under this condition, it can be shown (49) that the components of the permeability tensor must satisfy the following constraints:

$$\mu'' \geq 0$$
$$\mu'' \geq |\kappa''|$$

Examining Equation 14 it is apparent that the LL form of the permeability components satisfies these constraints. It is worthwhile noting at this point that the BB equations given as Equation 10 lead to permeability components that do not satisfy the nonnegative energy absorption constraints. Hence, extreme caution must be exercised in interpreting results obtained using these equations.

If the ferrite sample is not magnetically saturated, a more general form of the permeability tensor than that of Equation 14 must be used. A useful form of this tensor is derived in the next section.

Tensor Permeability In Unsaturated Ferrites. A saturated ferrite sample is composed of a single magnetic domain, i.e., all the microscopic moments in the material are aligned. If the dc magnetic bias field is reduced to a sufficiently small value, the microscopic magnetic moments in the material will no longer all be aligned. Instead, the sample will be composed of a number of

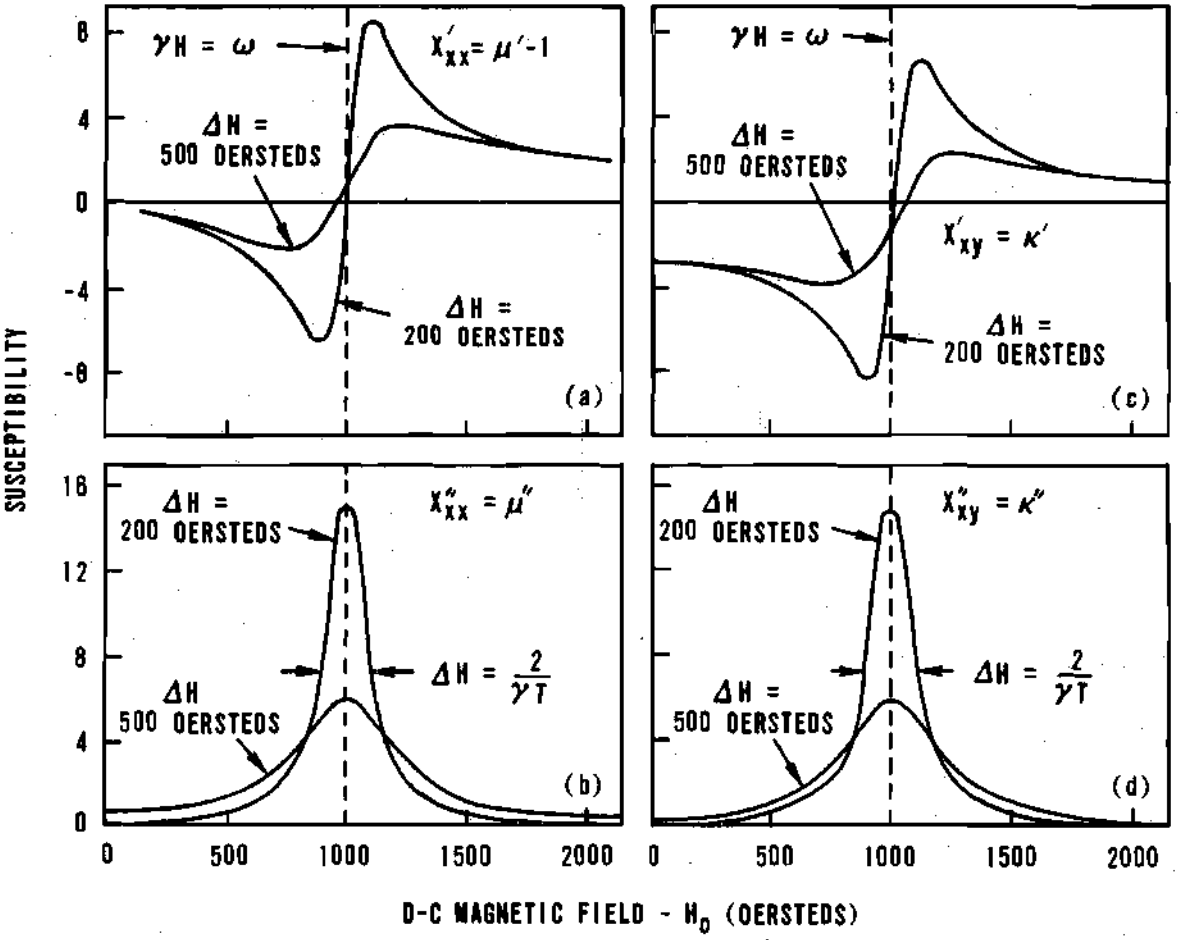

Figure 9. Real and Imaginary Parts of μ and κ, From Lax and Button, Figure 4-3, p. 155

magnetic domains, within each of which the moments are all aligned but with the moments in the various domains oriented in different directions. Under these conditions, the material is said to be magnetically unsaturated. For an unsaturated material, a spatial averaging process must be carried out to obtain the net magnetization in the x, y, or z direction, and the domain structure exerts an appreciable influence on the macroscopic properties of the material. This means that the components of the permeability tensor are in general dependent upon the distribution of the directions of the microscopic magnetic moments with respect to the applied bias field. In an attempt to establish and justify a general form for the permeability tensor, which would be applicable in unsaturated media, Rado (50) (51) made a detailed qualitative examination of an arbitrarily magnetized polycrystalline ferrite media. In such media he writes the intrinsic tensor relationship in the form

$$\begin{bmatrix} \langle b_x \rangle \\ \langle b_y \rangle \\ \langle b_z \rangle \end{bmatrix} = \mu_o \begin{bmatrix} \langle \mu_{11} \rangle & \langle \mu_{12} \rangle & \langle \mu_{13} \rangle \\ \langle \mu_{21} \rangle & \langle \mu_{22} \rangle & \langle \mu_{23} \rangle \\ \langle \mu_{31} \rangle & \langle \mu_{32} \rangle & \langle \mu_{33} \rangle \end{bmatrix} \begin{bmatrix} \langle h_x \rangle \\ \langle h_y \rangle \\ \langle h_z \rangle \end{bmatrix} \tag{16}$$

where $\langle b \rangle$ and $\langle h \rangle$ are the spatial averages of the time-varying components of the magnetic induction and the magnetic field intensity. The $\langle \mu_{j\kappa} \rangle$ are effective permeability components averaged over several domains and, as such, are directly measurable quantities. Under the assumptions of Rado's theory, the relation between the macroscopic "point" field quantities $\vec{b}$ and $\vec{h}$ (not average) is given by a spin wave equation at points within the domain walls and by a tensor inside the domains, but the experimentally important relation between the average quantities $\langle \vec{b} \rangle$ and $\langle \vec{h} \rangle$ is given by a tensor everywhere. Relating $\langle \mu_{j\kappa} \rangle$ to the measurable intrinsic magnetic properties of the ferrite is, in general, exceedingly difficult.

An interesting case in which the components of the effective tensor permeability can be related to the intrinsic properties of the ferrite was examined by Rado (50). Based on qualitative arguments, he established the following lossless form of the permeability tensor for an unsaturated medium with a bias field in the +z direction.

$$\vec{\mu} = \mu_o \begin{bmatrix} 1 & -j\frac{\omega_m}{\omega} & 0 \\ j\frac{\omega_m}{\omega} & 1 & 0 \\ 0 & 0 & 1 \end{bmatrix} = \mu_o \begin{bmatrix} \mu & -j\kappa & 0 \\ j\kappa & \mu & 0 \\ 0 & 0 & 1 \end{bmatrix} \tag{17}$$

Where $\omega_m = \gamma M$, ω = microwave radian frequency,

M = actual net static magnetization, γ = gyromagnetic ratio.

Since κ is directly proportional to the net magnetization of the material, it is given, as a function of the applied bias field, by curves of the same shape as the magnetization and hysteresis curves for the material. This form of the permeability tensor proved very useful in the analysis of Faraday rotation devices.

For the current problem, it has been necessary to include the effects of losses. The following procedure was utilized to obtain a tensor permeability for unsaturated media including losses.

As suggested by Rado (51), the relation $<\mu_{j\kappa}>$ between the effective rf fields $<\vec{b}>$ and $<\vec{h}>$ can sometimes be obtained by performing spatial averages on the relation $\mu_{j\kappa}$ between the "point" rf fields $\vec{b}$ and $\vec{h}$ of an appropriate saturated media problem. With this in mind, a ferrite sample consisting of a single domain magnetized by an applied magnetic field was considered. The saturation magnetization $\vec{M}_s$ of the domain and the net effective magnetic field $\vec{H}_i$ were assumed to be oriented in different directions as shown in Figure 10. The

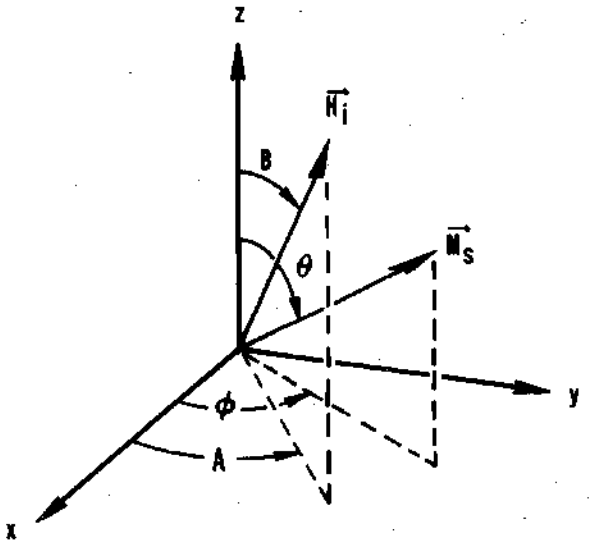

Figure 10. Relative Directions of the Saturation Magnetization $\vec{M}_s$ and of the Net Effective Static Magnetic Field Acting on a Single Domain

equation of motion for the macroscopic magnetization, including losses via the Landau-Lifshitz damping term, is

$$\frac{d\vec{M}}{dt} = \gamma_e (\vec{M} \times \vec{H}) - \frac{\alpha}{\vec{M}} \vec{M} \times \frac{d\vec{M}}{dt} \qquad (18)$$

where $\vec{M} = \vec{M}_s + \vec{m}e^{j\omega t}$ $\vec{H} = \vec{H}_i + \vec{h}e^{j\omega t}$

$\vec{M}_s = \left|\vec{M}_s\right| \left|\vec{i} \sin\theta\cos\phi + \vec{j} \sin\theta\sin\phi + \vec{\kappa}\cos\theta\right|$ = saturation magnetization

$\vec{h} = \vec{i}h_x + \vec{j}h_y + \vec{\kappa}h_z$ = rf magnetic field

$\vec{m} = \vec{i}m_x + \vec{j}m_y + \vec{\kappa}m_z$ = rf magnetization

$\gamma_e = \gamma(1+\alpha^2)$, $\alpha = \frac{1}{\omega\tau}$, τ = damping time-constant

$\vec{H}_i = \vec{i}H_x + \vec{j}H_y + \vec{\kappa}H_z$ = net effective field acting on a single domain

$= \left|\vec{H}_i\right| \left|\vec{i} \sin B \cos A + \vec{j} \sin B \sin A + \vec{\kappa}\cos B\right|$

Expanding Equation 18, equating coefficients of $e^{j\omega t}$, after considerable algebra the following small signal tensor permeability is obtained. The details of the analysis are given in Appendix A.

$$\vec{\mu} = \mu_o \begin{bmatrix} \mu_{11} & \mu_{12} & \mu_{13} \\ \mu_{21} & \mu_{22} & \mu_{23} \\ \mu_{31} & \mu_{32} & \mu_{33} \end{bmatrix} \tag{19}$$

$$\mu_{11} = 1 + \frac{\gamma_e |\vec{M}_s|}{\Delta} \Big\{ \Big[\gamma_e H_z (\cos\theta - \alpha \sin^2\theta \sin\phi \cos\phi) + \gamma_e H_y (\sin\theta \sin\phi + \alpha \sin\theta \cos\theta \cos\phi) \Big] + j \Big[\omega\alpha (\cos^2\theta + \sin^2\phi \sin^2\theta) + \frac{1}{\omega} (\gamma_e H_z \gamma_e H_x \sin\theta \sin\phi - \gamma_e H_x \gamma_e H_y \cos\theta) \Big] \Big\}$$

$$\mu_{12} = \frac{-j\gamma_e |\vec{M}_s|}{\Delta} \Big\{ \omega \cos\theta + \alpha \sin^2\theta \cos\phi \, (\omega \sin\phi + j \gamma_e H_z \cos\phi) - \frac{1}{\omega} (\gamma_e H_x) (\gamma_e H_x \cos\theta + \gamma_e H_z \sin\theta \cos\phi) + j(\alpha \gamma_e H_x \cos\theta - \gamma_e H_y) \sin\theta \cos\phi \Big\} \tag{20}$$

$$\mu_{13} = \frac{-j\gamma_e |\vec{M}_s|}{\Delta} \Big\{ -\omega \sin\theta \sin\phi + \omega\alpha \cos\theta \sin\theta \sin\phi + \frac{1}{\omega} \gamma_e H_x \sin\theta (\gamma_e H_x \sin\phi - \gamma_e H_y \cos\phi) + j\alpha \sin^2\theta \cos\phi (2 \gamma_e H_x \sin\phi - \gamma_e H_y \cos\phi) - j \gamma_e H_z \sin\theta \cos\phi \Big\}$$

$$\mu_{21} = \frac{-j\gamma_e |\vec{M}_s|}{\Delta} \Big\{ -\omega \cos\theta + \omega\alpha \sin^2\theta \sin\phi \cos\phi + \frac{1}{\omega} \gamma_e H_y (\gamma_e H_y \cos\theta - \gamma_e H_z \sin\theta \sin\phi) + j \sin\theta \sin\phi \, (\alpha \gamma_e H_y \cos\theta - \alpha \gamma_e H_z \sin\theta \sin\phi - \gamma_e H_x) \Big\}$$

$$\mu_{22} = 1 + \frac{\gamma_e |\vec{M}_s|}{\Delta} \Big\{ \gamma_e H_z (\cos\theta + \alpha \sin^2\theta \sin\phi \cos\phi)$$

$$+ \gamma_e H_z \sin\theta (\cos\phi - \alpha \cos\theta \sin\phi) + j\omega\alpha(\cos^2\theta + \cos^2\phi \sin^2\theta)$$

$$+ \frac{1}{\omega} \gamma_e H_y (\gamma_e H_x \cos\theta - \gamma_e H_z \sin\theta \cos\phi) \Big\}$$

$$\mu_{23} = \frac{-j\gamma_e |\vec{M}_s|}{\Delta} \Big\{ \omega \sin\theta \cos\phi + \omega\alpha \cos\theta \sin\theta \sin\phi$$

$$+ \frac{1}{\omega} \gamma_e H_y (\gamma_e H_x \sin\theta \sin\phi - \gamma_e H_y \sin\theta \cos\phi)$$

$$+ j\alpha \gamma_e H_x \sin^2\theta \sin^2\phi - j \gamma_e H_z \sin\theta \sin\phi - j \alpha \gamma_e H_y \sin^2\theta \sin\phi \cos\phi \Big\}$$

$$\mu_{31} = \frac{-j \gamma_e |\vec{M}_s|}{\Delta} \Big\{ \omega \sin\theta \sin\phi + \omega\alpha \sin\theta \cos\theta \cos\phi$$

$$+ \frac{1}{\omega} \gamma_e H_z (\gamma_e H_y \cos\theta - \gamma_e H_z \sin\theta \sin\phi)$$

$$+ j\alpha \gamma_e H_y \cos^2\theta - j \gamma_e H_x \cos\theta - j\alpha \gamma_e H_z \sin\theta \cos\theta \sin\phi \Big\}$$

$$\mu_{32} = \frac{-j \gamma_e |\vec{M}_s|}{\Delta} \Big\{ -\omega \sin\theta \cos\phi + \omega\alpha \sin\theta \cos\theta \sin\phi$$

$$+ \frac{1}{\omega} \gamma_e H_z (\gamma_e H_z \sin\theta \cos\phi - \gamma_e H_x \cos\theta)$$

$$-j\alpha \gamma_e H_x \cos^2\theta - j \gamma_e H_y \cos\theta + j\alpha \gamma_e H_z \cos\theta \sin\theta \cos\phi \Big\}$$

$$\mu_{33} = 1 + \frac{\gamma_e |\vec{M}_s|}{\Delta} \Big\{ \alpha \gamma_e H_x \sin\theta \cos\theta \sin\phi + \gamma_e H_y \sin\theta \sin\phi$$

$$- \alpha \gamma_e H_y \sin\theta \cos\theta \cos\phi + \gamma_e H_x \sin\theta \cos\phi$$

$$-j \frac{1}{\omega} \gamma_e H_z (\gamma_e H_x \sin\theta \sin\phi + \gamma_e H_y \sin\theta \cos\phi) + j\omega\alpha \sin^2\theta \Big\}$$

where $\Delta = \left[-\omega^2-(\omega\alpha)^2+(\gamma_e|\vec{H}_i|)^2\right]+j\left[2\omega\alpha\gamma_e H_x\sin\theta\cos\phi\right.$

$\left.+2\omega\alpha\gamma_e H_y\sin\theta\sin\phi+2\omega\alpha\gamma_e H_z\cos\theta\right]$

$H_x = |\vec{H}_i|\sin B\cos A$

$H_y = |\vec{H}_i|\sin B\sin A$

$H_z = |\vec{H}_i|\cos B$

If θ and B are both zero, corresponding to a saturated media with saturation magnetization and bias field oriented in the same direction, the permeability given in Equation 20 reduces to that given in Equation 14.

As previously noted, an unsaturated material is composed of many domains with the magnetizations of the individual domains oriented at different angles (θ-B, ϕ-A) relative to the effective internal magnetic field $\vec{H}_i$. The result of Equation 20 can be extended so that it applies in unsaturated media if spatial averages which extend over several domains can be performed. Since the distributions of the magnetizations of the domains as functions of ϕ and θ and of the $\vec{H}_i$'s as functions of B and A are not always known, the averaging cannot, in general, be carried out explicitly. However, observing that, in most cases of practical interest, there exists a physically preferred direction for the magnetization and the effective static magnetic field often permits the averaging with respect to angles in the plane perpendicular to the preferred direction to be performed explicitly. The physically preferred direction of magnetization may arise in various ways. For instance, if we apply even a very small dc bias field to the sample, a preferred direction of magnetization is established in the direction of the applied field. Alternatively, if we arrange the ferrite so that it forms a closed magnetic path, such as the toroids in the latching phase shifters, the geometry of the sample establishes preferred magnetization directions. Assume, then, that the preferred magnetization direction is the +z direction and that this also the preferred direction for the $\vec{H}_i$'s. For this

situation, all values of ϕ and of A between 0 and 2π are equally likely. If it is assumed that $|\vec{M}_s|$ and $|\vec{H}_i|$ have the same value for all of the "several domains" over which the spatial averaging is to be performed and that the angles between the $\vec{H}_i$'s and the z-axis are small, the tensor permeability of Equation 19 after averaging with respect to α and A becomes (see Appendix A for details)

$$\langle\vec{\mu}\rangle_{\phi,A} = \mu_o \begin{bmatrix} \langle\mu_{11}\rangle_{\phi,A} & \langle\mu_{12}\rangle_{\phi,A} & 0 \\ \langle\mu_{21}\rangle_{\phi,A} & \langle\mu_{22}\rangle_{\phi,A} & 0 \\ 0 & 0 & \langle\mu_{33}\rangle_{\phi,A} \end{bmatrix} \tag{21}$$

$$\langle\mu_{11}\rangle_{\phi,A} = \langle\mu_{22}\rangle_{\phi,A} = 1 + \frac{\gamma_e|\vec{M}_s|\left|\gamma_e|\vec{H}_i|\cos\theta + j\omega\alpha\left(\cos^2\theta + \frac{1}{2}\sin^2\theta\right)\right|}{\Delta} \tag{22}$$

$$\langle\mu_{12}\rangle_{\phi,A} = -\langle\mu_{21}\rangle_{\phi,A} = \frac{-j\,\gamma_e|\vec{M}_s|\left|\omega\cos\theta + j\frac{\alpha\gamma_e|\vec{H}_i|\sin^2\theta}{2}\right|}{\Delta}$$

$$\langle\mu_{33}\rangle_{\phi,A} = 1 + \frac{\left|j\omega\alpha\sin^2\theta\right|}{\Delta}$$

$$\langle\mu_{13}\rangle_{\phi,A} = \langle\mu_{31}\rangle_{\phi,A} = \langle\mu_{23}\rangle_{\phi,A} = \langle\mu_{32}\rangle_{\phi,A} = 0$$

where $\Delta = \left[(\gamma_e|\vec{H}_i|)^2 - \omega^2 - (\omega\alpha)^2\right] + j\left[2\,\gamma_e|\vec{H}_i|\omega\alpha\cos\theta\right]$

It is now convenient to revert to the earlier notation and write

$$\langle\mu\rangle_{\phi,A} = \langle\mu_{11}\rangle_{\phi,A} = \langle\mu_{22}\rangle_{\phi,A}$$

$$-j\langle k\rangle_{\phi,A} = \langle\mu_{12}\rangle_{\phi,A} = -\langle\mu_{21}\rangle_{\phi,A}$$

$$\langle\mu_z\rangle_{\phi,A} = \langle\mu_{33}\rangle_{\phi,A}$$

Separating $\langle \mu \rangle_{\phi,A}$, $\langle \kappa \rangle_{\phi,A}$, and $\langle \mu_z \rangle_{\phi,A}$ into real and imaginary parts yields after some simplifying algebra

$$\langle \mu' \rangle_{\phi,A} = 1 + \frac{\gamma_e |\vec{M}_s| \gamma_e |\vec{H}_i| \cos\theta \left\{ \left[\gamma_e |\vec{H}_i| \right]^2 - \omega^2 - (\omega\alpha)^2 \cos^2\theta \right\}}{\Delta} \tag{23}$$

$$\langle \mu'' \rangle_{\phi,A} = \frac{\gamma_e |\vec{M}_s| \omega\alpha \cos^2\theta \left[\frac{3}{2} (\gamma_e |\vec{H}_i|)^2 + \frac{1}{2} \omega^2 + \frac{1}{2} (\omega\alpha)^2 \right]}{\Delta} - \frac{1}{2} \left[(\gamma_e |\vec{H}_i|)^2 - \omega^2 - (\omega\alpha)^2 \right]$$

$$\langle \kappa' \rangle_{\phi,A} = \frac{\gamma_e |\vec{M}_s| \omega \cos\theta \left\{ (\gamma_e |\vec{H}_i|)^2 \alpha^2 \sin^2\theta + \left[(\gamma_e |\vec{H}_i|)^2 - \omega^2 - (\omega\alpha)^2 \right] \right\}}{\Delta}$$

$$\langle \kappa'' \rangle_{\phi,A} = \frac{\gamma_e |\vec{M}_s| \omega\alpha \gamma_e |\vec{H}_i| \left\{ 2\omega - \frac{\sin^2\theta}{\omega} \left[\frac{1}{2} (\gamma_e |\vec{H}_i|)^2 + \frac{3}{2} \omega^2 - \frac{1}{2} (\omega\alpha)^2 \right] \right\}}{\Delta}$$

$$\langle \mu_z' \rangle_{\phi,A} = 1 + \frac{\gamma_e |\vec{M}_s| \left\{ (\omega\alpha)^2 (\gamma_e |\vec{H}_i|) (2 \sin^2\theta \cos\theta) \right\}}{\Delta}$$

$$\langle \mu_z'' \rangle_{\phi,A} = \frac{\gamma_e |\vec{M}_s| \left\{ \omega\alpha \sin^2\theta \left[\omega^2 + (\omega\alpha)^2 - (\gamma_e |\vec{H}_i|)^2 \right] \right\}}{\Delta}$$

where $\Delta = \left[(\gamma_e |\vec{H}_i|)^2 - \omega^2 - (\omega\alpha)^2 \right]^2 + \left[2 \gamma_e |\vec{H}_i| \omega\alpha \cos\theta \right]^2$

If the angle between $\vec{H}_i$ and the z-axis is large, the expressions for the components of the permeability tensor are somewhat more complicated, as can be seen in Appendix A. In this more general situation the permeability components, after averaging with respect to angles in the xy-plane, are functions of

both θ and B. To perform the averages with respect to θ and B, it is necessary to know the distributions of these angles as functions of the other parameters of the problem (e.g., as a function of the applied bias field).

For the case in which the angle between $\vec{H}_i$ and the z-axis is small, the permeability components, as given in Equation 23, are functions of θ alone. Even in this case, the average with respect to θ cannot be performed explicitly without making specific assumptions about the distributions of θ as a function of the applied bias field. However, because the average with respect to θ is intimately related to measurable physical quantities, a very useful form of the permeability tensor for unsaturated media can be obtained as follows. Write the average of the permeability components given in Equation 23 with the operator $\langle \rangle_\theta$ denoting spatial average with respect to θ. Collecting terms and recognizing their physical significance leads to the desired permeability components. Writing out the average with respect to θ, the following expressions are obtained

$$\langle \mu' \rangle_{\phi,A,\theta} = 1 + \frac{1}{\Delta}\left\{\gamma_e|\vec{H}_i|\left[(\gamma_e|\vec{H}_i|)^2 - \omega^2\right]\gamma_e|\vec{M}_s|\,\langle\cos\theta\rangle_\theta + \gamma_e|\vec{H}_i|\,(\omega\alpha)^2\,\gamma_e|\vec{M}_s|\,\langle\cos^3\theta\rangle_\theta\right\} \tag{24}$$

$$\langle \mu'' \rangle_{\phi,A,\theta} = \frac{\omega\alpha}{\Delta}\left\{\left[\frac{3}{2}(\gamma_e|\vec{H}_i|)^2 + \frac{1}{2}\,\omega^2 + \frac{1}{2}(\omega\alpha)^2\right]\gamma_e|\vec{M}_s|\,\langle\cos^2\theta\rangle_\theta - \frac{\gamma_e|\vec{M}_s|}{2}\left[(\gamma_e|\vec{H}_i|)^2 - \omega^2 - (\omega\alpha)^2\right]\right\}$$

$$\langle \kappa' \rangle_{\phi,A,\theta} = \frac{1}{\Delta}\left\{(\gamma_e|\vec{H}_i|)^2\,\alpha^2\,\gamma_e|\vec{M}_s|(\langle\cos\theta\rangle_\theta - \langle\cos^3\theta\rangle_\theta) + \left[(\gamma_e|\vec{H}_i|)^2 - \omega^2 - (\omega\alpha)^2\right]\gamma_e|\vec{M}_s|\,\langle\cos\theta\rangle_\theta\right\}$$

$$\langle \kappa'' \rangle_{\phi,A,\theta} = \frac{\omega\alpha\gamma_e|\vec{H}_i|}{\Delta}\left\{2\omega\gamma_e|\vec{M}_s| - \frac{1}{\omega}\left[\frac{1}{2}(\gamma_e|\vec{H}_i|)^2 + \frac{3}{2}\omega^2 - \frac{1}{2}(\omega\alpha)^2\right]\gamma_e|\vec{M}_s|(1 - \langle\cos^2\theta\rangle_\theta)\right\}$$

$$\langle \mu_z' \rangle_{\phi,A,\theta} = 1 + \frac{1}{\Delta}\left|(\omega\alpha)^2(\gamma_e|\vec{H}_i|)(2\gamma_e|\vec{M}_s|)(\langle\cos\theta\rangle_\theta - \langle\cos^3\theta\rangle_\theta)\right|$$

$$\langle \mu_z'' \rangle_{\phi,A,\theta} = \frac{\omega\alpha}{\Delta}\left|\left[\omega^2 + (\omega\alpha)^2 - (\gamma_e|\vec{H}_i|)^2\right]\left[\gamma_e|\vec{M}_s|\right]\left[1 - \langle\cos^2\theta\rangle_\theta\right]\right|$$

Where it has been recognized that the second term of Δ is very small compared to the first term for parameter values corresponding to the normal operating range of phase shifters so that $\Delta \approx \left[-\omega^2 + (\gamma_e|\vec{H}_i|)^2 - (\omega\alpha)^2\right]^2$.

Examining the permeability components of Equation 24, terms of the form $|\vec{M}_s|\langle\cos\theta\rangle_\theta$, $|\vec{M}_s|\langle\cos^2\theta\rangle_\theta$, and $|\vec{M}_s|\langle\cos^3\theta\rangle_\theta$ are observed to occur. The first term, $|\vec{M}_s|\langle\cos\theta\rangle_\theta$, is physically just the remanent magnetization, M_r, in the z-direction. The second and third terms can be related to the remanence ratio, R_r, which is defined by

$R_r = \frac{M_r}{|\vec{M}_s|} = \langle\cos\theta\rangle_\theta$. If M_r is to be greater than zero, the distribution of the magnetizations of the domains with respect to θ must be "peaked" in the first quadrant so that $\langle\cos\theta\rangle_\theta > 0$. If this is true, it is easily shown that

$$|\vec{M}_s|\langle\cos^2\theta\rangle_\theta \geq |\vec{M}_s|\left[\langle\cos\theta\rangle_\theta\right]^2 = |\vec{M}_s| R_r^2$$

and

$$|\vec{M}_s|\langle\cos^3\theta\rangle_\theta \leq |\vec{M}_s| \cdot \langle\cos\theta\rangle_\theta = |\vec{M}_s| R_r.$$

The saturation magnetization $|\vec{M}_s|$ and the remanent magnetization can easily be measured by independent methods. The damping constant α (or ΔH) is measured in the usual manner using a saturated sample. Since ω, the microwave radian frequency, will be known this leaves only $|\vec{H}_i|$ as an unknown factor in Equation 24. $|\vec{H}_i|$ can often be estimated by using Kittel's equation (52) to

compute an effective field for the "major" domain. The demagnetizing factors for the "major" domain can be estimated from the geometry of the sample.

It is significant that the real and imaginary parts of the permeability components depend in different ways upon $\langle \cos\theta \rangle_\theta$, $\langle \cos^2\theta \rangle_\theta$, and $\langle \cos^3\theta \rangle_\theta$. The following special case vividly displays these differences. Suppose that $\left|\vec{H}_i\right| \approx 0$ in Equation 24. The permeability components then become

$$\langle \mu' \rangle_{\phi,\, A,\theta} \approx 1$$

$$\langle \kappa' \rangle_{\phi,\, A,\theta} \approx \frac{-\omega \gamma_e \left|\vec{M}_s\right| \langle \cos\theta \rangle_\theta}{\left[\omega^2 + (\omega\alpha)^2\right]}$$

$$\langle \mu_z' \rangle_{\phi,\, A,\theta} \approx 1$$

$$\langle \mu'' \rangle_{\phi,\, A,\theta} \approx \frac{\omega\alpha\left[\frac{\gamma_e \left|\vec{M}_s\right|}{2}\left(1 + \langle \cos^2\theta \rangle_\theta\right)\right]}{\left[\omega^2 + (\omega\alpha)^2\right]}$$

$$\langle \kappa'' \rangle_{\phi,\, A,\theta} \approx 0$$

$$\langle \mu_z'' \rangle_{\phi,\, A,\theta} \approx \frac{\omega\alpha\gamma_e \left|\vec{M}_s\right|}{\left[\omega^2 + (\omega\alpha)^2\right]}\left(1 - \langle \cos^2\theta \rangle_\theta\right)$$

where

$\left|\vec{M}_s\right| \langle \cos\theta \rangle_\theta$ = remanent magnetization = M_r

$\langle \cos\theta \rangle_\theta$ = remanent ratio = R_r

Then $\frac{1}{2}\left|\vec{M}_s\right| \langle 1 + \cos^2\theta \rangle_\theta = \frac{1}{2}\left|\vec{M}_s\right| \left\{1 + \langle \cos^2\theta \rangle_\theta\right\}$

$$\geq \frac{1}{2}\left|\vec{M}_s\right| \left(1 + \left[\langle \cos\theta \rangle_\theta\right]^2\right).$$

Therefore, $\frac{1}{2}\left|\vec{M}_s\right| < 1 + \cos^2\theta >_\theta \stackrel{d}{=} M_{L_{xy}} \geq \frac{1}{2}\left|\vec{M}_s\right| (1 + R_r^2)$.

Similarly, $\left|\vec{M}_s\right| < 1 - \cos^2\theta >_\theta = \left|\vec{M}_s\right| \left\{1 - < \cos^2\theta >\right\}$

$$\leq \left|\vec{M}_s\right| \left(1 - \left[< \cos\theta >_\theta\right]^2\right) \text{ or } \left|\vec{M}_s\right| < 1 - \cos^2\theta >_\theta \stackrel{d}{=} M_{L_z}$$

$\leq \left|\vec{M}_s\right| (1 - R_r^2)$. Thus the magnetization enters the real and imaginary parts of the permeability components in different manners. The appropriate effective magnetization to use in the real (phase shift) part is the remanent magnetization, M_r, while the proper effective magnetization to use in the imaginary (loss) parts is $M_{L_{xy}}$ for the xy-components and M_{L_z} for the z-component. The bounds on the M_L's are

$$\frac{1}{2}\left|\vec{M}_s\right| (1 + R_r^2) \leq M_{L_{xy}} \leq \left|\vec{M}_s\right|$$

$$0 \leq M_{L_z} \leq \left|\vec{M}_s\right| (1 - R_r^2)$$

The magnetic losses represented by the imaginary parts of the permeability components of Equation 24 physically represent the spatial averages of losses due to damping of the precessional motion of the magnetization within the individual domains. The effective static magnetic field H_i is to be interpreted as an effective internal field which includes anisotropy and demagnetizing effects. With this interpretation, the high-frequency portion of the "low-field" losses (53) are accounted for directly by the model. The model does not include domain-wall losses. However, in high-density, unstressed ferrites domain-wall losses are usually confined to the frequency region below 100 Mc (54) and will, therefore, not be important in predicting losses at microwave frequencies.

Scalar Representation of Magnetic Losses. In the special case where a ferrite sample exhibits zero net static magnetization, the tensor relating $\langle \vec{b} \rangle$ to $\langle \vec{h} \rangle$ reduces to a complex scalar permeability

$$\mu_i = \mu_i' - j\,\mu_i'' \tag{25}$$

It has been suggested by Ince and Stern (29) and others that the partially magnetized ferrites in latching phase shifters can be treated as though the ferrite were magnetically saturated so far as phase shift is concerned and totally unmagnetized so far as losses are concerned. Thus, the phase properties are determined using the lossless permeability tensor of Equation 3 with the saturation magnetization M_s set equal to the measured remanence magnetization M_r of the ferrite toroid and with the internal magnetic field H_i set equal to zero. Losses are computed using a measured loss tangent $\tan\delta_m = \mu_i''/\mu_i'$ in analogy with Equation 25. In the opinion of Ince and Stern (29) this "bulk" loss representation is necessary because "... it is not feasible to write a tensor loss mechanism for the ferrite in the remanent state." One distinct disadvantage of this or of any other bulk loss representation is that the relation of the losses to intrinsic material parameters is obscured. Hence, no insight is provided into how the composition of the material might be modified to improve its loss characteristics. This disadvantage would not be too severe if the procedure led to accurate results. However, as will be shown in Chapter IV, the proposed bulk representation does not provide a satisfactory quantitative prediction of magnetic losses. The tensor permeability for unsaturated ferrites developed in the preceding section does, however, permit accurate quantitative prediction of magnetic losses for ferrites in the remanent state.

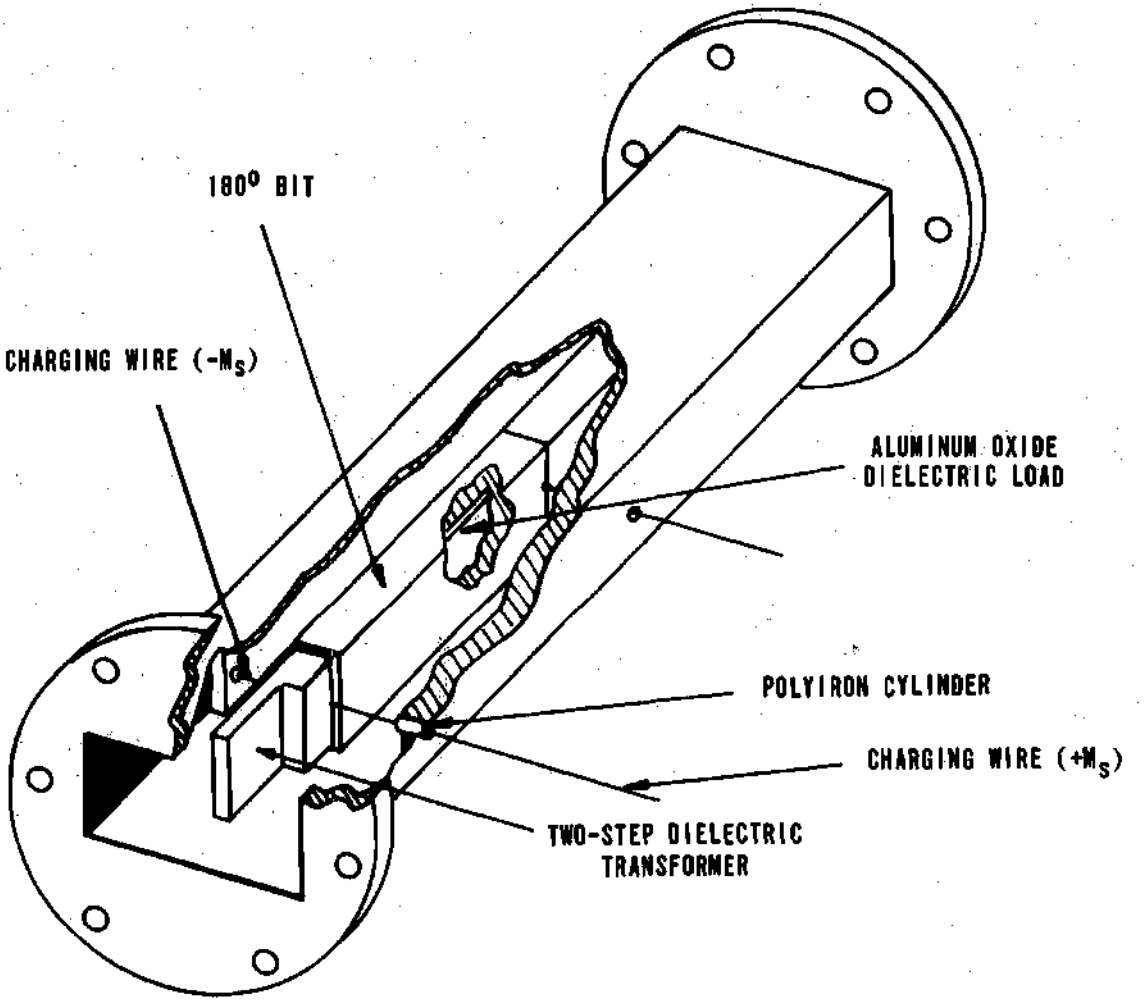

Figure 11. Cutaway View of a Waveguide Latching Phase Shifter

Specific Phase Shifters and Models

"Latching" Phase Shifters

A cutaway view of a particularly useful (22) latching or digital ferrite phase shifter structure is shown in Figure 11. In this structure, a rectangular toroid of "square loop" ferrite positioned along the axis of the waveguide is used as the phase shifting element. A single turn of wire coaxial to the ferrite toroid provides a path for the current pulses which magnetize the ferrite to

either of two remanent magnetization states ($+M_r$ or $-M_r$). Corresponding to these states, there are phase shifts $+\phi_r$ and $-\phi_r$ and their difference, $\Delta\phi_r$, is the nonreciprocal, differential phase shift of the ferrite "bit". In the device several bits of different values can be used in cascade to achieve step-wise variable, or digital, phase shift by activating (changing to $+M_r$) the appropriate combinations of bits, with the remaining bits left in the "inactive" ($-M_r$) state. The dielectric core of the toroid helps to concentrate the rf energy in the ferrite.

In the normal operational mode of this phase shifter (i.e., the fundamental TE mode), the rf magnetic field is entirely in the xy-plane. The magnetization in the top and bottom "crossbars" of the toroid is principally in the $\pm x$ direction, while in the vertical legs the magnetization tends to be in the $\pm z$ direction. To first order, when the incident rf magnetic field and the direction of magnetization of a sample are mutually parallel, there is no interaction between the field and the magnetization. Therefore, the crossbars of the toroid "look" approximately like pieces of dielectric to the incident rf field. In the vertical legs the magnetization is normal to the rf magnetic field and a strong interaction takes place.

From the above observations, it is apparent that the single-toroid latching phase shifter can be represented by the twin slab model shown in Figure 12. When the dielectric core and the ferrite toroid of the practical device have the same dielectric constant, that value is, of course, used for the dielectric constant of the dielectric load of the model. If the dielectric constants of the dielectric core and the ferrite are different, an "effective" dielectric constant is used for the dielectric load of the model.

Two variations on the basic structure of Figure 11, both of which can be represented by the same model as that of the basic structure, are shown in Figure 13. The parameters of these structures are normally such that the rf fields are concentrated near the center of the waveguide. The configuration of Figure 13a uses an external "driver" ferrite to complete the magnetic circuit and offers the advantage that temperature stabilization of the properties of the

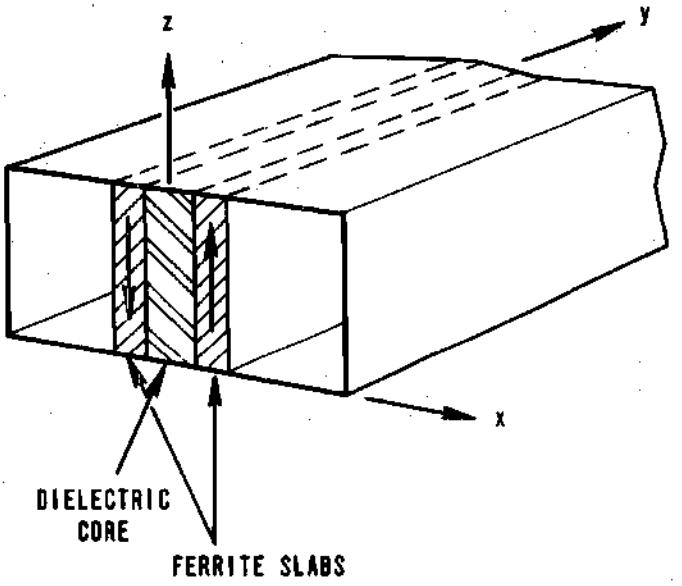

Figure 12. Twin-Slab Model for "Single-Toroid" Ferrite Latching Phase Shifter

phase shifter can be accomplished more or less independently of the properties of the internal ferrite sections (55). Thus, the portion of the material inside the waveguide can be selected to "optimize" the microwave performance of the device at a given temperature, while a good square-loop, high-Curie-temperature "driver" ferrite can be selected to insure adequate temperature stability without regard for its microwave properties. It is also possible in many cases to temperature compensate the characteristics of this structure or those of any of the other structures discussed by making the toroid out of a material with good microwave properties which have been temperature stabilized by adjusting

the material composition (56). The double-toroid structure of Figure 13b permits the switching wires to be positioned in a region of low rf field intensity. Also the width of the dielectric load is easily adjusted in contrast with the single internal toroid model where a new toroid is required if the width of the core is to be changed. Only the inner "leg" of each toroid exerts an appreciable effect on the microwave characteristics of the device.

A configuration closely related to the basic structure of Figure 11 is shown in Figure 14. This particular structure is very useful when high average rf power is to be controlled. The performance characteristics of a ferrite phase shifter normally deteriorate as the rf average power level increases due to heating effects. The removal of heat from the ferrite is considerably improved by placing slabs of dielectric material having a high thermal conductivity (such as boron nitride) in contact with the ferrite and the waveguide as shown in the figure. Combining this technique with the use of a temperature compensated material as the phase shift element leads to considerable improvement in average power handling capabilities. The model for this structure is shown in Figure 15.

As the peak rf power is increased, a threshold power level will be reached behond which the insertion loss of the device will increase appreciably due to the inherent nonlinearities of the system of precessing dipole moments. The peak power threshold for the onset of nonlinear effects for any of the above structures or for the applied field devices discussed below is partially determined by the critical field strength of the ferrite, h_{crit}, which is in turn largely determined by the intrinsic parameters of the ferrite (62) (63) (64). However, the threshold power level is also strongly influenced by the geometry of the structure, since the actual field strength in the ferrite is a function of the dimensional and electrical parameters of the components of the structure, the input power level, and frequency. Thus, for high peak power operation the

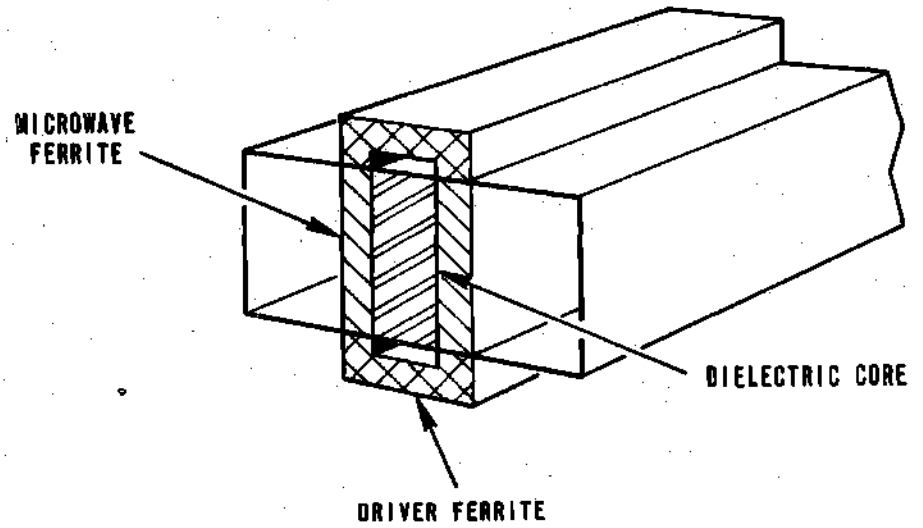

Figure 13a. Composite Circuit Latching Phase Shifter

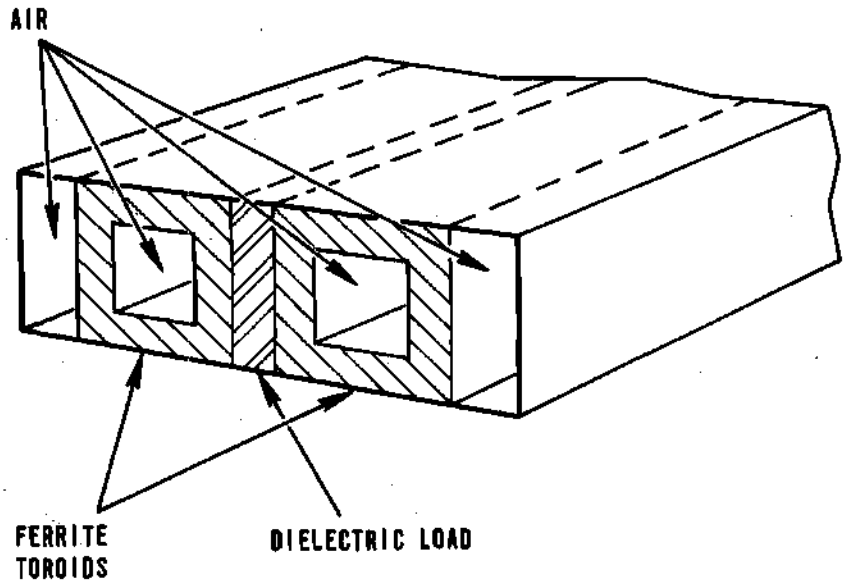

Figure 13b. Double Toroid Latching Phase Shifter

dimensional parameters of the structure and the permittivity of the dielectric load must be adjusted to minimize the rf magnetic field components in the ferrite while maintaining adequate phase shift.

"Applied-Field" Phase Shifters

Two useful applied-field or analog phase shifter structures and their models are shown in Figures 16 and 17. The phase shift for both of these devices can be varied by changing the magnitude and/or the direction of the applied bias field. The magnitude of the bias field is normally sufficiently large to magnetically saturate the ferrite. These structures can be adapted to high average power applications by using dielectrics having high thermal conductivity and temperature compensated ferrites.

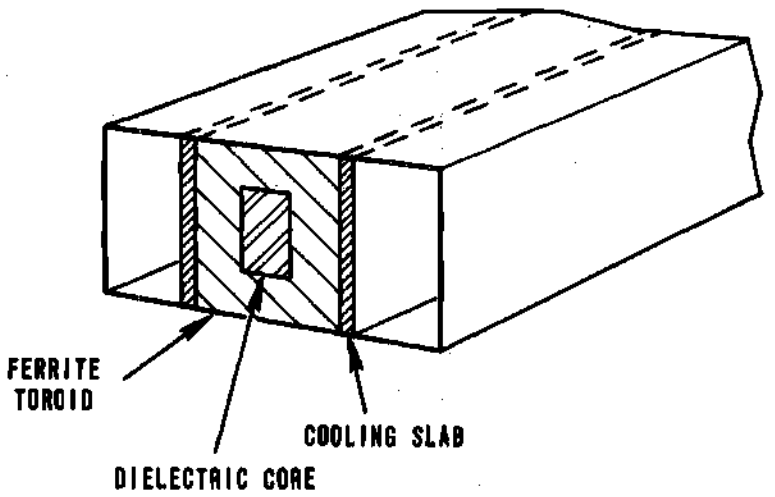

Figure 14. Latching Phase Shifter for High Average Power Applications

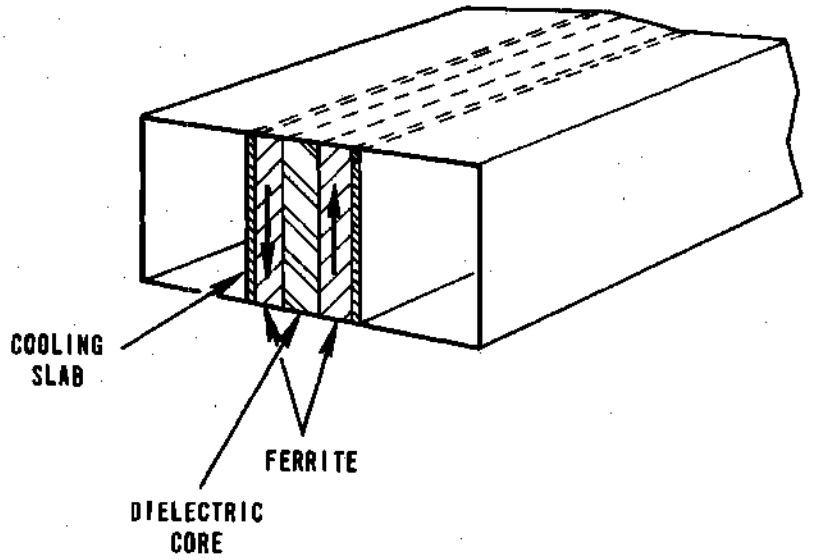

Figure 15. Model for the Structure of Figure 14

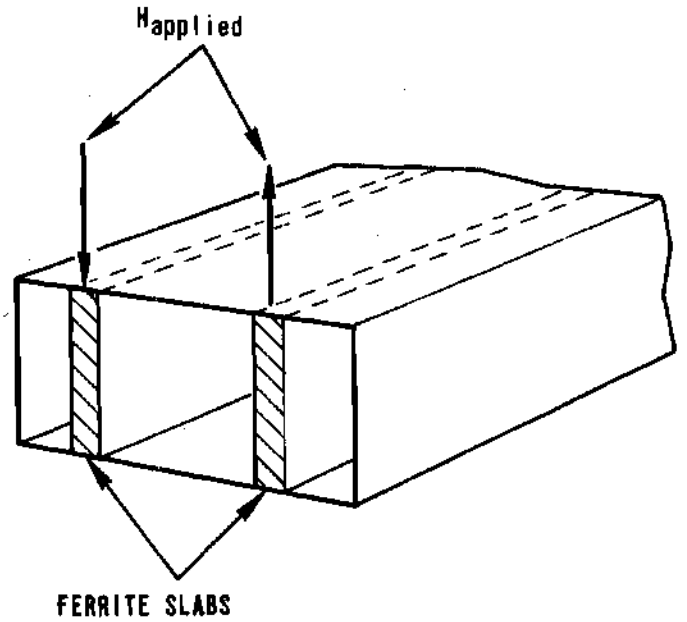

Figure 16. Twin-Slab Ferrite Analog Phase Shifter

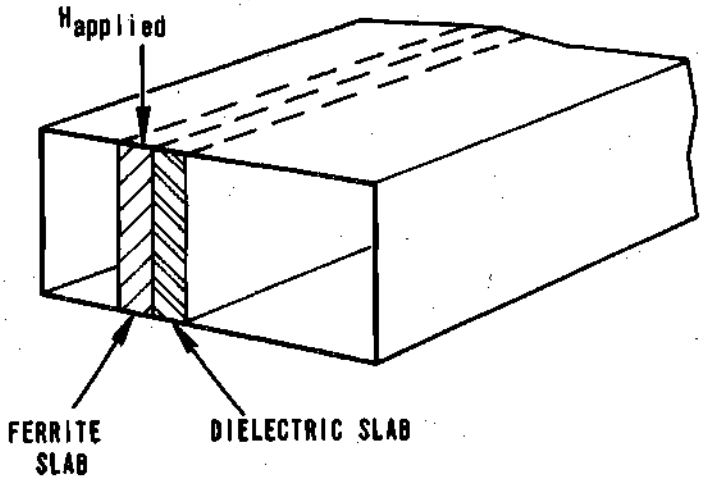

Figure 17. Single-Slab, Dielectric Loaded Ferrite Analog Phase Shifter

CHAPTER III

MODEL ANALYSIS PROCEDURES

Introduction

To establish quantitative relationships between the transfer characteristics of a ferrite device and its dimensional and material parameters, it is necessary to solve the boundary value problem for the device structure. Before the boundary value problem can be solved, mathematical models must be established which account for the electromagnetic properties of the materials used in the device, and a geometrical model established which accounts for the configurational properties of the structure. These two procedures have been carried out in Chapter II for a number of ferrite phase shifters. It is the purpose of this chapter to present procedures for solving the boundary value problems. The phase shifter models of Chapter II are used to illustrate the specifics of the procedures, but the methods presented are applicable to problems of a more general nature.

Three formally different procedures for obtaining the characteristic equation for the boundary value problem (i.e., the propagation constant equation) are presented. The first, which is referred to as the "direct method", is the direct solution of Maxwell's equations subject to appropriate boundary conditions. The second, which is due to Seidel (57), is called the "transverse operator" method and is similar to the A B C D matrix formulation for transmission line circuits. The third, referred to as "transverse resonance", is due to Frank (58) and consists of matching transverse impedances at appropriate points. The three methods are, naturally, closely related.

Direct Method

The starting point for the direct method is Maxwell's equations which must be solved in an appropriate coordinate system subject to specified boundary conditions. Since the structures of principal interest in this thesis consist of interleaved vertical slabs of dielectric and transversely magnetized ferrite in a section of rectangular waveguide, a rectangular coordinate system is used with the +z-direction pointing, as in Chapter II, in the preferred magnetization direction of the ferrite. The positive direction of propagation is taken to be the +y-direction. Sinusoidal steady state conditions are assumed, so that the field components have $e^{j\omega t}$ time dependence and $e^{-\gamma y}$ spatial dependence in the direction of propagation. The general form of the microwave permeability of the ferrite whose components are given in Equation 24 is repeated here for convenience.

$$\langle \overleftrightarrow{\mu} \rangle_{\phi,A,\theta} = \mu_o \begin{bmatrix} \langle \mu \rangle_{\phi,\,A,\,\theta} & -j\langle \kappa \rangle_{\phi,\,A,\theta} & 0 \\ j\langle \kappa \rangle_{\phi,\,A,\,\theta} & \langle \mu \rangle_{\phi,\,A,\,\theta} & 0 \\ 0 & 0 & \langle \mu_z \rangle_{\phi,A,\theta} \end{bmatrix} \tag{26}$$

For the following discussion, the angular brackets representing the spatial averaging are suppressed.

Under the above conditions, the Maxwell curl equations for the ferrite

$$\nabla \times \vec{E} = -\frac{\partial}{\partial t}\vec{b} = -\frac{\partial}{\partial t}[\overleftrightarrow{\mu}\, h] \tag{27}$$

$$\nabla \times \vec{h} = \epsilon_o \epsilon_f \vec{E}$$

can be written in expanded form as

$$-\gamma E_z - \frac{\partial E_y}{\partial z} = -j\omega\mu_o\left[\mu h_x - j\kappa h_y\right] \tag{28}$$

$$\frac{\partial E_x}{\partial z} - \frac{\partial E_z}{\partial x} = -j\omega\mu_o\left[j\kappa h_x + \mu h_y\right]$$

$$\frac{\partial E_y}{\partial x} + \gamma E_x = -j\omega\mu_o\mu_z h_z$$

$$-\gamma h_z - \frac{\partial h_y}{\partial z} = j\omega\epsilon_o\epsilon_f E_x \tag{29}$$

$$\frac{\partial h_x}{\partial z} - \frac{\partial h_z}{\partial x} = j\omega\epsilon_o\epsilon_f E_y$$

$$\frac{\partial h_y}{\partial x} + \gamma h_x = j\omega\epsilon_o\epsilon_f E_z$$

The propagation modes of interest for the present class of problems are transverse electric modes with no variation of the rf fields in the direction of the magnetization of the ferrite (z-direction). With these constraints (i.e., $E_y = 0$, $\frac{\partial}{\partial z} = 0$) imposed, the curl equations can be manipulated to yield

$$\frac{\partial^2 E_z}{\partial x^2} + \left[\gamma^2 + \frac{k^2}{\rho}\right] E_z = 0 \tag{30}$$

$$E_x = h_z = 0$$

$$h_y = \frac{\rho}{j\omega\mu_o}\left[\frac{\partial E_z}{\partial x} + \frac{\gamma}{\theta} E_z\right]$$

$$h_x = \frac{\rho}{j\omega\mu_o}\left[\gamma E_z - \frac{1}{\theta}\frac{\partial E_z}{\partial x}\right]$$

where

$$\rho = \frac{\mu}{\mu^2 - \kappa^2}$$

$$\theta = \frac{\mu}{j\kappa}$$

$$k^2 = \omega^2 \mu_o \epsilon_o \epsilon_f$$

For magnetization in the -z direction μ has the same sign but κ reverses in sign. For a dielectric region $\mu = 1$, $\kappa = 0$ and Equation 30 reduces to

$$\frac{\partial^2 E_z}{\partial x^2} + [\gamma^2 + k^2] E_z = 0 \qquad (31)$$

$$E_x = h_z = 0$$

$$h_y = \frac{1}{j\omega\mu_o} \frac{\partial E_z}{\partial x}$$

$$h_x = \frac{1}{j\omega\mu_o} \gamma E_z$$

The well-known solutions of Equations 30 and 31 constitute the admissible field forms in the dielectric and the ferrite, respectively. A set of functions with arbitrary coefficients which permit the boundary conditions of the specific structure being analyzed to be satisfied are selected from the admissible functions. Applying the boundary conditions then leads to a set of equations that are linear and homogeneous in the arbitrary constants. For a nontrivial solution, the determinent of the coefficients of the "arbitrary constants" must vanish. This requirement yields, by expanding the determinent, a transcendental equation for the propagation constant which can be solved by numerical methods. With the propagation constant known, all of the constants in the field equations except one can be related to the remaining constant and the other parameters of

the problem. The one remaining constant is usually evaluated from some auxiliary conditions such as a specified value for the input power.

As an example of the application of this procedure, consider the electromagnetically symmetric structure of Figure 18. The form of the electric field intensity in each of the three regions is (suppressing the time dependence)

$$E_{z1} = [A \cos k_d x]\, e^{-\gamma y} \tag{32}$$

$$E_{z2} = \left[Be^{jk_m x} + Ce^{-jk_m x}\right] e^{-\gamma y}$$

$$E_{z3} = [D \sin k_a (x - x_3)]\, e^{-\gamma y}$$

$$k_a^2 = \gamma^2 + \omega^2 \mu_o \epsilon_o \epsilon_a, \quad k_d^2 = \gamma^2 + \omega^2 \mu_o \epsilon_o \epsilon_d, \quad k_m^2 = \gamma^2 + \frac{\omega^2 \mu_o \epsilon_o \epsilon_f}{\rho}$$

where the boundary condition $E_z = 0$ at $x = x_3$ has already been imposed. The remaining boundary conditions to be applied are that tangential $\vec{E}$ and $\vec{h}$ be continuous at the $x = x_1$ and $x = x_2$ interfaces, i.e.,

$$E_{z1}\Big|_{x = x_1} = E_{z2}\Big|_{x = x_1} \qquad E_{z2}\Big|_{x = x_2} = E_{z3}\Big|_{x = x_2} \tag{33}$$

$$h_{y1}\Big|_{x = x_1} = h_{y2}\Big|_{x = x_1} \qquad h_{y2}\Big|_{x = x_2} = h_{y3}\Big|_{x = x_2}$$

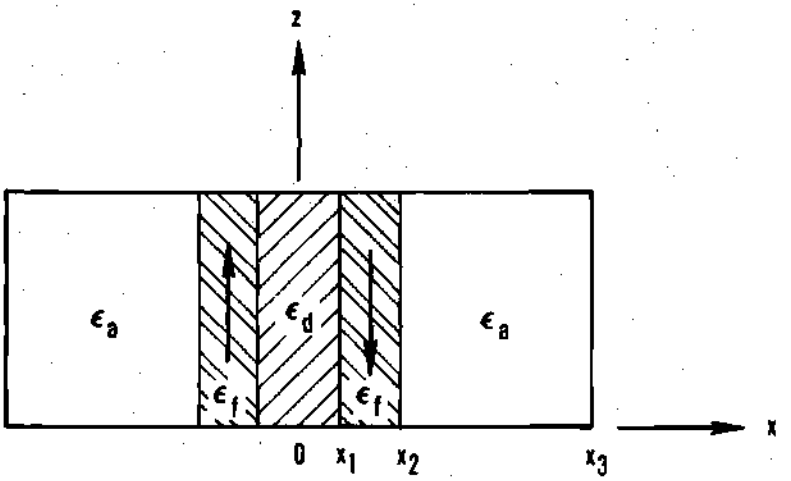

Figure 18. Dielectric Loaded Twin Slab Structure

Solving for the rf magnetic fields using Equations 30 and 31 yields

$$h_{y1} = \frac{1}{j\omega\mu_o}\left[-A\,k_d \sin k_d x\right]e^{-\gamma y} \tag{34}$$

$$h_{y2} = \frac{\rho}{j\omega\mu_o}\left[\left(j\,k_m + \frac{\gamma}{\theta}\right)Be^{jk_m x} + \left(-j\,k_m + \frac{\gamma}{\theta}\right)Ce^{-jk_m x}\right]e^{-\gamma y}$$

$$h_{y3} = \frac{1}{j\omega\mu_o}\left[k_a D \cos k_a (x - x_3)\right]e^{-\gamma y}$$

$$h_{x1} = \frac{1}{j\omega\mu_o}\left[\gamma A \cos k_d x\right]e^{-\gamma y} \tag{35}$$

$$h_{x2} = \frac{\rho}{j\omega\mu_o}\left[e^{jk_m x}\left(\gamma - j\frac{k_m}{\theta}\right)B + e^{-jk_m x}\left(\gamma + j\frac{k_m}{\theta}\right)C\right]e^{-\gamma y}$$

$$h_{x3} = \frac{1}{j\omega\mu_o}\left[\gamma D \sin k_a (x - x_3)\right]e^{-\gamma y}$$

Applying the boundary conditions on $\vec{E}$ and $\vec{h}$ tangential, the following set of equations are obtained

$$[\cos k_d x_1] A + \left[- e^{j k_m x_1}\right] B + \left[- e^{-j k_m x_1}\right] C + [o] D = 0 \qquad (36)$$

$$[j k_d \sin k_d x_1] A + \left[\rho e^{j k_m x_1} \left(- k_m + j \frac{\gamma}{\theta}\right)\right] B$$

$$+ \left[\rho e^{-j k_m x_1} \left(k_m + j \frac{\gamma}{\theta}\right)\right] C + [o] D = 0$$

$$[o] A + \left[e^{j k_m x_2}\right] B + \left[e^{-j k_m x_2}\right] C + \left[\sin k_a (x_3 - x_2)\right] D = 0$$

$$[o] A + \left[-\rho e^{j k_m x_2} \left(- k_m + j \frac{\gamma}{\theta}\right)\right] B + \left[-\rho e^{-j k_m x_2} \left(k_m + j \frac{\gamma}{\theta}\right)\right] C$$

$$+ \left[j k_a \cos k_a (x_3 - x_2)\right] D = 0$$

For a nontrivial solution the determinant of coefficients of the parameters A, B, C, D must vanish. Expanding this determinant yields, after a great deal of algebra, the following transcendental equation relating the propagation constant to the dimensional and material parameters of the structure.

$$\left[\frac{k_m}{\rho}(k_a - k_d) \cot k_m (x_2 - x_1) - \frac{\gamma}{\rho\theta}(k_a + k_d)\right] \cos\left\{k_d x_1 - k_a (x_3 - x_2)\right\} \qquad (37)$$

$$+ \left[\frac{k_m}{\rho}(k_a + k_d) \cot k_m (x_2 - x_1) - \frac{\gamma}{\rho\theta}(k_a - k_d)\right] \cos\left\{k_d x_1 + k_a (x_3 - x_2)\right\}$$

$$+ \left[k_m^2 + \frac{\gamma^2}{\theta^2} - \frac{k_a k_d}{\rho^2}\right] \sin\left\{k_d x_1 - k_a (x_3 - x_2)\right\}$$

$$- \left[k_m^2 + \frac{\gamma^2}{\theta^2} + \frac{k_a k_d}{\rho^2}\right] \sin\left\{k_d x_1 + k_a (x_3 - x_2)\right\} = 0$$

where $k_m^2 = \frac{\omega^2 \mu_o \epsilon_o \epsilon_f}{\rho} + \gamma^2$ $\qquad$ $k_d^2 = \omega^2 \mu_o \epsilon_o \epsilon_d + \gamma^2$

$k_a^2 = \omega^2 \mu_o \epsilon_o \epsilon_a + \gamma^2$ $\qquad$ $\rho = \frac{\mu}{\mu^2 - \kappa^2}$

$\theta = j\frac{\mu}{\kappa}$ $\qquad$ $\gamma = \alpha + j\beta$

$\mu = \mu' - j\mu''$ $\qquad$ $\kappa = \kappa' - j\kappa''$

$\epsilon_d = \epsilon'_d - j\epsilon''_d$ $\qquad$ $\epsilon_f = \epsilon'_f - j\epsilon''_f$

$\epsilon_a = \epsilon'_a - j\epsilon''_a$

If the dimensional and material parameters of the structure are specified, this equation can be solved numerically for the propagation constant γ. Equations can then be solved for B, C, and D in terms of A and substituted into Equations 32, 34 and 35 to obtain the electric and magnetic field intensities. B, C and D in terms of A are

$$B = \frac{e^{-jk_m x_1}}{2k_m}\left\{\frac{j k_d \sin k_d x_1}{\rho} + \left(k_m + j\frac{\gamma}{\theta}\right)\cos k_d x_1\right\}A \qquad (38)$$

$$C = \frac{e^{jk_m x_1}}{2k_m}\left\{\frac{-j k_d \sin k_d x_1}{\rho} - \left(-k_m + j\frac{\gamma}{\theta}\right)\cos k_d x_1\right\}A$$

$$D = e^{jk_m x_1}\left\{\frac{-j k_d \sin k_d x_1}{\rho} - \left(-k_m + j\frac{\gamma}{\theta}\right)\cos k_d x_1\right\}$$

$$\left\{\frac{1}{e^{jk_m x_2}\left[\left(-k_m + j\frac{\gamma}{\theta}\right)\sin k_a (x_3 - x_2) + j\frac{k_a}{\rho}\cos k_a (x_3 - x_2)\right]}\right\}$$

From the computed values of the propagation constant and the rf field intensities, various transfer characteristics can be obtained. These data are normally presented in the form of families of curves relating the device transfer characteristics to its dimensional and material parameters.

Transverse Operator Method

The transverse operator method, developed by Seidel, permits the equation for the propagation constant equation to be obtained rapidly and in a form convenient for numerical solution. The technique is based on the fact that in a TE mode waveguide where the rf field components have no variation in the direction of the E field, the electromagnetic field is completely specified by the E field and the longitudinal h component alone. For example, the electromagnetic field in the structure of Figure 15 has components E_z, h_x, and h_y but is completely specified by E_z and h_y since h_x is linearly related to h_y through the divergence condition on the induction field. Both E_z and h_y are continuous at the interfaces of the strata of the waveguide cross section. Hence, in analogy with the ABCD matrix representation of cascaded transmission lines, a transverse transfer matrix is defined which "transfers" the quantities E_z and h_y from one point along a transverse axis to another.

$$\begin{bmatrix} E_{za} \\ h_{ya} \end{bmatrix} = \begin{bmatrix} A & B \\ C & D \end{bmatrix} \begin{bmatrix} E_{zb} \\ h_{yb} \end{bmatrix} \tag{39}$$

The overall transverse operator matrix relating the fields at point a to the fields at point b is the matrix product of the transfer operators of the individual regions separating the point. If points a and b are taken to be the walls of the waveguide, then $E_{za} = E_{zb} = 0$ and

$$\begin{bmatrix} 0 \\ h_{ya} \end{bmatrix} = \begin{bmatrix} A & B \\ C & D \end{bmatrix} \begin{bmatrix} 0 \\ h_{yb} \end{bmatrix} \tag{40}$$

or

$$\begin{aligned} 0 &= B\, h_{yb} \\ h_{ya} &= D\, h_{yb} \end{aligned} \tag{41}$$

For a nontrivial solution h_{yb} must be nonzero. Therefore, B must be zero. From this condition the equation for the propagation constant is easily determined. If the structure analyzed has electromagnetic symmetry about some point, for example, point o is such a point in the structure of Figure 19; the y-component of the h field must be zero about that point and a simplification in the computations necessary to obtain the propagation equation results. The operator relating the fields at point o to those at the wall can be written as

$$\begin{bmatrix} 0 \\ h_{ya} \end{bmatrix} = \begin{bmatrix} A & B \\ C & D \end{bmatrix} \begin{bmatrix} E_{zo} \\ 0 \end{bmatrix} \tag{42}$$

or

$$\begin{aligned} 0 &= A\, E_{zo} \\ h_{ya} &= C\, E_{zo} \end{aligned} \tag{43}$$

For a nontrivial solution E_{zo} must be different from zero, and A must, therefore, be identically zero. This condition leads to the equation for the propagation constant of symmetrical structures.

The ABCD parameters for ferrite and dielectric regions are easily obtained from Maxwell's equations. A derivation for these parameters is given in Appendix C. The derivation follows that of Seidel but the notation used is based on the notation of the "direct method" of the preceeding section. The ABCD parameters for a ferrite region of width δ and a dielectric region of width W are

Ferrite Region of Width δ

$$A = \cos k_m \delta + \frac{\gamma}{k_m \theta} \sin k_m \delta \tag{44}$$

$$B = \frac{-j\omega\mu_o}{\rho k_m} \sin k_m \delta$$

$$C = \frac{j\rho}{\omega\mu_o k_m}\left(\frac{-\gamma^2}{\theta} - k_m^2\right)\sin k_m \delta$$

$$D = \cos k_m \delta - \frac{\gamma}{k_m \theta} \sin k_m \delta$$

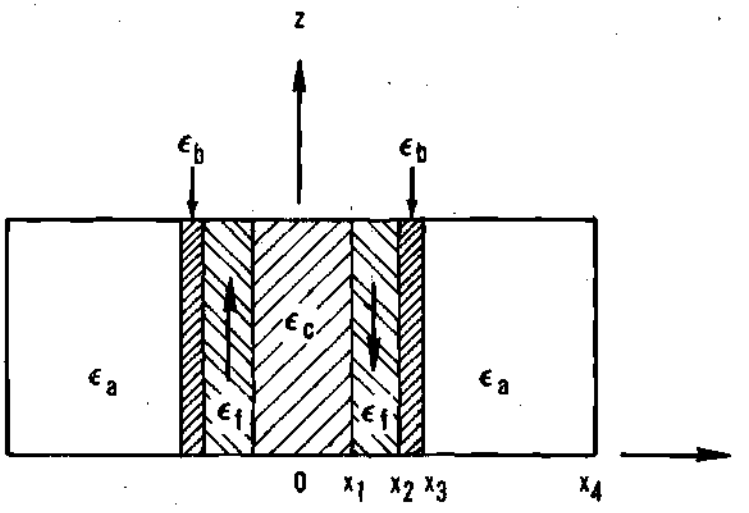

Figure 19. A Structure with Electromagnetic Symmetry about o

Dielectric Region of Width W

$$A = \cos k_d W \tag{45}$$

$$B = \frac{-j\omega\mu_o}{k_d} \sin k_d W$$

$$C = \frac{-j k_d}{\omega\mu_o} \sin k_d W$$

$$D = \cos k_d W$$

The definitions of the symbols and a discussion of algebraic sign changes with static field reversal are given in Appendix C.

As an example of the application of this method, consider the structure shown in Figure 19. This structure has electromagnetic symmetry about o. The overall transfer matrix is

$$\begin{bmatrix} A & B \\ C & D \end{bmatrix} = \begin{bmatrix} A_1 & B_1 \\ C_1 & D_1 \end{bmatrix} \begin{bmatrix} A_2 & B_2 \\ C_2 & D_2 \end{bmatrix} \begin{bmatrix} A_3 & B_3 \\ C_3 & D_3 \end{bmatrix} \begin{bmatrix} A_4 & B_4 \\ C_4 & D_4 \end{bmatrix} \tag{46}$$

Carrying out this multiplication and setting A = 0 yields

$$A = (A_1A_2 + B_1C_2)(A_3A_4 + B_3C_4) + (A_1B_2 + B_1D_2)(C_3A_4 + D_3C_4) = 0 \tag{47}$$

Substituting for the A's, B's, C's, and D's from Equations 44 and 45, the following equation for the propagation constant is obtained

$$\left[\left(k_a k_b\right)\left(\cos k_a W_1\right)\left(\cos k_b W_2\right) + \left(-k_b^2\right)\left(\sin k_a W_1\right)\left(\sin k_b W_2\right)\right] \otimes \qquad (48)$$

$$\left[\left(\frac{k_m}{\rho}\cos k_m W_3 - \frac{\gamma}{\rho\theta}\sin k_m W_3\right)\left(\cos k_c W_4\right) + \left(\frac{-\sin k_m W_3}{\rho 2}\right)\left(k_c \sin k_c W_4\right)\right]$$

$$+ \left[\left(k_a \cos k_a W_1\right)\left(\sin k_b W_2\right) + \left(\sin k_a W_1\right)\left(k_b \cos k_b W_2\right)\right] \otimes$$

$$\left[\left\{\left(\frac{-\gamma^2}{\theta^2} - k_m^2\right)\sin k_m W_3\right\}\left\{\cos k_c W_4\right\} + \left\{\frac{k_m}{\rho}\cos k_m W_3 + \frac{\gamma}{\rho\theta}\sin k_m W_3\right\} \otimes \right.$$

$$\left.\left\{-k_c \sin k_c W_4\right\}\right] = 0$$

$$k_a^2 = \omega^2 \mu_o \epsilon_o \epsilon_a + \gamma^2 \qquad k_b^2 = \omega^2 \mu_o \epsilon_o \epsilon_b + \gamma^2$$

$$k_c^2 = \omega^2 \mu_o \epsilon_o \epsilon_c + \gamma^2 \qquad k_m^2 = \frac{\omega^2 \mu_o \epsilon_o \epsilon_f}{\rho} + \gamma^2$$

$\otimes$ = multiplication $\qquad W_1 = x_4 - x_3 \qquad W_3 = x_2 - x_1$

$$W_2 = x_3 - x_2 \qquad W_4 = x_1$$

If the field intensities are required, they can be obtained from Maxwell's equations by the same procedure used in the direct method.

Transverse Resonance

The transverse resonance method of obtaining the equation for the propagation constant is based on the same observations about the fields in a TE mode waveguide as was the transverse operator method. The difference between the methods is that the transverse resonance technique deals with ratios of E_z to h_y while the transverse operator method deals with the fields themselves. Since E_z and h_y are both continuous at the interface between two media, their ratio must also be continuous. The ratio of E_z to h_y is usually referred to as the transverse wave impedance. By matching wave impedances at the

interfaces between the strata of the waveguide cross section, the equation for the propagation constant may be obtained.

As an example of the application of this procedure, consider the structure shown in Figure 18, which was used as an example for the direct method.

The $\vec{E}$ field and $\vec{h}$ fields in regions 1, 2, and 3 are given by Equations 32, 34 and 35 of the section on the direct method. The conditions to be satisfied by the transverse wave impedances are

$$\left.\frac{E_{z3}}{h_{y3}}\right|_{x = x_2} = \left.\frac{E_{z2}}{h_{y2}}\right|_{x = x_2} \tag{49}$$

$$\left.\frac{E_{z2}}{h_{y2}}\right|_{x = x_1} = \left.\frac{E_{z1}}{h_{y1}}\right|_{x = x_1}$$

Substituting for the fields and manipulating the resulting two equations, the following equation is obtained for the propagation constant.

$$\frac{\tan k_m (x_2 - x_1)}{k_m} = \frac{k_a \cot k_a (x_2 - x_3) + k_d \tan k_d x_1}{\Delta} \tag{50}$$

$$\Delta = \frac{k_a k_d}{\rho} \tan k_d x_1 \cot k_a (x_2 - x_3) - \rho \left(k_m^2 + \frac{\gamma^2}{\theta^2}\right) + k_a \frac{\gamma}{\theta} \cot k_a (x_2 - x_3)$$

$$- k_d \frac{\gamma}{\theta} \tan k_d x_1$$

Equation 50 can be shown to be equivalent to Equation 37 obtained earlier by the direct method.

The effects of dielectric and magnetic losses can be included exactly in the characteristic equation obtained using any of the above methods by simply using the appropriate complex permeability (Equation 15, 24, or 25) and permittivities. Solution of the characteristic equation then yields directly the theoretically predicted values of attenuation and phase shift per unit length for the device. It is often desirable to include waveguide conductor losses in the theoretical prediction of the overall losses for a ferrite device. For this purpose, a standard small-loss technique (67), which is quite satisfactory for computing waveguide losses is presented in Appendix B.

CHAPTER IV

EXPERIMENTAL VALIDITY CHECKS ON LOSS REPRESENTATIONS IN SATURATED AND UNSATURATED FERRITES

Introduction

In Chapter II the following observations were made on loss representations in polycrystalline ferrites. (a) It is commonly believed that the Landau-Lifshitz loss representation is not valid for quantitative prediction of losses in saturated polycrystalline ferrites biased from resonance. (b) It is the contention of some current investigators that losses for ferrites in a remanent magnetization state must be represented as bulk losses. In the same chapter, a method by means of which losses for ferrites in a remanent or unsaturated state can in fact be represented by a "lossy" tensor permeability was presented. It is the purpose of the current chapter to present and compare the results of numerical computations and experimental measurements which were carried out to test the validity of the three loss representations mentioned above, i.e., the LL representation for saturated ferrites, and the "tensor" and "bulk" representations for ferrites in the remanent state. The numerical calculations were carried out with the aid of a Burrough's B-5500 digital computer which was made available by the Rich Electronic Computer Center of the Georgia Institute of Technology. All experimental data were furnished by the Sperry Microwave Electronics Company of Clearwater, Florida.

Both the theoretical and the experimental data are presented in normalized form. Physical dimensions are normalized with respect to the free space wavelength at the center operating frequency, f_c. Frequency and the frequency equivalents of static magnetic fields and of remanence and saturation magneti-

zations are normalized with respect to the center operating frequency. Differential phase shift is given in degrees per GHz-cm. To unnormalize this quantity with respect to frequency, multiply by the center frequency in GHz. Losses are given either as decibels per 360^{o} of differential phase shift or decibels per centimeter.

Ferrite parameters and the phase shift and loss characteristics of the various devices were measured using standard techniques and equipment as described briefly below.

Measurement Equipment and Techniques

Measurement of Saturation Magnetization

Saturation magnetizations were measured using a vibrating sample magnetometer. This measurement is based on the detection of the ac magnetic field set up by the vibrating magnetic sample. A small sphere of the ferrite is placed in a strong saturating dc magnetic field. The sample is vibrated at a low audio frequency (100 cps) and the oscillating dipole field thus generated is detected by two coils so positioned as to minimize stray pickup. The magnitude of this dipole field is compared to the signal detected by two similar coils from a known calibrated sample attached to the same vibrating rod. This system, first proposed by Foner (66), is capable of accurate, continuous readout and lends itself well to the measurement of saturation magnetization as a function of temperature. The magnetometer can also be used to measure coercive force on spherical samples.

Measurement of Remanence Ratio

A hysteresisograph, or "square loop tester," was used to obtain the remanence ratio for toroidal samples. A brief schematic of the device is shown in Figure 20. The equipment operates at 60 cps and consists of a coaxial drive probe, integrator, function generator, peak reading voltmeter and scope display.

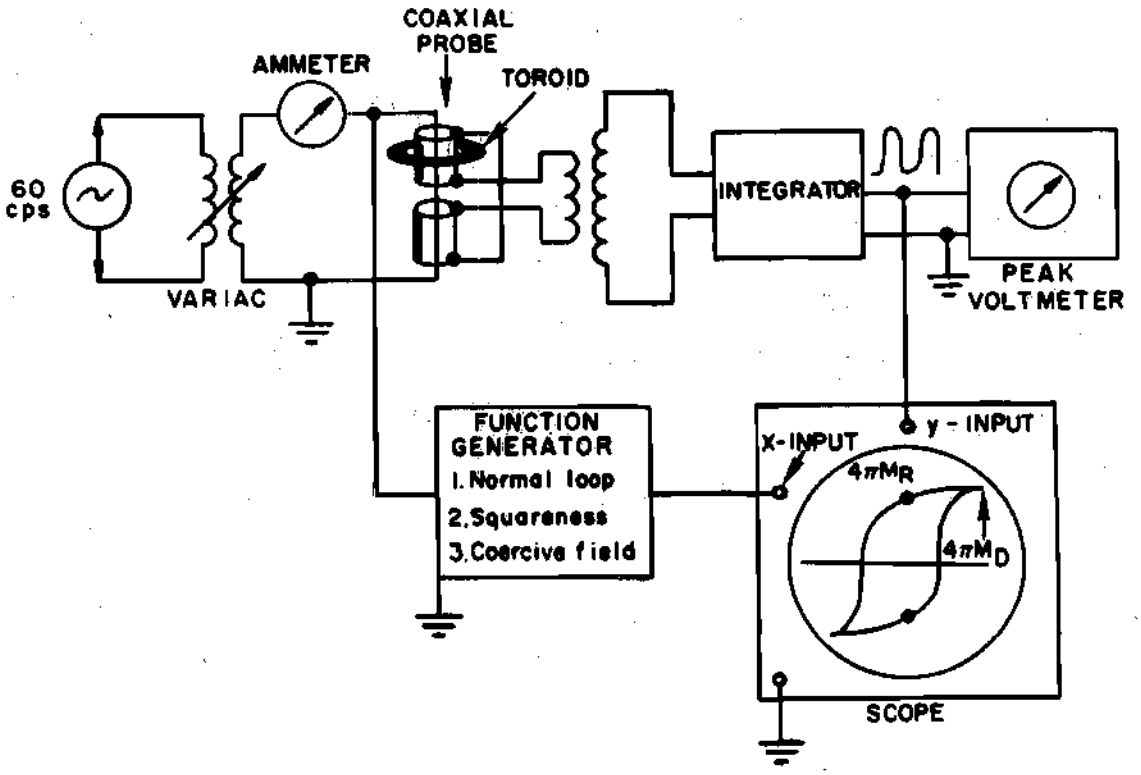

Figure 20. **Schematic of Square Loop Tester Modified for Measuring the Remanent Magnetization**

Measurement of Resonance Linewidth

Resonance linewidths were obtained using a reflection type, X band, resonance spectrometer. The samples measured were generally in the form of spheres 20 ± 2 mils in diameter polished to a 4/0 finish.

Measurement of Dielectric Constant and Dielectric Loss Tangent

Measurements of dielectric constant and dielectric loss tangent were made at X band. A small cylindrical sample of the material to be measured is inserted in a transmission cavity at a point of maximum electric field and zero magnetic field. If the Q and the resonant frequency of the cavity are known before and after a sample is inserted, tan δ and ϵ' can be calculated.

Measurement of Attenuation and VSWR

Measurements of attenuation and VSWR were carried out using the so-called ratio detector depicted in Figure 21A. This method, described by Hunton et al (67), permits a continuous display of the loss and VSWR across the frequency band.

Measurement of Differential Phase Shift

Differential phase shift was measured in the phase bridge shown in Figure 21B. At the power splitter the rf energy divides. The losses of the phase shifter under test are balanced and monitored by the calibrated attenuator in the upper arm. The ferrite is magnetized first clockwise and then counterclockwise and the calibrated phase shifter is adjusted to provide a null for each direction of magnetization. The difference of the calibrated phase shifter readings is the differential phase shift.

Loss Representation in Saturated Ferrites

Magnetic losses in saturated ferrites are usually accounted for analytically by the Landau-Lifshitz phenomenological representation of Equation 14 (Chapter II). As pointed out earlier, this representation is commonly believed to be quantitatively correct only at resonance. As a test of its quantitative accuracy over a wide operating region far from resonance, the Landau-Lifshitz loss formulation was utilized in the solution of the boundary value problem for the configuration of Figure 22. The loss and phase characteristics predicted by the analysis were then compared with the measured properties of a laboratory model of the device. Magnetic and dielectric losses were included exactly in the boundary value problem. Waveguide losses were computed using the small loss technique discussed in Appendix B. The internal dc magnetic field is determined from the measured bias field and the demagnetizing factors of the ferrite slab. Because the boundary value is solved exactly, the demagnetizing factors associated with the rf magnetic field are accounted for automatically by the boundary

conditions imposed on the rf fields at the surfaces of the ferrite. The equation for the propagation constant is

$$\left[\left(\cos k_a W_1\right)\left(\cos k_m W_3 + \frac{\gamma}{k_m \theta}\sin k_m W_3\right) + \left(\frac{\sin k_a W_1}{k_a}\right)\left(\frac{\rho}{k_m}\left\{\frac{-\gamma^2}{\theta^2} - k_m^2\right\}\sin k_m W_3\right)\right]$$

$$\circledast\left[\left(\cos k_b W_2\right)\left(\frac{\sin k_c W_4}{k_c}\right) + \left(\frac{\sin k_b W_2}{k_b}\right)\left(\cos k_c W_4\right)\right]$$

$$+ \left[\left(\cos k_a W_1\right)\left(\frac{\sin k_m W_3}{\rho k_m}\right) + \left(\frac{\sin k_a W_1}{k_a}\right)\left(\cos k_m W_3 - \frac{\gamma}{k_m \theta}\sin k_m W_3\right)\right]$$

$$\circledast\left[\left(-k_b \sin k_b W_2\right)\left(\frac{\sin k_c W_4}{k_c}\right) + \left(\cos k_b W_2\right)\left(\cos k_c W_4\right)\right] = 0$$

where

$$k_a^2 = \omega^2 \mu_o \epsilon_o \epsilon_a + \gamma^2 \qquad \epsilon_a = \epsilon'_a - j\,\epsilon''_a$$

$$k_b^2 = \omega^2 \mu_o \epsilon_o \epsilon_b + \gamma^2 \qquad \epsilon_b = \epsilon'_b - j\,\epsilon''_b$$

$$k_c^2 = \omega^2 \mu_o \epsilon_o \epsilon_c + \gamma^2 \qquad \epsilon_c = \epsilon'_c - j\,\epsilon''_c$$

$$k_m^2 = \frac{\omega^2 \mu_o \epsilon_o \epsilon_m + \gamma^2}{\rho} \qquad \epsilon_m = \epsilon'_m - j\,\epsilon''_m$$

$$\rho = \frac{\mu}{\mu^2 - \kappa^2} \qquad \mu = \mu' - j\,\mu''$$

$$\kappa = \kappa' - j\,\kappa''$$

$$\theta = j\frac{\mu}{\kappa} \qquad \gamma = \alpha + j\,\beta$$

μ', μ'', κ', κ'' are given by Equation 15 (Chapter II).

A variety of parameter combinations were examined. Typical theoretical and experimental results are compared in Figures 23 and 24. The agreement between predicted and measured results is good, and the conclusion is that the Landau-Lifshitz representation is satisfactory for quantitative prediction of magnetic losses far from resonance.

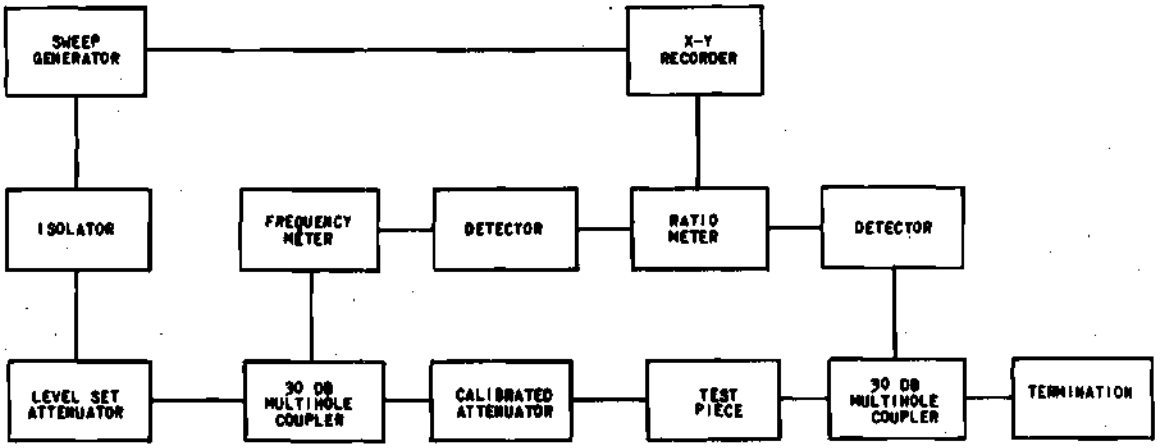

A. RATIO DETECTOR SETUP FOR MEASURING ATTENUATION AND VSWR

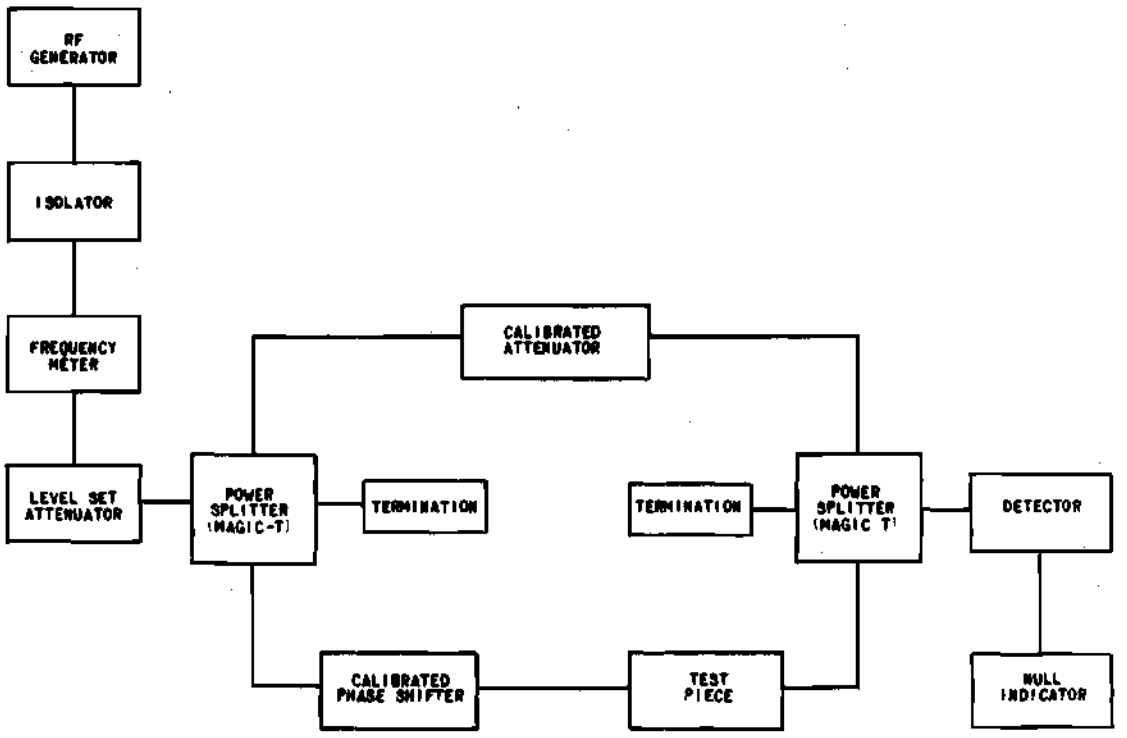

B. PHASE BRIDGE SETUP FOR MEASURING PHASE SHIFT

Figure 21. Laboratory Setups for Measurement of Attenuation and Phase Shift at Low Power Levels

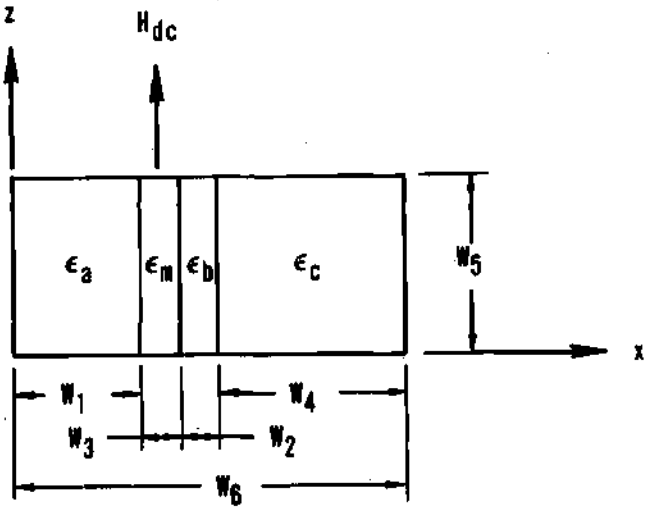

Figure 22. An Applied Field Type Phase Shifter

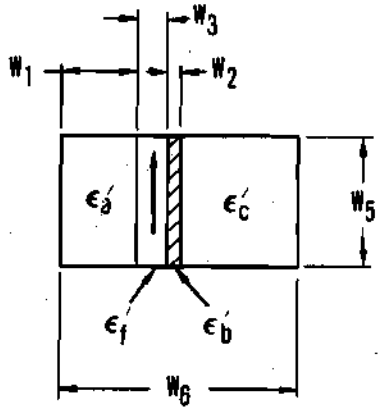

$m_s = \frac{\gamma 4\pi M_s}{\omega_c} = 0.48$

f_c = 9 Gc
ΔH = 48 Oe.
$W_1 = 0.139\ \lambda_c$
$W_2 = 0.0245\ \lambda_c$
$W_3 = 0.0405\ \lambda_c$
$W_5 = 0.305\ \lambda_c$
$W_6 = 0.383\ \lambda_c$
$\epsilon'_a = \epsilon'_c = 1.0$
$\epsilon'_b = 16.62$

$\epsilon'_f = 16.13$
$\tan \delta_a = \tan \delta_c = 0$
$\tan \delta_b = 0.0007$
$\tan \delta_f = 0.0003$
Length = 3 Inches

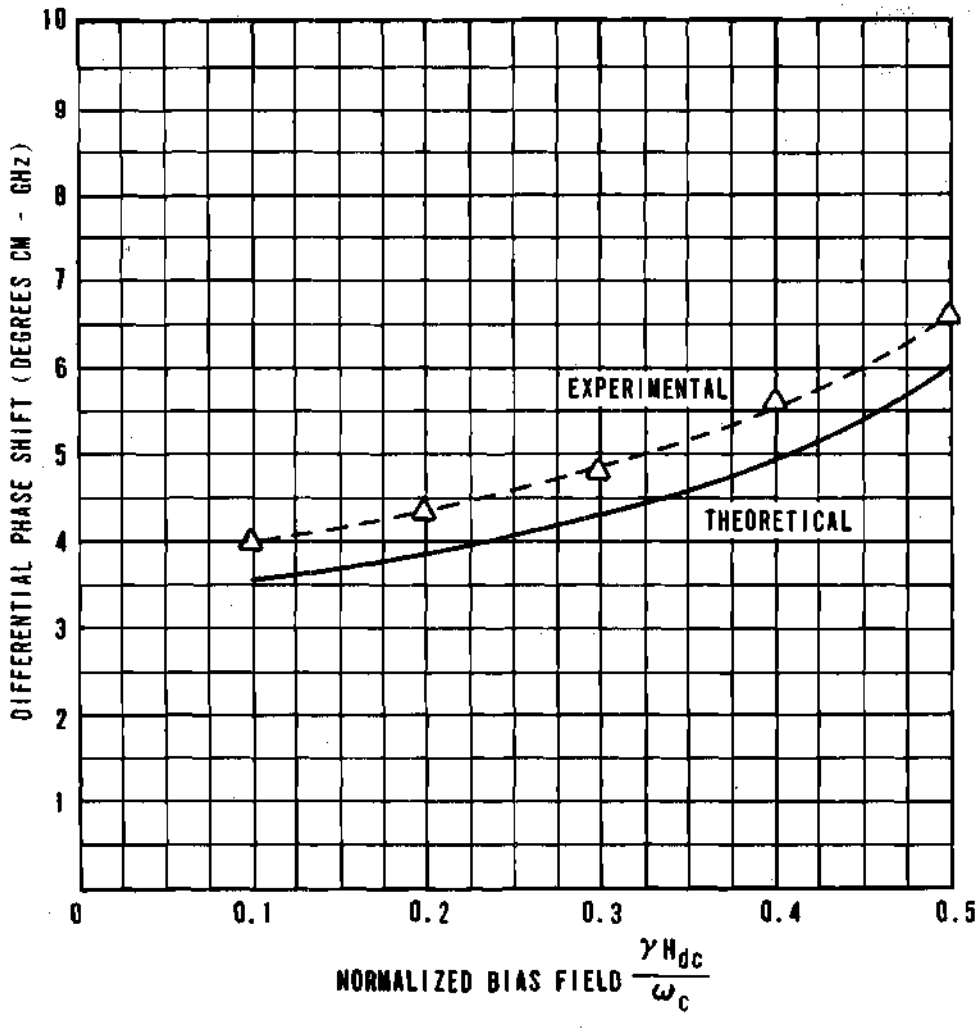

Figure 23. Differential Phase Shift vs Normalized Bias Field For An Analog Phase Shifter

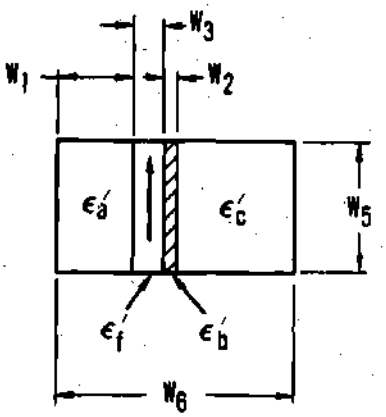

$m_s = \frac{\gamma 4\pi M_s}{\omega_c} = 0.48$

f_c = 9 Gc

ΔH = 48 Oe.

$W_1 = 0.139\ \lambda_c$

$W_2 = 0.0245\ \lambda_c$

$W_3 = 0.0405\ \lambda_c$

$W_5 = 0.305\ \lambda_c$

$W_6 = 0.383\ \lambda_c$

$\epsilon'_a = \epsilon'_c = 1.0$

$\epsilon'_b = 16.62$

$\epsilon'_f = 16.13$

$\tan \delta_a = \tan \delta_c = 0$

$\tan \delta_b = 0.0007$

$\tan \delta_f = 0.0003$

Length = 3 Inches

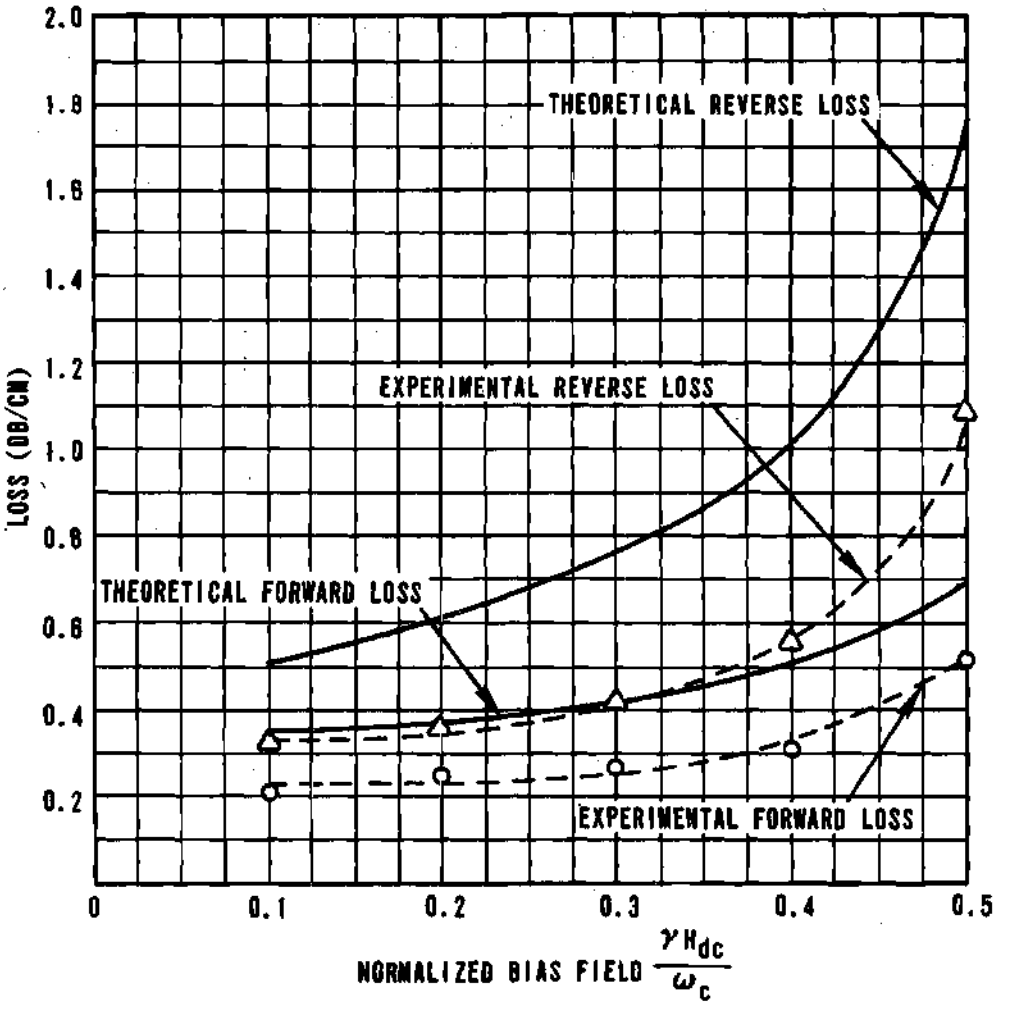

Figure 24. Insertion Loss vs Normalized Bias Field For An Analog Phase Shifter

Loss Representations in Unsaturated Ferrites

Two possible ways of representing magnetic losses in unsaturated ferrites (i.e., the "tensor" and the "bulk" representations) were presented in Chapter II. To test and compare the accuracy of these two magnetic loss representations for the prediction of losses in ferrite devices, the configuration of Figure 18 was analyzed for the case of the ferrite in a remanent magnetization state with magnetic losses included by both of the proposed methods. The predicted loss and phase characteristics were then compared with the measured performance characteristics of a laboratory model of the device. The propagation constant equation for the model analyzed is given in Equation 37 (Chapter III). The experimental phase shifter was of the latching type discussed in Chapter II and illustrated in Figure 11.

Because the latching phase shifter operates in the remanence state, no dc magnetic field is applied. The question then arises as to what value should be assigned to the effective internal field H_i. A possible starting point is to assume that H_i is also zero. This is the procedure followed by Ince and Stern and by Schloemann. However, this assumption, which in essence ignores the possibility of precessional resonance, is not in agreement with experimental results obtained by the research group of the Sperry Microwave Electronics Company. Their measurements on ferrite toroids in a remanent state show a pronounced resonance loss peak. This loss is believed to be the result of precessional resonance in the various magnetic domains of the toroid, which implies a non-zero effective field H_i. To establish a reasonable value for H_i requires some understanding of the domain structure of the material. For material geometries which lead to an appreciable remanence ratio (0.5 or greater), the domain structure of the ferrite will most likely consist of a few large domains and some smaller domains in "unmagnetized" parts of the material. Each domain may have different demagnetizing factors, and in each domain the magnetization will exhibit precessional resonance at a characteristic frequency determined by the anisotropy field of the material and the demagnetizing fields.

It is important to observe that, although the rf demagnetizing factors at the surfaces of the ferrite are accounted for by the applied boundary conditions, the rf demagnetizing factors of the various internal domains are not included by that procedure and must be accounted for in the average effective field H_i. Based on this domain model, the major portion of the resonance losses will be determined by the effective field of the largest domains whose magnetizations are oriented orthogonal to the rf magnetic field. The geometry of these major domains should be related to the overall sample dimensions.

Based on this thought, H_i can be estimated using Kittel's equation and the estimated demagnetizing factors of the major domain. Because the applied dc magnetic field is identically zero Kittel's equation can be written as

$$H_i = \left\{\left[\left(N_x + N_x^a - N_z\right) 4\pi M_s\right]\left[\left(N_y + N_y^a - N_z\right) 4\pi M_s\right]\right\}^{1/2}$$

where N_x^a, N_y^a are the effective demagnetizing factors arising from anisotropy effects and are given by:

$$N_x^a = \frac{K_1}{4\pi M_s^2}\left[2 - \sin^2\theta - 3\sin^2 2\theta\right]$$

$$N_y^a = \frac{2K_1}{4\pi M_s^2}\left[1 - 2\sin^2\theta - \frac{3}{8}\sin^2 2\theta\right]$$

Here θ is the angle the magnetization makes with a <100> direction of the crystallites as measured in a <110> plane. If the magnetization is assumed to lie along the easy direction of a negative anisotropy material, the resonance equation reduces to:

$$H_i = \left\{\left(\frac{4}{3}\frac{K_1}{M_s} + N_x 4\pi M_s\right)\left(\frac{4}{3}\frac{K_1}{M_s} + N_y 4\pi M_s\right)\right\}^{1/2}$$

where N_z has been set equal to zero in accordance with the toroidal geometry. The parameter K_1 is the first order magnetocrystalline anisotropy constant. For a typical garnet toroid with $\frac{K_1}{M_s} \approx 60$ oe., $4\pi M_s = 1200$ gauss, and a length to width ratio of 10 to 1 for the toroid legs, the estimated effective field for the major domain is

$$H_i = \sqrt{(80 + 120)(80 + 1080)}$$

$$H_i \approx 480 \text{ oe.}$$

In Figures 25 and 26, the theoretical differential phase shift and loss per 360° of differential phase shift for a latching phase shifter are shown for several values of the normalized effective internal field as functions of the width of the waveguide. In addition, the experimentally observed loss and differential phase shift for the same structure are given. It is encouraging to note that as the effective field approaches the value predicted by the simple arguments given above, both the predicted loss and differential phase shift for the structure approach the observed values more closely. The theoretical predictions and the experimental results are in fact in excellent agreement. Figures 27 and 28 illustrate the effect on loss and differential phase shift of variations in H_i over a small range of values when all other parameters are fixed. Additional curves comparing theoretical with experimental results are given in Appendix D.

Figure 29 presents a comparison of the experimental losses for a latching phase shifter with theoretical losses computed by - (a) a "small loss" technique (see Appendix B) with magnetic losses represented by a bulk loss tangent, (b) solving the exact boundary value problem with magnetic losses represented by a bulk loss tangent, and (c) solving the exact boundary value problem with magnetic losses represented by the "lossy" tensor permeability. These results imply

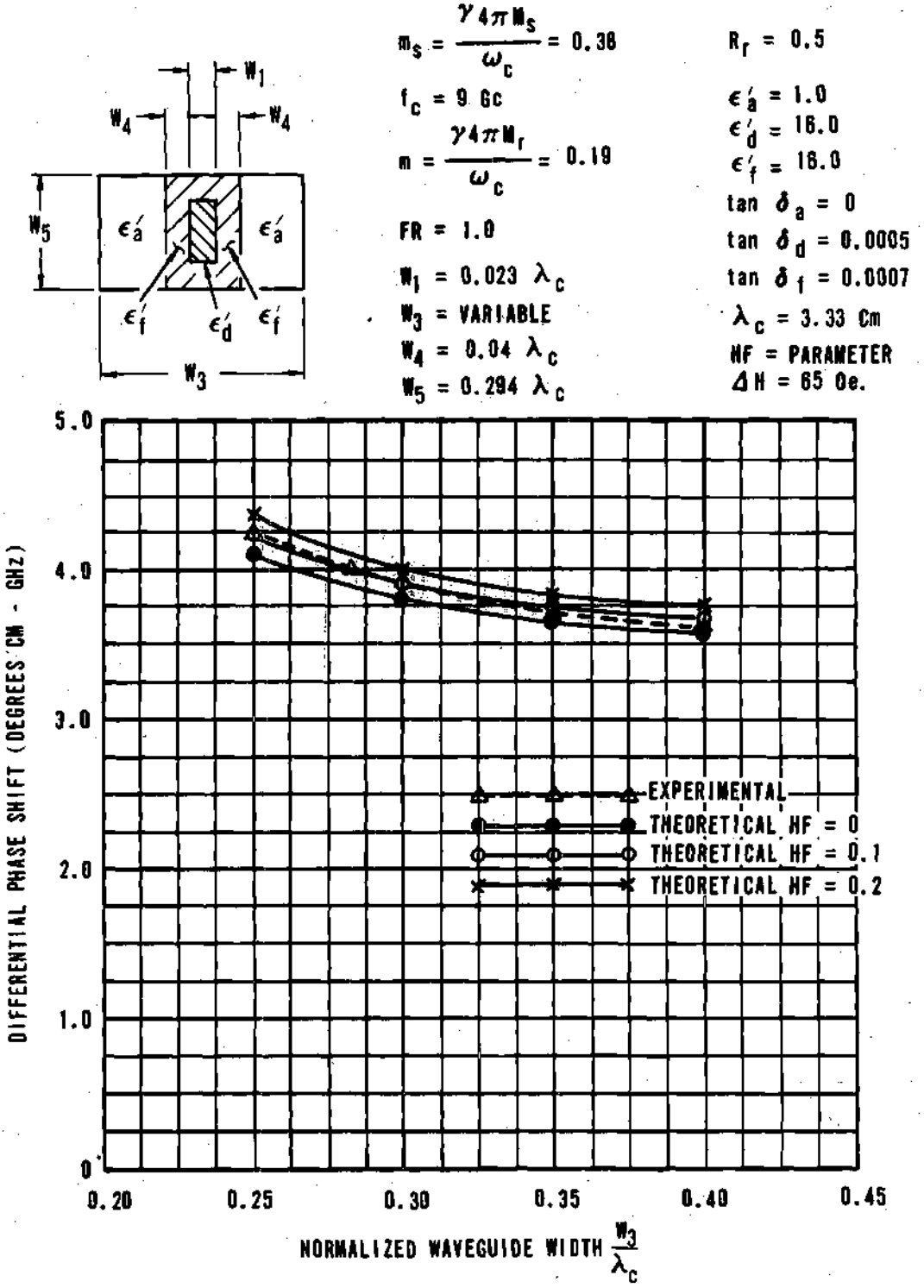

Figure 25. Differential Phase Shift vs Normalized Waveguide Width For A Latching Phase Shifter With Effective Internal Field As A Parameter

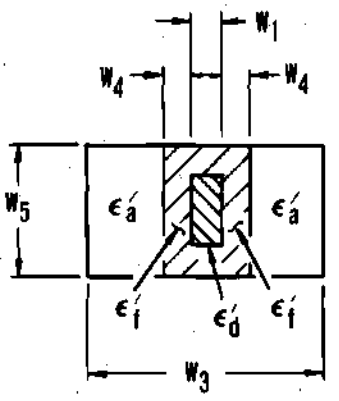

$m_s = \frac{\gamma 4\pi M_s}{\omega_c} = 0.38$

$f_c = 9$ Gc

$m = \frac{\gamma 4\pi M_f}{\omega_c} = 0.19$

FR = 1.0

$W_1 = 0.023\ \lambda_c$

W_3 = VARIABLE

$W_4 = 0.04\ \lambda_c$

$W_5 = 0.294\ \lambda_c$

$R_f = 0.5$

$\epsilon'_a = 1.0$

$\epsilon'_d = 16.0$

$\epsilon'_f = 16.0$

$\tan \delta_a = 0$

$\tan \delta_d = 0.0005$

$\tan \delta_f = 0.0007$

$\lambda_c = 3.33$ Cm

HF = PARAMETER

$\Delta H = 65$ Oe.

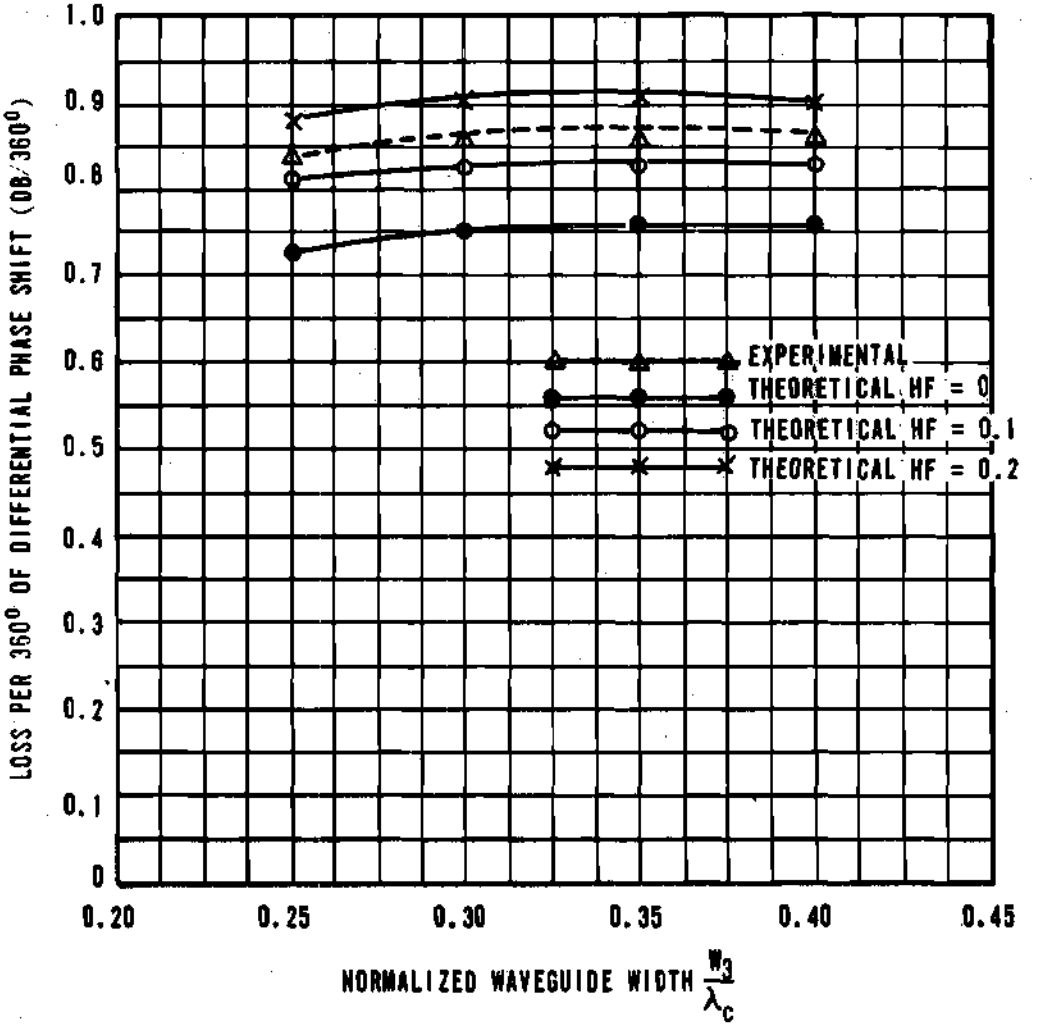

Figure 26. Loss Per 360° Of Differential Phase Shift vs Normalized Waveguide Width For A Latching Phase Shifter With Effective Internal Field As A Parameter

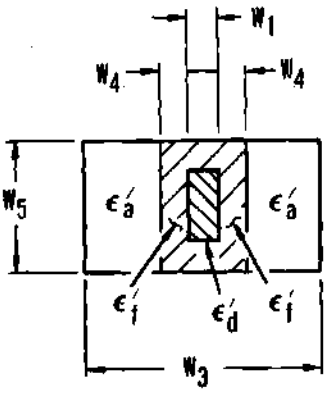

$m_s = \frac{\gamma 4\pi M_s}{\omega_c} = 0.38$

$f_c = 9$ Gc

$m = \frac{\gamma 4\pi M_r}{\omega_c} = 0.19$

FR = 1.0

$W_1 = 0.023\ \lambda_c$

$W_3 = 0.3\ \lambda_c$

$W_4 = 0.04\ \lambda_c$

$W_5 = 0.294\ \lambda_c$

$R_r = 0.5$

$\epsilon'_a = 1.0$

$\epsilon'_d = 16.0$

$\epsilon'_f = 16.0$

$\tan \delta_a = 0$

$\tan \delta_d = 0.0005$

$\tan \delta_f = 0.0007$

$\lambda_c = 3.33$ Cm

HF = VARIABLE

$\Delta H = 65$ Oe.

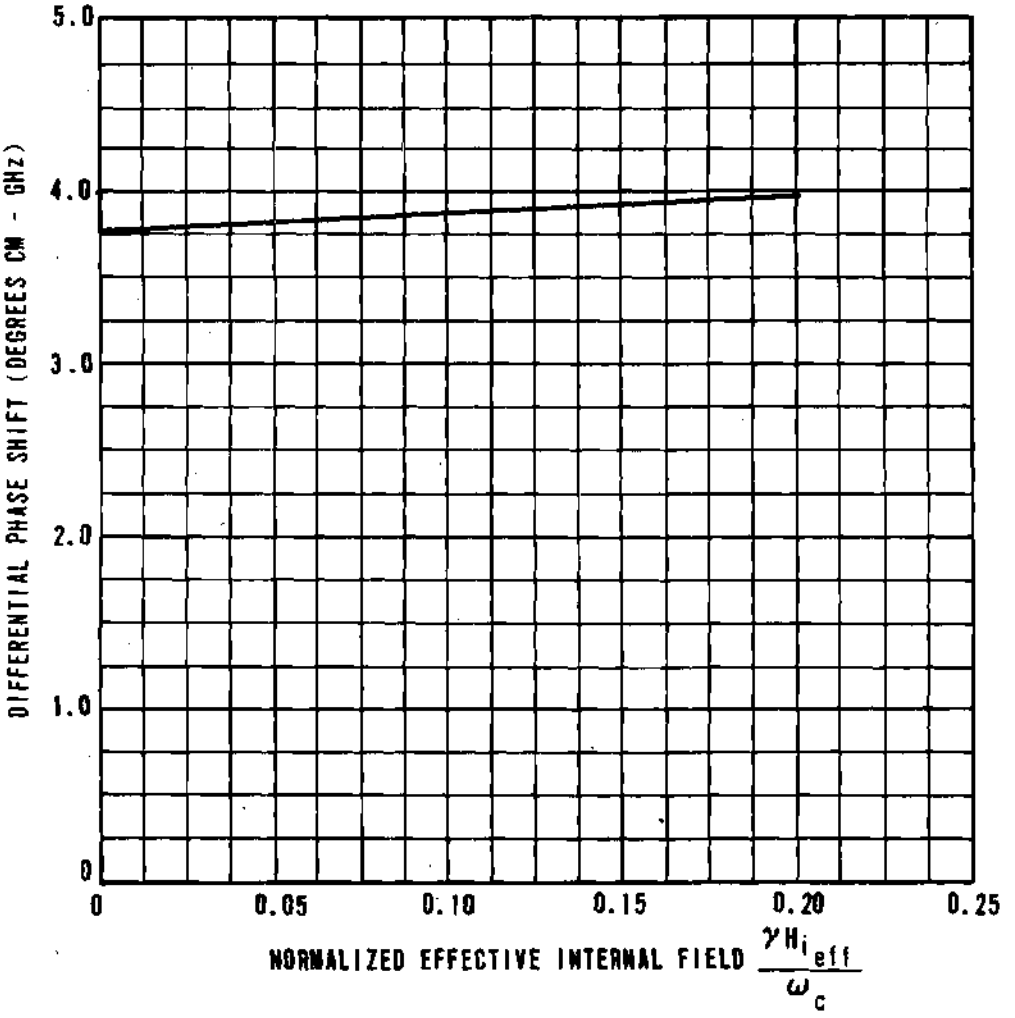

Figure 27. Differential Phase Shift vs Effective Internal Field For A Latching Phase Shifter

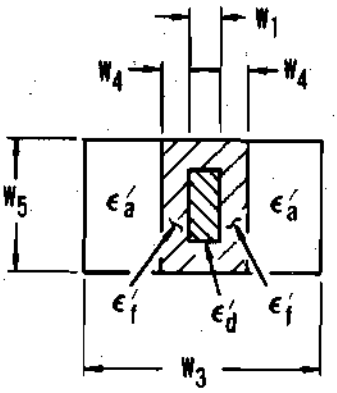

$m_s = \frac{\gamma 4\pi M_s}{\omega_c} = 0.38$

$f_c = 9$ Gc

$m = \frac{\gamma 4\pi M_r}{\omega_c} = 0.19$

FR = 1.0

$W_1 = 0.023\ \lambda_c$

$W_3 = 0.3\ \lambda_c$

$W_4 = 0.04\ \lambda_c$

$W_5 = 0.294\ \lambda_c$

$R_r = 0.5$

$\epsilon'_a = 1.0$

$\epsilon'_d = 16.0$

$\epsilon'_f = 16.0$

$\tan \delta_a = 0$

$\tan \delta_d = 0.0005$

$\tan \delta_f = 0.0007$

$\lambda_c = 3.33$ Cm

HF = VARIABLE

$\Delta H = 65$ Oe.

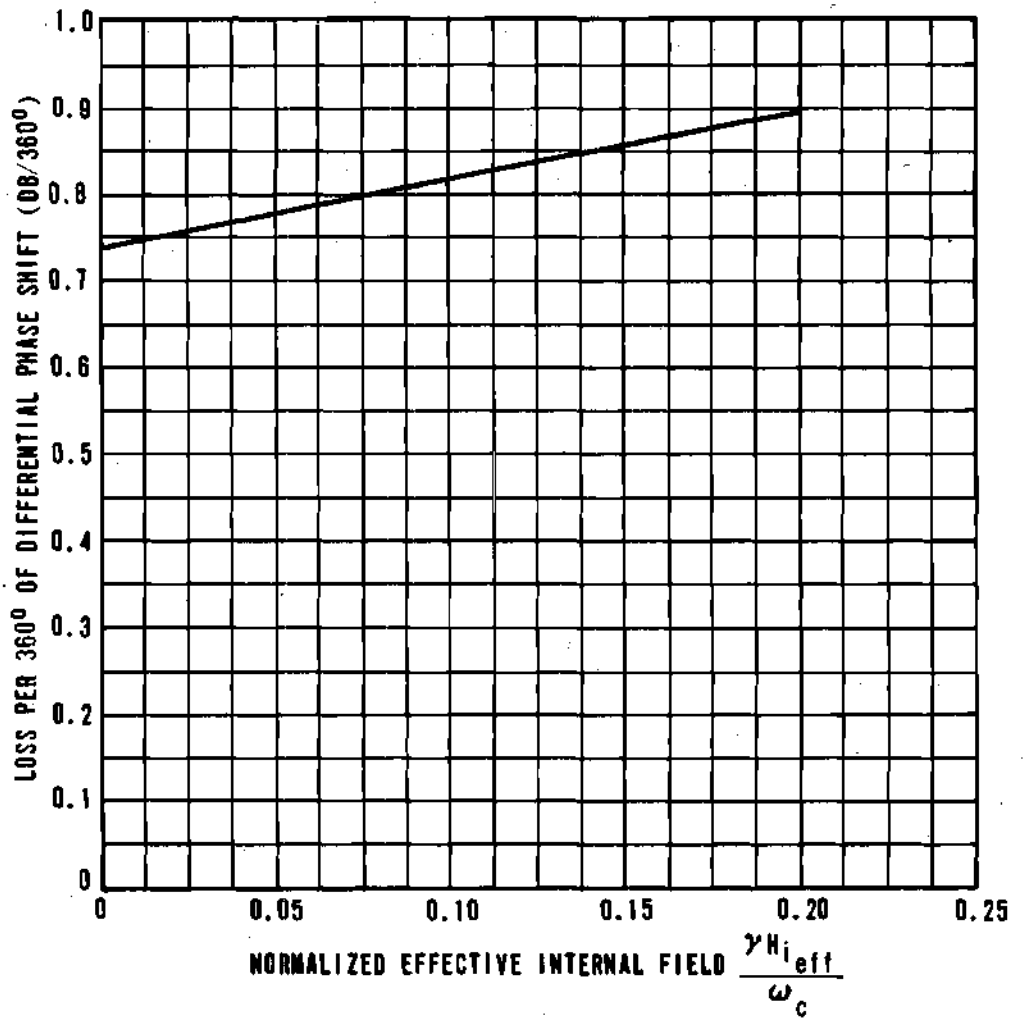

Figure 28. Loss Per 360° Of Differential Phase Shift vs Effective Internal Field For A Latching Phase Shifter

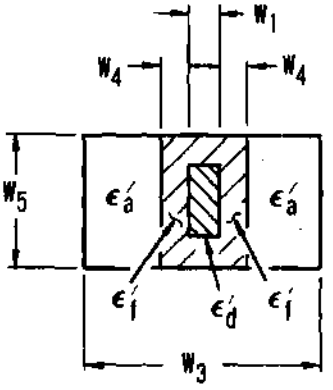

$m_s = \frac{\gamma 4\pi M_s}{\omega_c} = 0.38$

$f_c = 9$ Gc

$m = \frac{\gamma 4\pi M_r}{\omega_c} = 0.19$

FR = 1.0

$W_1 = 0.023\ \lambda_c$

W_3 = VARIABLE

$W_4 = 0.04\ \lambda_c$

$W_5 = 0.294\ \lambda_c$

$R_r = 0.5$

$\epsilon'_a = 1.0$

$\epsilon'_d = 16.0$

$\epsilon'_f = 16.0$

$\tan \delta_a = 0$

$\tan \delta_d = 0.0005$

$\tan \delta_f = 0.0007$

$\lambda_c = 3.33$ Cm

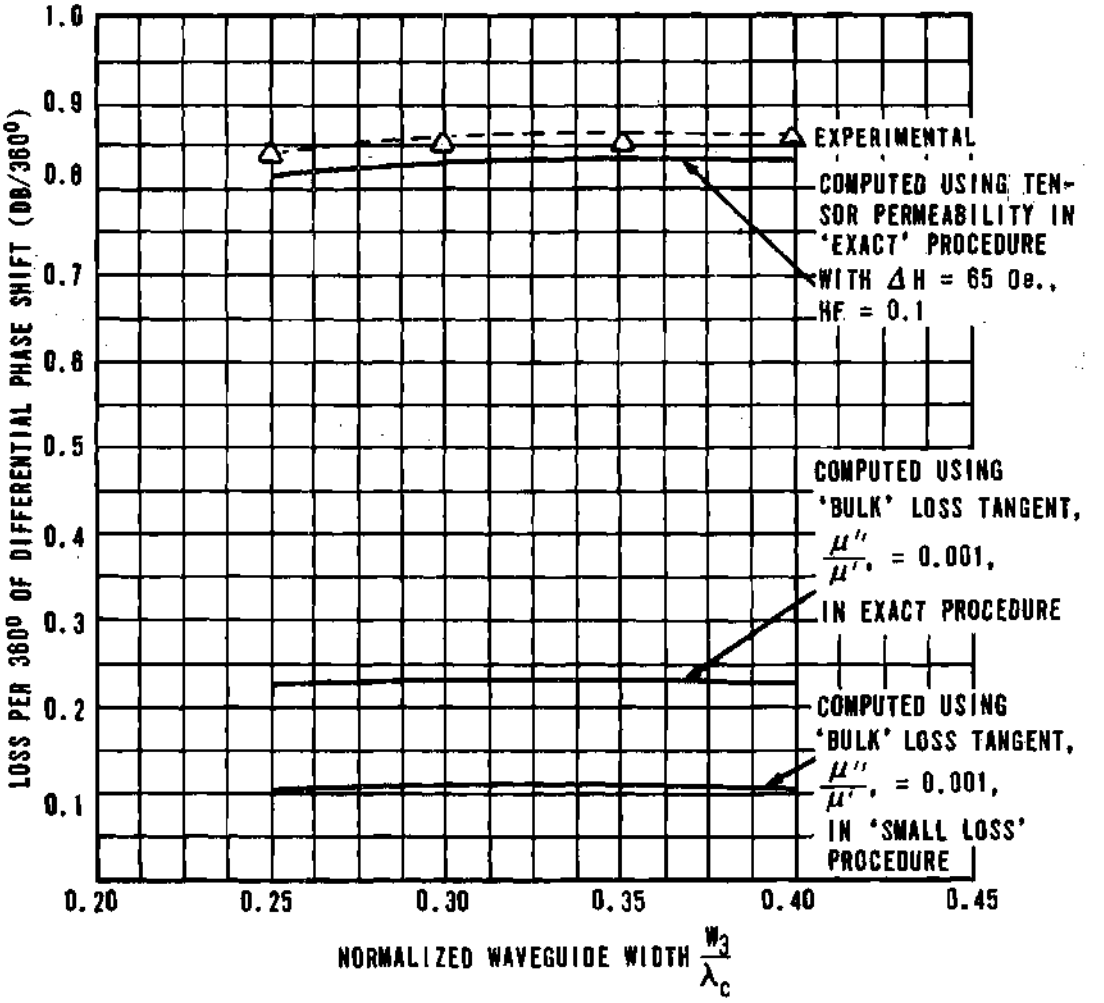

Figure 29. Loss Per 360° Of Differential Phase Shift vs Normalized Waveguide Width For A Latching Phase Shifter With Method Of Computation As A Parameter

that neither the bulk magnetic loss representation or the small loss computational technique are sufficiently accurate for quantitative prediction of losses in ferrite phase shifters.

A critical test for the tensor representation of magnetic losses in unsaturated ferrites arose when the theoretical analysis predicted an unexpected strong dependence of loss on resonance linewidth ΔH. To test the validity of this surprising prediction, a special series of experiments were carried out. The results, shown in Figure 30, conclusively verify the validity of the tensor representation of losses in unsaturated ferrites. The materials used were yttrium dysprosium aluminum iron garnet (8% Al, 10% Dy, ΔH = 379 oe.), yttrium dysprosium aluminum iron garnet (8% Al, 4% Dy, ΔH = 163 oe.), yttrium dysprosium aluminum iron garnet (8% Al, 2% Dy, ΔH = 100 oe.), yttrium gadolinium iron garnet (30% Gd, ΔH = 70 oe.), yttrium aluminum iron garnet (5% Al, ΔH = 30 oe.). The data points have been normalized to correspond to a remanence ratio of one half.

Resonance Linewidth

Resonance linewidth has been shown to be a very strong factor in determining the magnitude of magnetic losses in ferrite phase shifters. For this reason, the various damping mechanisms which contribute to the broadening of the resonance linewidth and their significance in the current problem are discussed briefly below*. The linewidth utilized in all the computations in this thesis is the experimentally determined polycrystalline linewidth. The linewidth observed on polycrystalline ferrimagnetic materials arises from several different sources. The various line broadening mechanisms can be categorized as intrinsic damping, corruption or porosity broadening, and anisotropy broadening. Obviously, all damping mechanisms are line broadening mechanisms since, in the absence of damping, the resonance line is infinitely narrow.

---

*This discussion is based on private correspondence with Dr. G. P. Rodrigue of the Sperry Microwave Electronics Company.

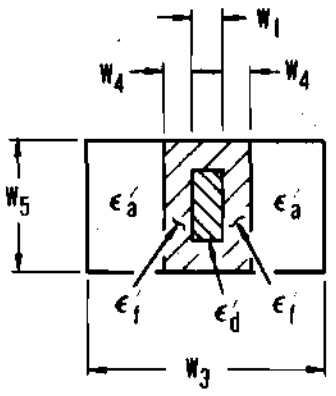

$m_s = \frac{\gamma 4\pi M_s}{\omega_c} = 0.38$

$f_c = 9$ Gc

$m = \frac{\gamma 4\pi M_r}{\omega_c} = 0.19$

FR = 1.0

$W_1 = 0.06\ \lambda_c$

$W_3 = 0.382\ \lambda_c$

$W_4 = 0.04\ \lambda_c$

$W_5 = 0.294\ \lambda_c$

$R_r = 0.5$

$\epsilon'_a = 1.0$

$\epsilon'_d = 16.0$

$\epsilon'_f = 16.0$

$\tan \delta_a = 0$

$\tan \delta_d = 0.0005$

$\tan \delta_f = 0.0007$

$\lambda_c = 3.33$ Cm

HF = 0.1

ΔH = VARIABLE

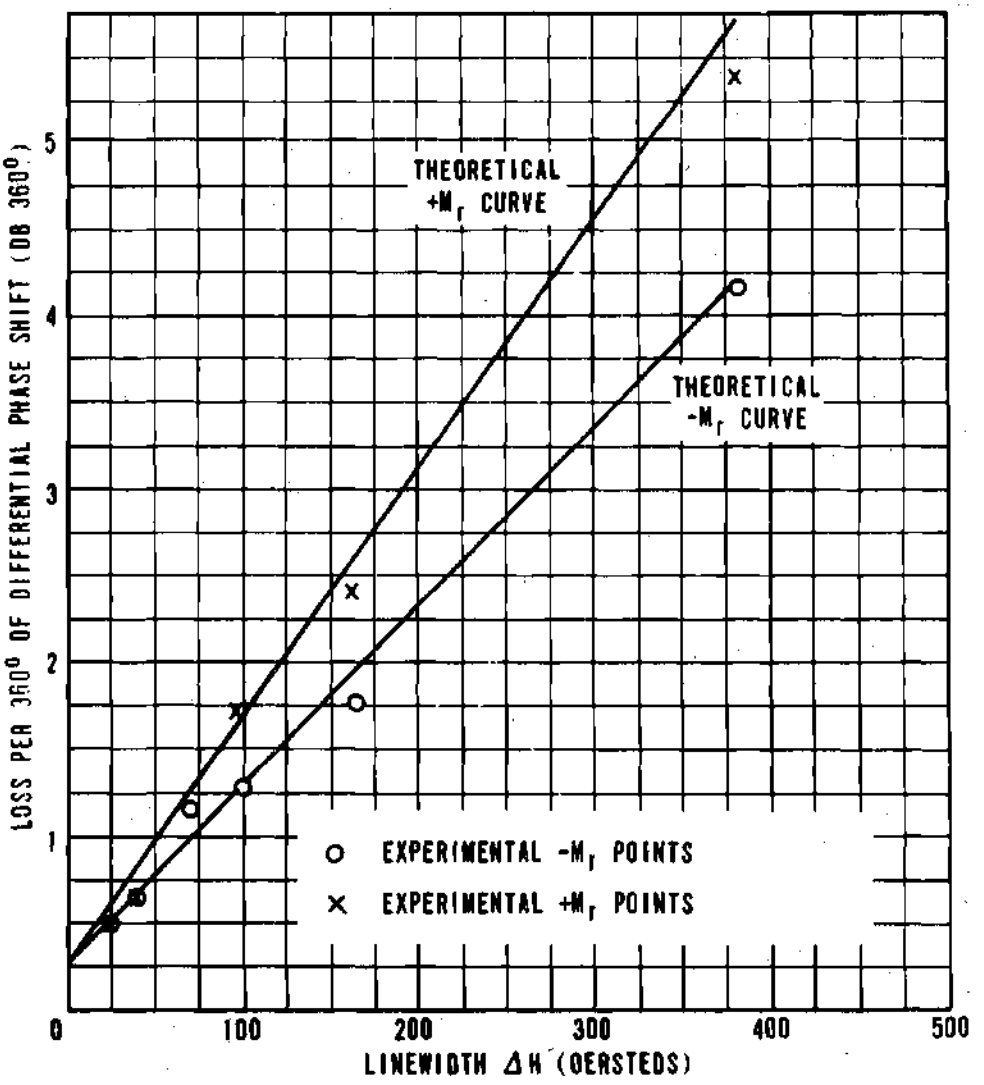

Figure 30. Loss Per 360° Of Differential Phase Shift vs Polycrystalline Linewidth For A Latching Phase Shifter

Intrinsic damping contributes the linewidth that is observed on pure single crystals, free from surface effects and so forth. This certainly represents a lower limit on polycrystalline linewidth, as all other effects will broaden this intrinsic resonance linewidth. The intrinsic linewidth of a polycrystalline sample is the same as the intrinsic linewidth of a single crystal sample of the same material and of equal purity. The equal purity should be kept in mind since lower purity oxides (99.9) are normally used in polycrystalline materials than are used in single crystal work (99.9999). Intrinsic linewidth is rather intimately related to the spin wave linewidth, ΔH_K. In fact, as a good approximation, one can take ΔH_K to be equal to the intrinsic ΔH at the same frequency. A frequency dependence of intrinsic linewidth has been observed on many single crystal samples and some polycrystals. The observed shape of the loss curve and the frequency dependence of linewidth for losses due to intrinsic damping are in excellent agreement with the predictions of the Landau-Lifshitz loss formulation.

Intrinsic linewidths vary widely. Prime examples are found in the garnet family. For example, pure yttrium iron garnet single crystals may have linewidths of a few tenths of an oersted, while the yttrium dysprosium iron garnets may have linewidths of several thousands of oersteds. In fact in the rare earth garnets, intrinsic linewidths are often so broad that the single and polycrystalline samples exhibit essentially the same linewidth --- all other contributing factors being almost negligible. This dominance of the intrinsic damping also manifests itself in the observed frequency dependence of the polycrystalline linewidth of rare earth and even of rare earth doped garnets. Thus, the linewidth of a heavily dysprosium doped yttrium iron garnet may show a marked frequency dependence. When intrinsic damping is dominant, X-band linewidths may actually be many times larger than L- or S-band linewidths.

Corruption or porosity broadening occurs in all polycrystalline samples to some extent. The more porous or less dense a polycrystalline sample is, the broader will be its resonance linewidth. Porosity broadening will contribute

a line broadening proportional to the percent porosity and to the saturation magnetization. Porosity broadening seems to be independent of frequency.

Anisotropy broadening has long been recognized as a source of linewidth in polycrystalline materials. Since each grain or crystallite may have its crystallographic axes aligned different from its neighbor, the effective anisotropy field varies from one grain to the next. Thus, each grain will resonate at slightly different field values, and this spread in effective field values gives rise to a spreading out of the resonance loss. This type of line broadening is independent of frequency and is the dominant mechanism in many common ferrites and garnets.

If porosity and anisotropy broadening are the dominant factors in determining the linewidth, there is some question as to whether the loss profile in the phase shift region (i.e., far from resonance) follows the Lorentzian curve predicted by the Landau-Lifshitz loss formulation or not. Some experimental results have been reported which seem to indicate that the loss profile in the region far from resonance does not follow the Lorentzian curve calculated using the measured polycrystalline linewidth, but that it may follow such a curve computed using the linewidth measured on a single grain taken from the polycrystalline sample. However, excellent agreement, as shown in Figure 30, was found between the losses in a latching phase shifter computed using the measured polycrystalline linewidth and the experimentally observed losses for the same configuration both for materials in which intrinsic damping dominated and for materials in which anisotropy and porosity damping dominated. This tends to indicate that the Lorentzian curve computed using the polycrystalline linewidth may be valid even in the region far from resonance.

In summary, polycrystalline linewidth of many ferrites and garnets is determined predominately by anisotropy broadening and is rather independent of frequency. In very porous samples, porosity broadening may be the dominant mechanism. It, too, is independent of frequency. In some rare earth doped garnets (or single crystals), intrinsic damping may be the dominant mechanism, and this linewidth will vary almost linearly with frequency.

Separation of Loss Contributions

One of the distinct advantages of an analytical approach to ferrite device design is that changes in device performance due to variations in material and dimensional parameters of the structure can be separated and the effects examined parameter by parameter. This permits evaluation of the relative importance of each parameter on the overall performance of the device. Figure 31 shows a separation of overall losses for a typical latching phase shifter into magnetic, dielectric, and waveguide loss contributions. Magnetic losses obviously dominate. The fact that magnetic losses vary linearly with linewidth has been demonstrated by the data shown in Figure 30. Thus, the losses of the phase shifter can be reduced by using a material with a smaller linewidth. Figures 32 and 33 show the variation of dielectric losses in a twin slab structure as a function of dielectric loss tangent for several values of dielectric constant and various spacings between slabs. In these and all other examples in this thesis except where otherwise specifically noted magnetic and dielectric losses are computed exactly. The relatively small waveguide losses are computed using the small loss technique discussed in Appendix B.

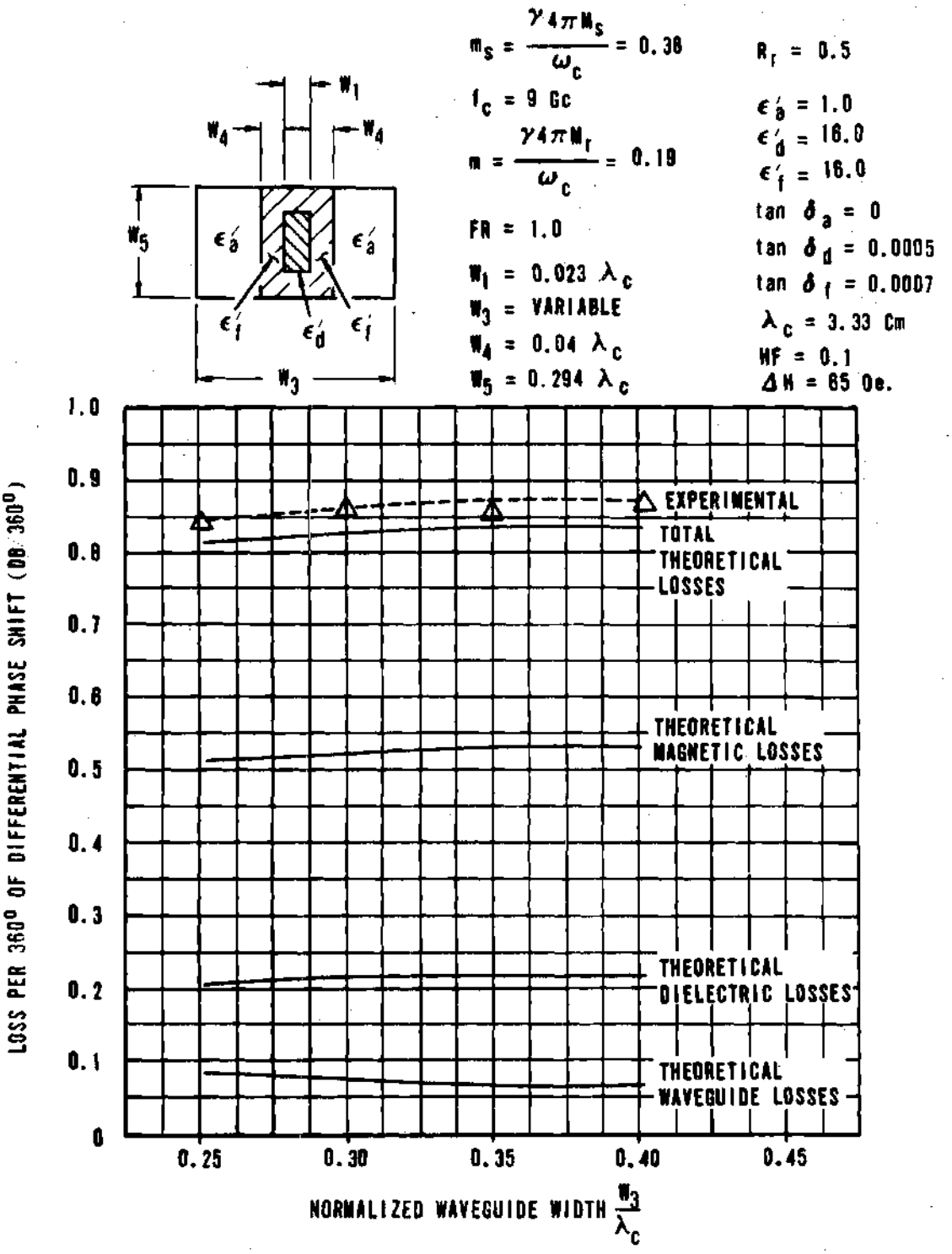

Figure 31. Separation of Losses In A Latching Phase Shifter

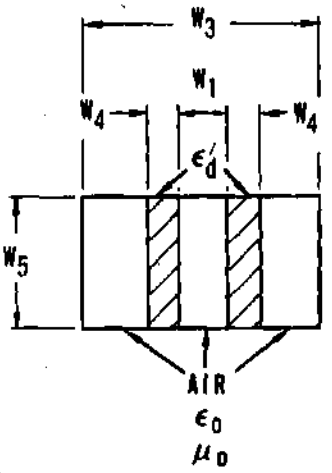

$W_1 = 0$
$W_3 = 0.7\ \lambda_c$
$W_4 = 0.04\ \lambda_c$
$W_5 = 0.294\ \lambda_c$
$f_c = 9$ Gc
ϵ'_d = PARAMETER

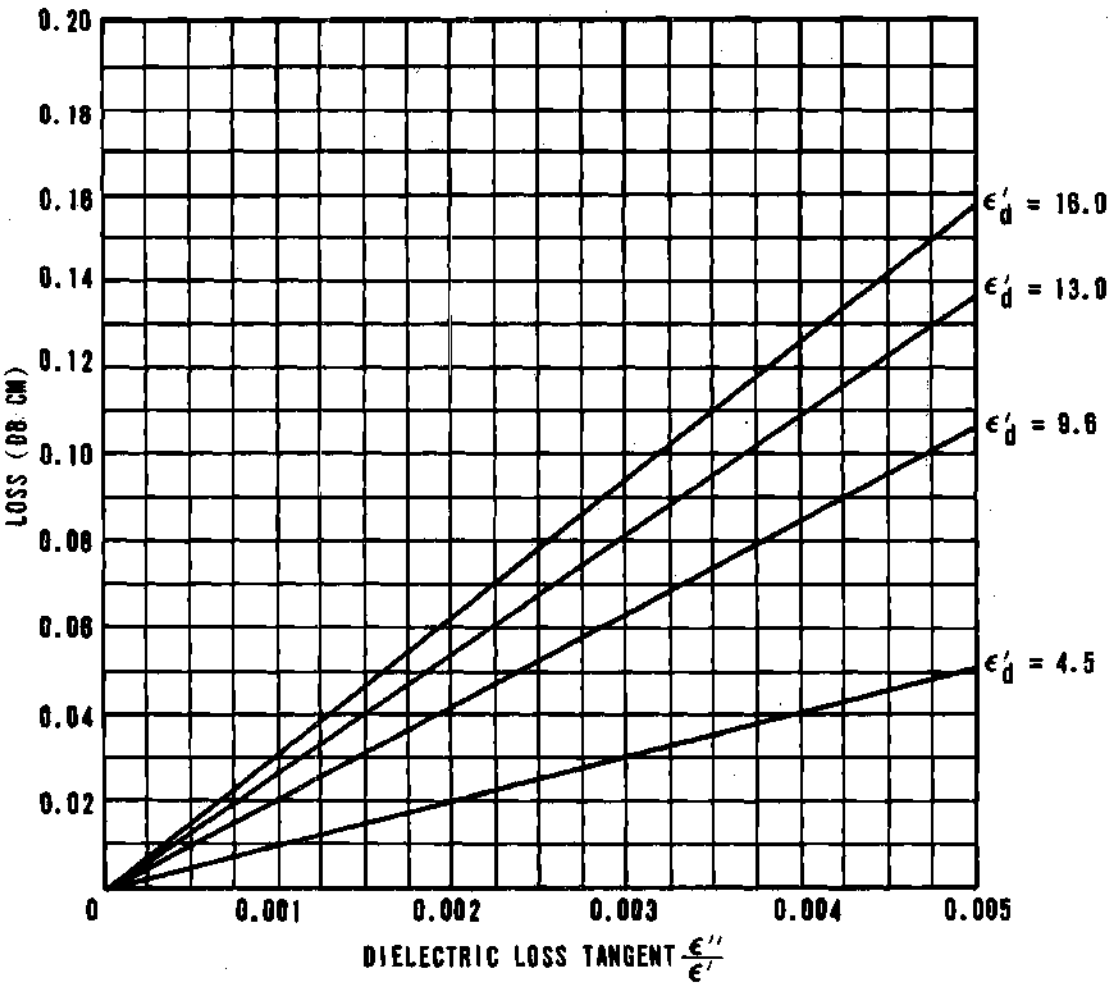

Figure 32. Insertion Loss vs Dielectric Loss Tangent For A Twin Dielectric Slab Structure With Dielectric Constant As A Parameter

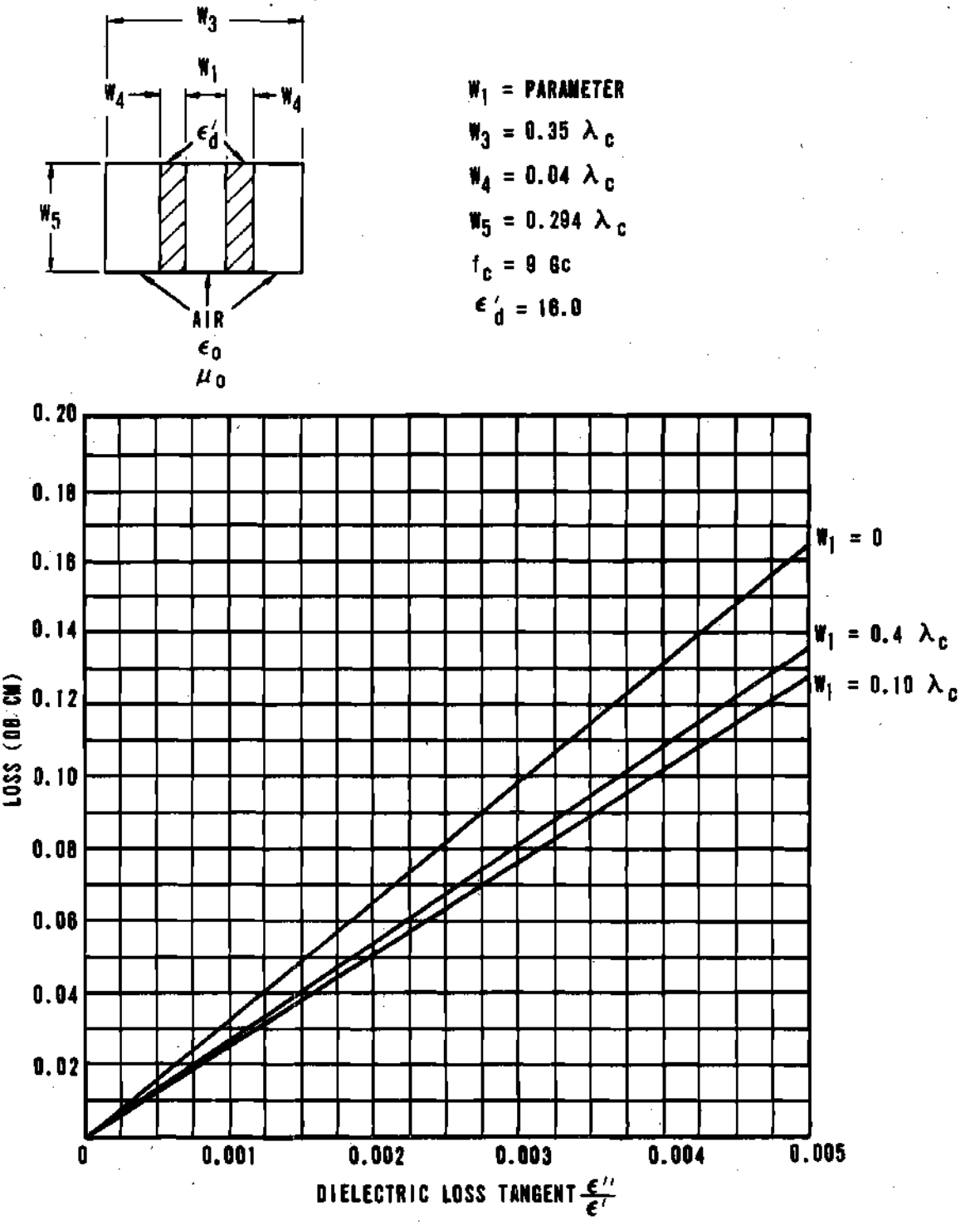

Figure 33. Insertion Loss vs Dielectric Loss Tangent For A Twin Dielectric Slab Structure With Distance of Separation As A Parameter

CHAPTER V

PHASE SHIFTER DESIGN DATA

Introduction

Ferrite devices have traditionally been designed primarily on the basis of "cut-and-try" experimental methods with general guide lines provided by qualitative theoretical results. The analytical procedures developed in this thesis, when used as design tools, permit the loss and phase characteristics of ferrite phase shifters to be predicted with great accuracy. Equally important to the device designer, the procedures enable the overall device loss and phase characteristics to be determined as functions of the dimensional and material parameters of the structure. Thus, the relative importance of the various parameters in determining device performance is easily evaluated. With the aid of a moderately high speed digital computer such as the Burrough's B-5500, loss and phase characteristics corresponding to more than one hundred sets of structural parameters can be computed per minute. It is, thus, possible to examine a very wide variety of parameter combinations. In the following section, a number of calculated design curves for ferrite phase shifters of both the latching and the applied field types are presented. These families of curves, normalized in the manner discussed in Chapter IV, are typical of the type of design data obtainable with the procedures developed.

Design Data

Latching Phase Shifters

The basic model analyzed is the dielectric loaded twin slab structure shown in Figure 18. The design curves which follow are directly applicable in the design of composite loop structures, such as the one shown in Figure 13a. For structures using a single internal toroid, like the one shown in Figure 34, the dielectric constant of the dielectric slab in the model should be treated as

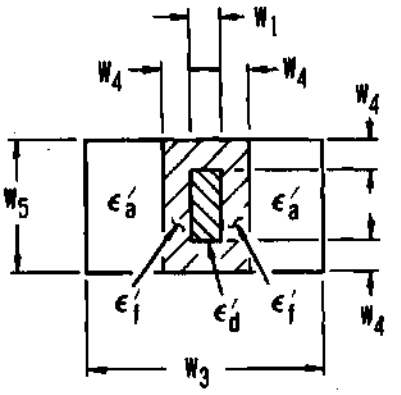

Figure 34. An Internal Toroid Latching Phase Shifter

an effective value. A simple procedure for computing the effective values of dielectric constant and dielectric loss tangent which leads to quite accurate results is to use volume ratios. That is

$$\epsilon'_{\text{effective}} = \epsilon'_f\left(\frac{2W_4}{W_5}\right) + \epsilon'_d\left(\frac{W_5 - 2W_4}{W_5}\right)$$

$$\tan\delta_{\text{effective}} = \tan\delta\left(\frac{2W_4}{W_5}\right) + \tan\delta\left(\frac{W_5 - 2W_4}{W_5}\right)$$

Differential Phase Shift. Differential phase shift is found to be an almost linear function of remanence magnetization as illustrated by Figures 35 and 36. In Figure 35 the remanence ratio is fixed and normalized saturation magnetization is the variable, while in Figure 36 the saturation magnetization has a fixed value and remanence ratio is the variable.

The variation of differential phase shift as a function of dielectric load thickness is illustrated in Figures 37 and 38. Dielectric constant of the load

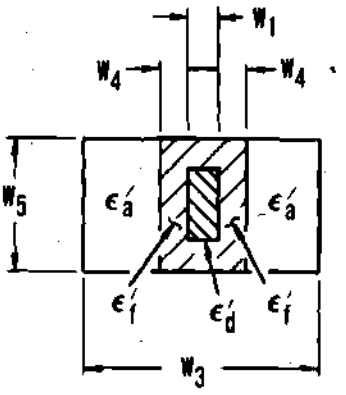

$m_s = \frac{\gamma 4\pi M_s}{\omega_c}$ = VARIABLE

f_c = 9 Gc

$m = \frac{\gamma 4\pi M_r}{\omega_c} = R_f M_s$

FR = 1.0

$W_1 = 0.04\ \lambda_c$
$W_3 = 0.781\ \lambda_c$
$W_4 = 0.05\ \lambda_c$
$W_5 = 0.294\ \lambda_c$

$R_f = 0.5$

$\epsilon'_a = 1.0$
$\epsilon'_d = 13.0$
$\epsilon'_f = 12.0$
$\tan \delta_a = 0$
$\tan \delta_d = 0.00005$
$\tan \delta_f = 0.0001$
$\lambda_c = 3.33$ Cm
MF = 0
$\Delta H = 65$ Oe.

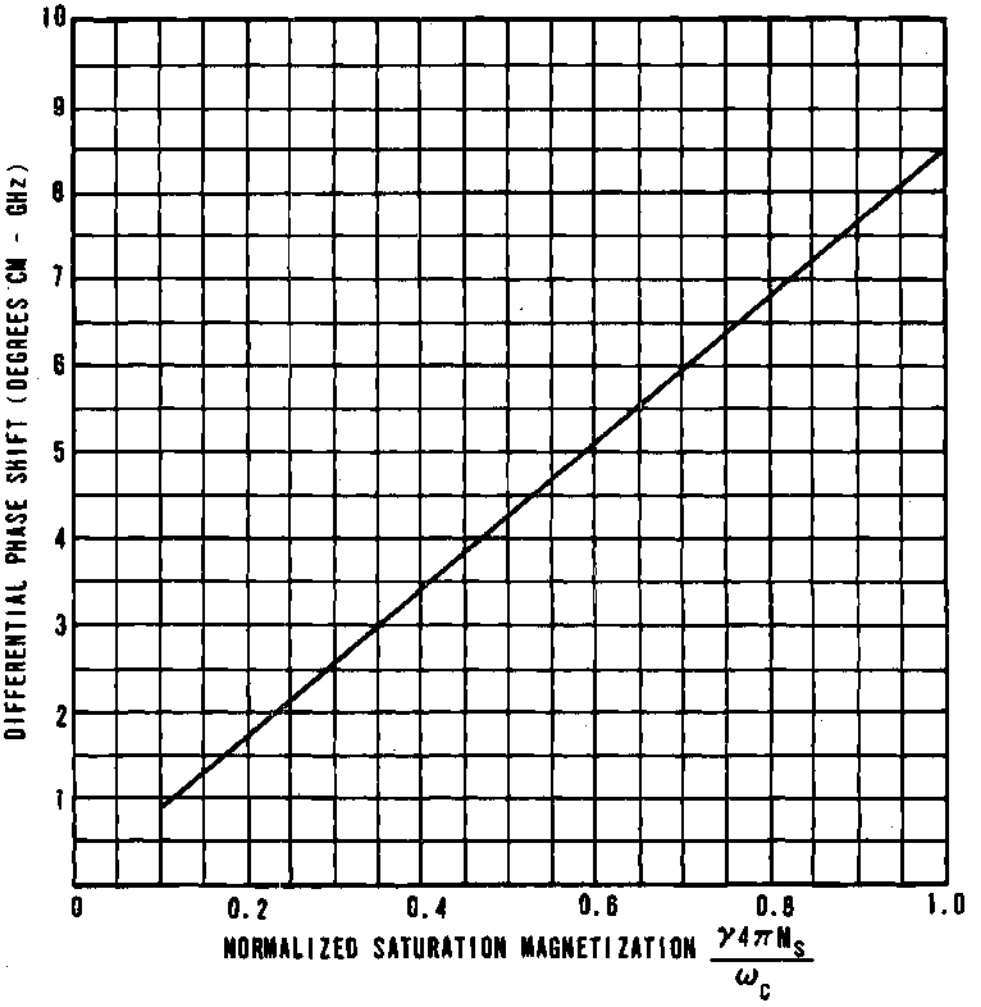

Figure 35. Differential Phase Shift vs Normalized Saturation Magnetization For Constant Remanence Ratio

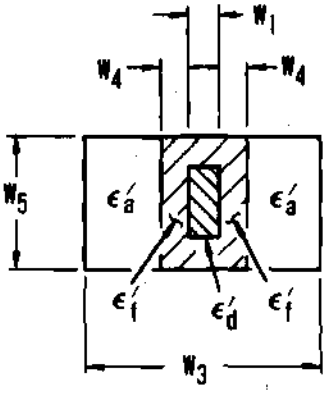

$m_s = \frac{\gamma 4\pi M_s}{\omega_c}$ = PARAMETER

f_c = 9 Gc

$m = \frac{\gamma 4\pi M_r}{\omega_c} = R_r M_s$

FR = 1.0

$W_1 = 0.08\ \lambda_c$

$W_3 = 0.382\ \lambda_c$

$W_4 = 0.04\ \lambda_c$

$W_5 = 0.294\ \lambda_c$

R_r = VARIABLE

$\epsilon'_a = 1.0$

$\epsilon'_d = 16.0$

$\epsilon'_f = 16.0$

$\tan \delta_a = 0$

$\tan \delta_d = 0.0005$

$\tan \delta_f = 0.0007$

$\lambda_c = 3.33$ Cm

HF = 0

ΔH = 70 Oe.

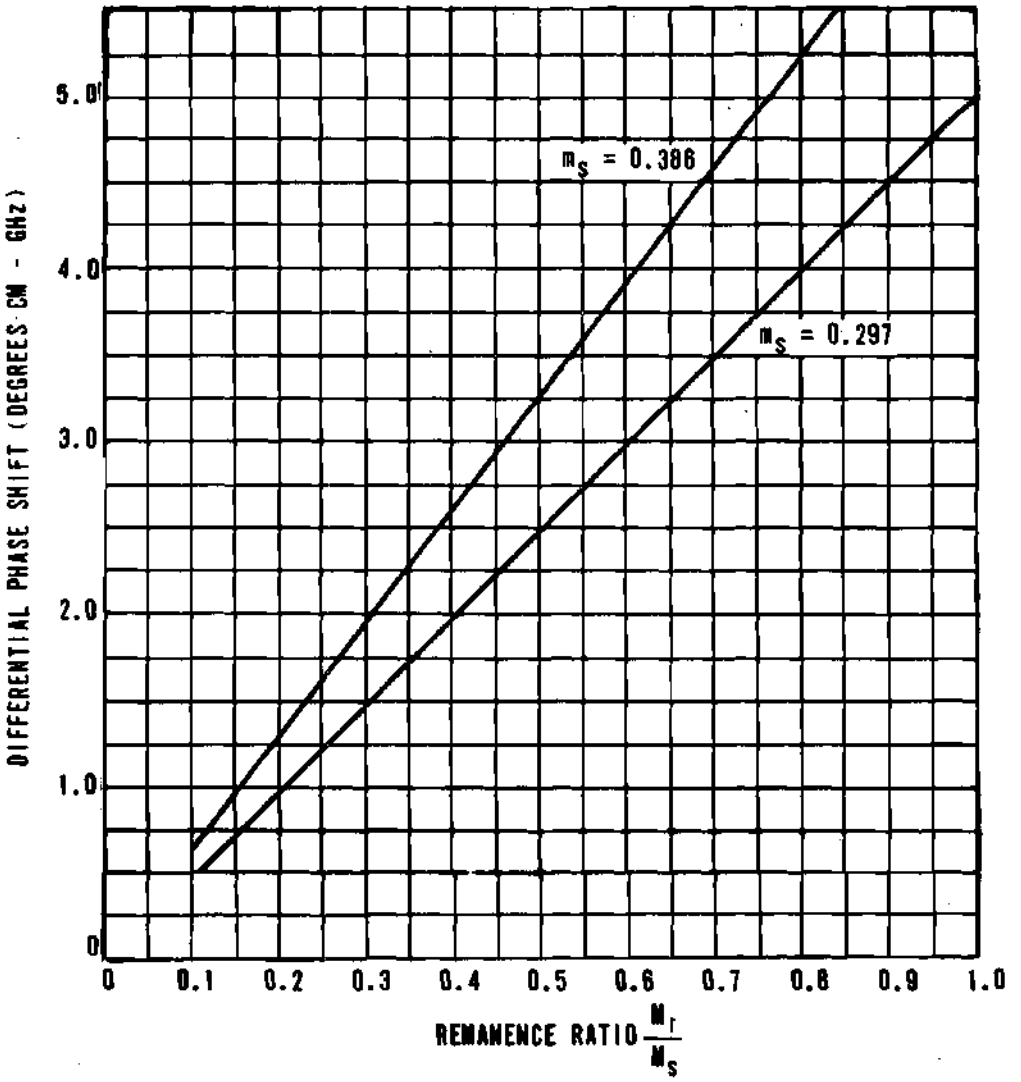

Figure 36. Differential Phase Shift vs Remanence Ratio For Two Values Of Saturation Magnetization

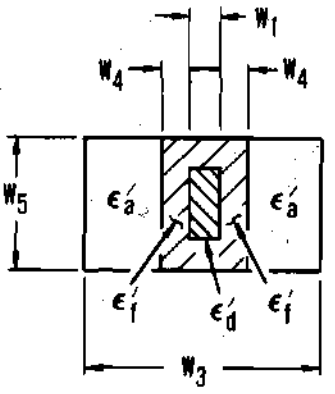

$m_s = \frac{\gamma 4\pi M_s}{\omega_c} = 1.6$

$f_c = 9$ Gc

$m = \frac{\gamma 4\pi M_f}{\omega_c} = 0.19$

FR = 1.0

W_1 = VARIABLE

$W_3 = 0.761\ \lambda_c$

$W_4 = 0.04\ \lambda_c$

$W_5 = 0.294\ \lambda_c$

$R_f = 0.5$

$\epsilon'_a = 1.0$

ϵ'_d = PARAMETER

$\epsilon'_f = 16.0$

$\tan \delta_a = 0$

$\tan \delta_d = 0.0005$

$\tan \delta_f = 0.0007$

$\lambda_c = 3.33$ Cm

HF = 0

$\Delta H = 65$ Oe.

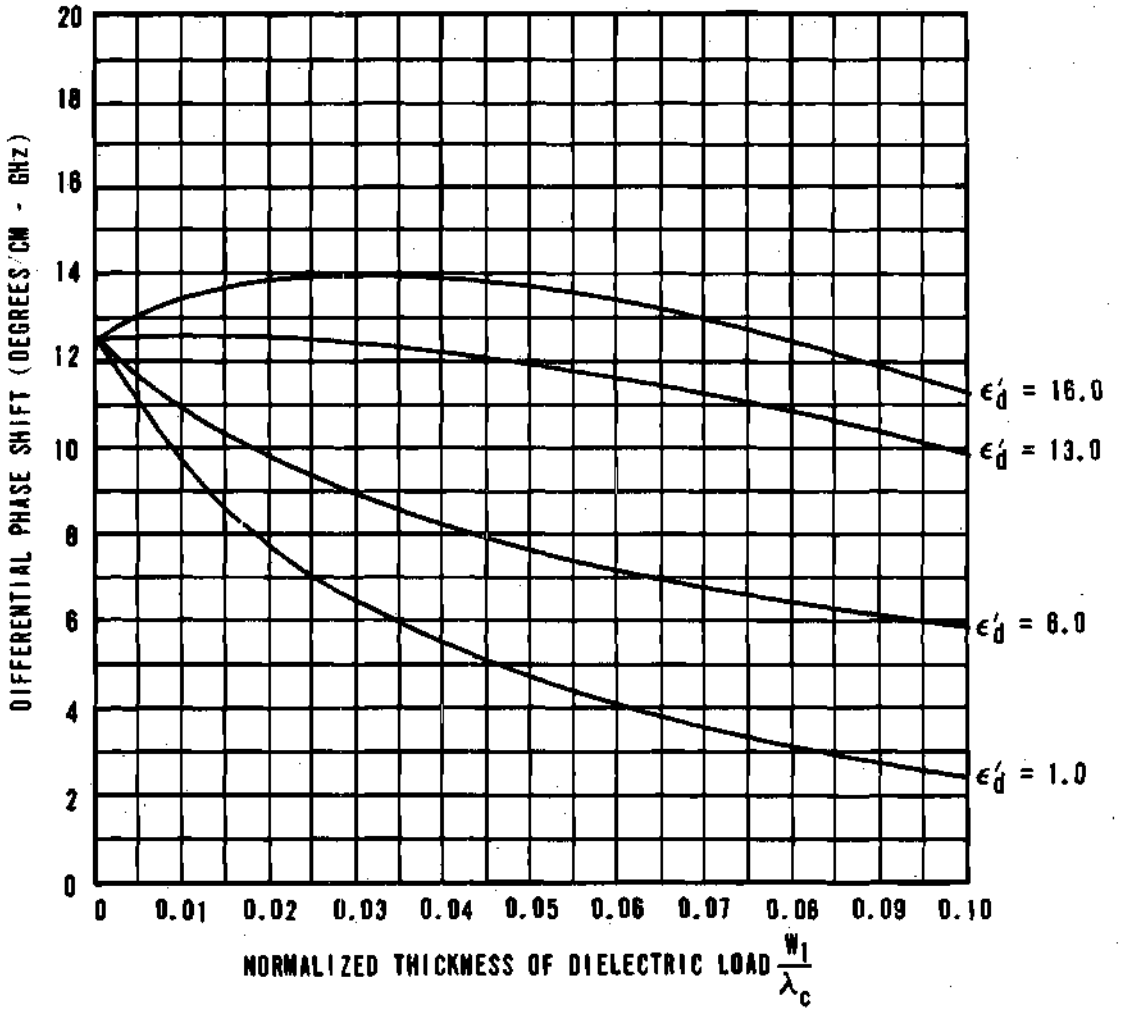

Figure 37. Differential Phase Shift vs Normalized Dielectric Load Thickness With Load Dielectric Constant As A Parameter

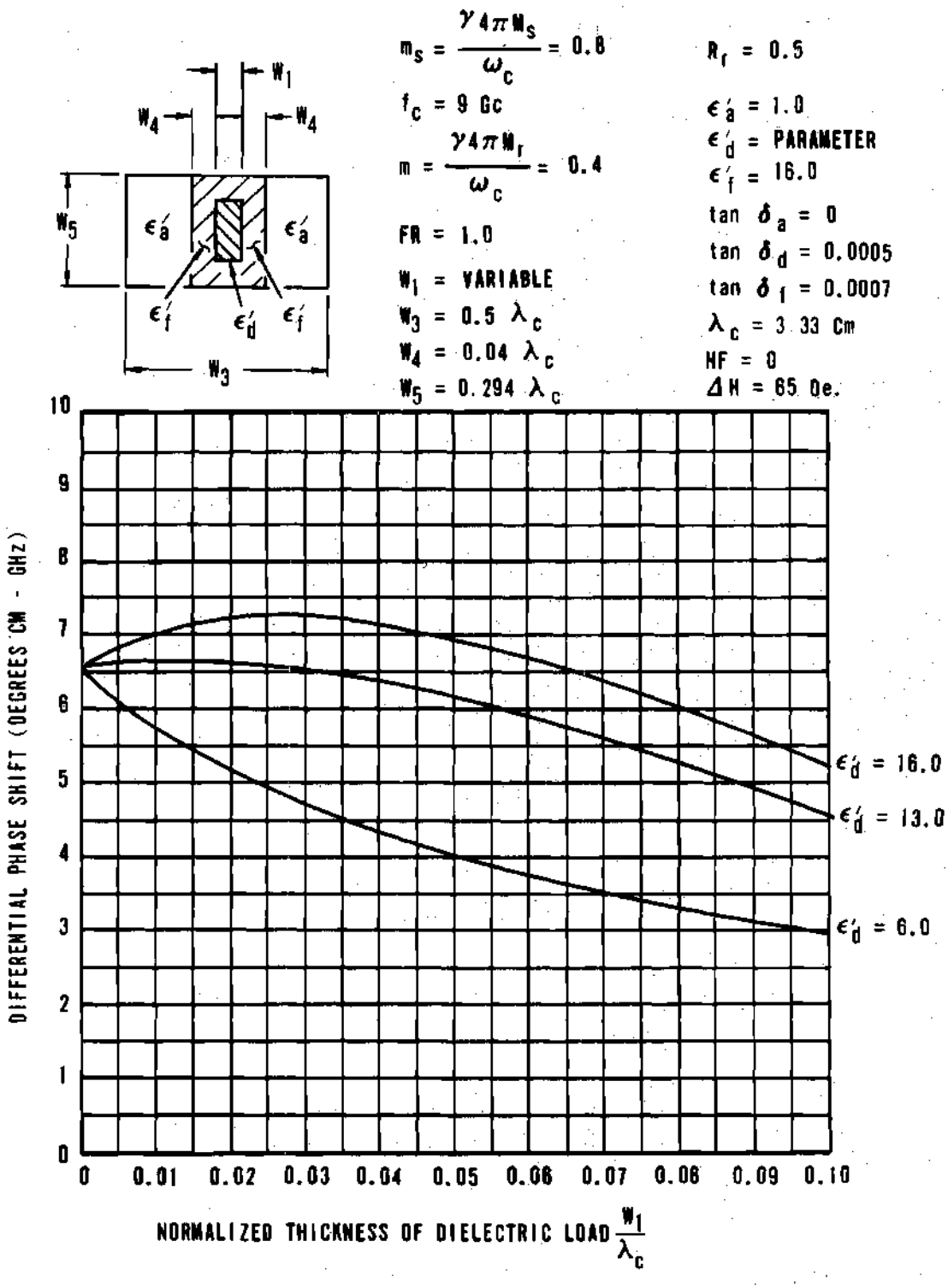

Figure 38. Differential Phase Shift vs Normalized Dielectric Load Thickness With Load Dielectric Constant As A Parameter

slab is a parameter in these two figures. Increasing the load dielectric constant causes a pronounced increase in the differential phase shift. Definite maxima are seen in the differential phase shift curves as a function of W_1 for loading slabs with sufficiently high dielectric constants.

Differential phase shift is found to be a nonlinear function of ferrite thickness as shown in Figures 39 and 40. These figures clearly illustrate the saturation of the differential phase shift at large values of ferrite thickness for several values of dielectric load thickness.

Frequency Sensitivity of Differential Phase Shift. The variation of differential phase shift can be controlled to some extent by proper selection of waveguide width and dielectric load thickness. Figures 41 and 42 show the frequency variation of differential phase shift for several values of waveguide width and of dielectric load thickness, respectively. It can be seen that in either case there are values of W_3 and W_1 that yield a differential phase shift which is essentially independent of frequency over a wide band of frequencies. The slope of the phase shift curve is quite important in many applications. Phase slope is defined as the change in differential phase shift over a 0.1 increment in normalized frequency centered at the operating frequency. Figure 43 is a plot of phase slope versus waveguide width with dielectric load thickness as a parameter. Note that combinations of W_1 and W_3 values may be selected which will result in zero phase slope.

Insertion Loss. A useful figure of merit for nonreciprocal phase shifters is the loss per 360° of differential phase shift (LP360). Figure 44 shows the variation of LP360 as a function of dielectric load thickness for the structure whose phase characteristics are shown in Figure 37. Note the broad minima in LP360 at about the value of W_1 for which the differential phase shift is maximum. Sharper minima are seen in the curves of LP360 versus ferrite thickness shown in Figure 45. The frequency variation of LP360 is illustrated in Figures 46 and 47 with waveguide width and dielectric load thickness as parameters, respectively.

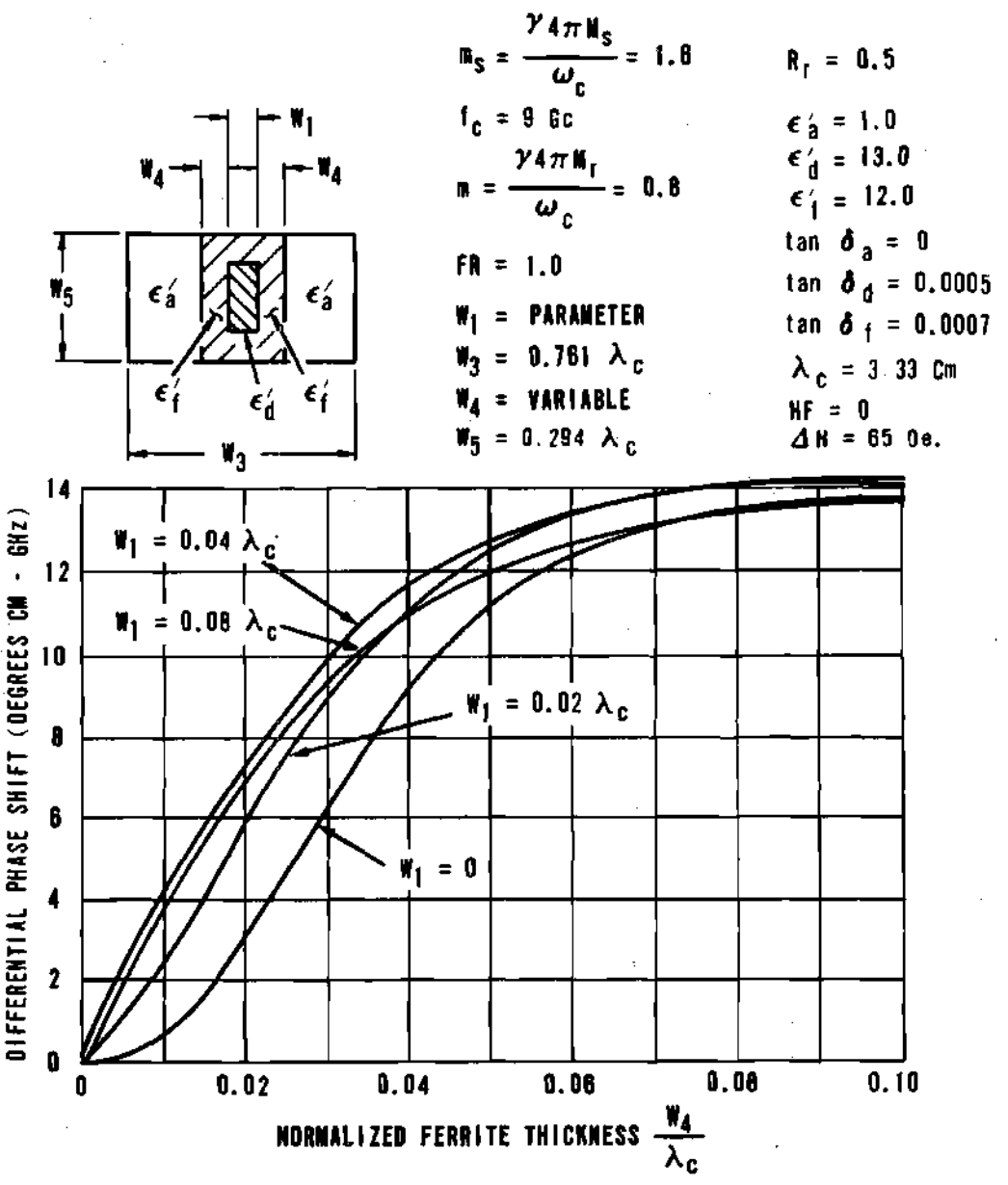

Figure 39. Differential Phase Shift vs Normalized Ferrite Thickness With Dielectric Load Thickness As A Parameter

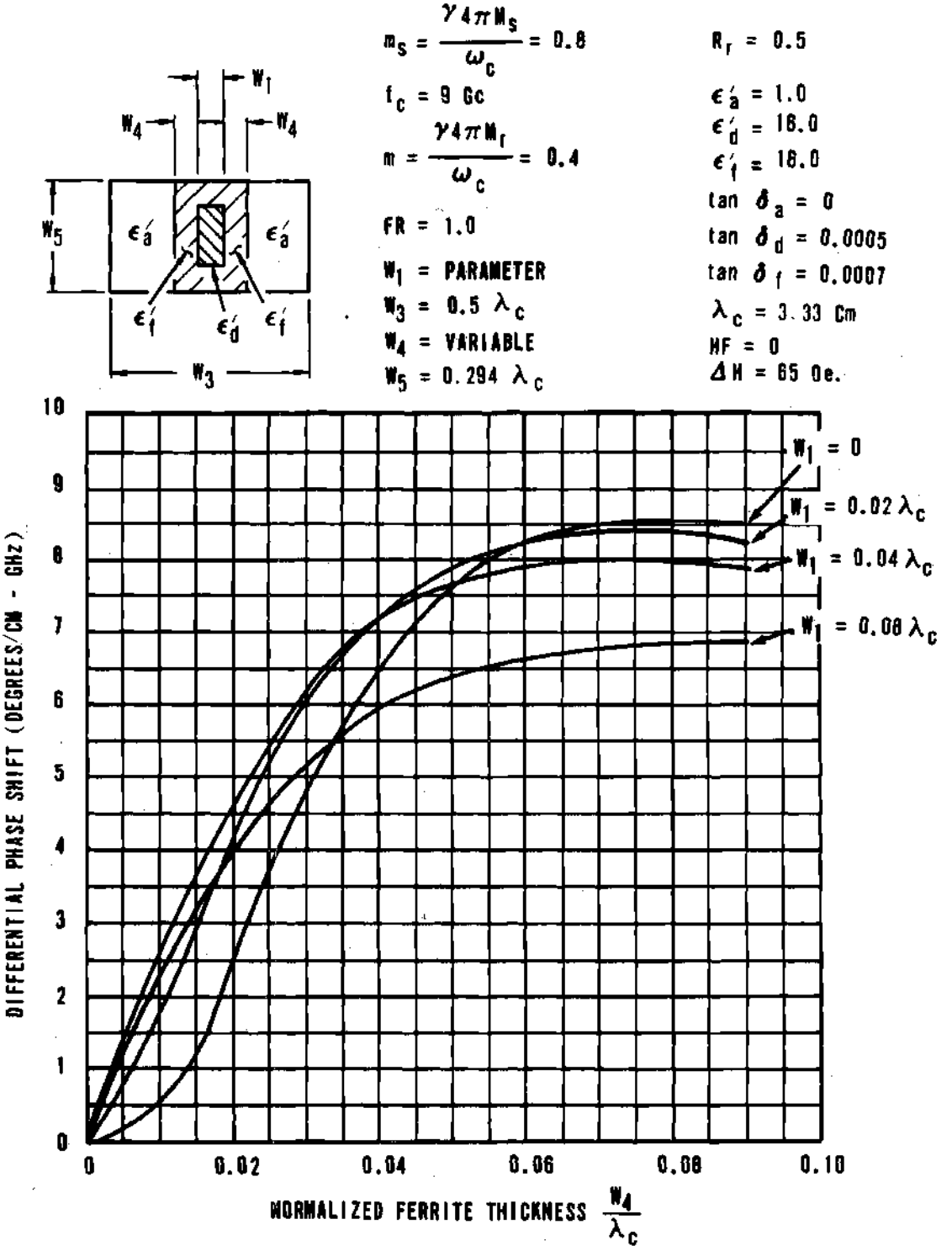

Figure 40. Differential Phase Shift vs Normalized Ferrite Thickness With Dielectric Load Thickness As A Parameter

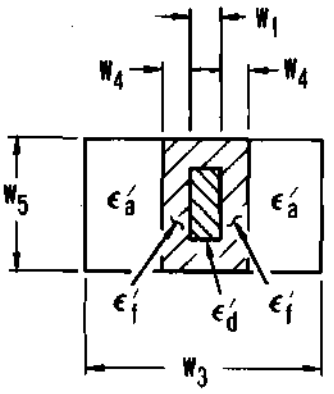

$m_s = \dfrac{\gamma 4\pi M_s}{\omega_c} = 0.38$

$f_c = 9$ Gc

$m = \dfrac{\gamma 4\pi M_r}{\omega_c} = 0.19$

FR = VARIABLE

$W_1 = 0.023\ \lambda_c$

W_3 = PARAMETER

$W_4 = 0.04\ \lambda_c$

$W_5 = 0.294\ \lambda_c$

$R_r = 0.5$

$\epsilon'_a = 1.0$

$\epsilon'_d = 16.0$

$\epsilon'_f = 16.0$

$\tan \delta_a = 0$

$\tan \delta_d = 0.0005$

$\tan \delta_f = 0.0007$

$\lambda_c = 3.33$ Cm

$HF = 0.137 = \gamma |\vec{H}_i| / \omega_c$

$\Delta H = 65$ Oe.

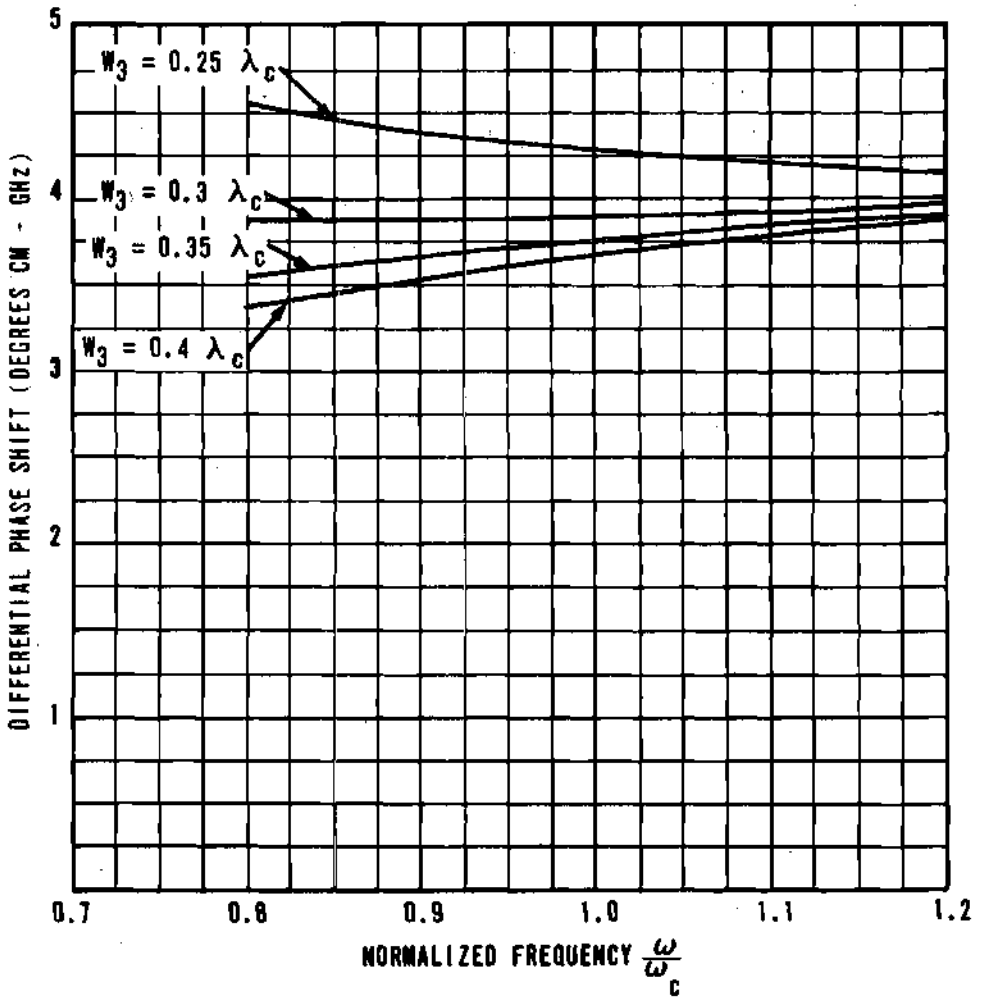

Figure 41. Differential Phase Shift vs Normalized Frequency With Waveguide Width As A Parameter

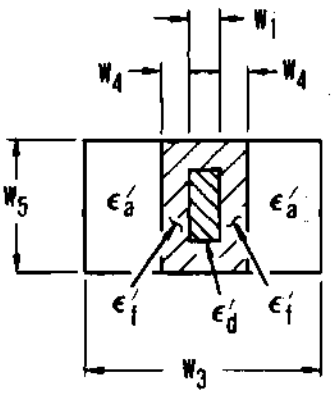

$m_s = \frac{\gamma 4\pi M_s}{\omega_c} = 0.38$

$f_c = 9$ Gc

$m = \frac{\gamma 4\pi M_r}{\omega_c} = 0.19$

FR = VARIABLE

W_1 = PARAMETER

$W_3 = 0.25\ \lambda_c$

$W_4 = 0.04\ \lambda_c$

$W_5 = 0.294\ \lambda_c$

$R_r = 0.5$

$\epsilon'_a = 1.0$

$\epsilon'_d = 16.0$

$\epsilon'_f = 16.0$

$\tan \delta_a = 0$

$\tan \delta_d = 0.0005$

$\tan \delta_f = 0.0007$

$\lambda_c = 3.33$ Cm

HF = 0

$\Delta H = 65$ Oe.

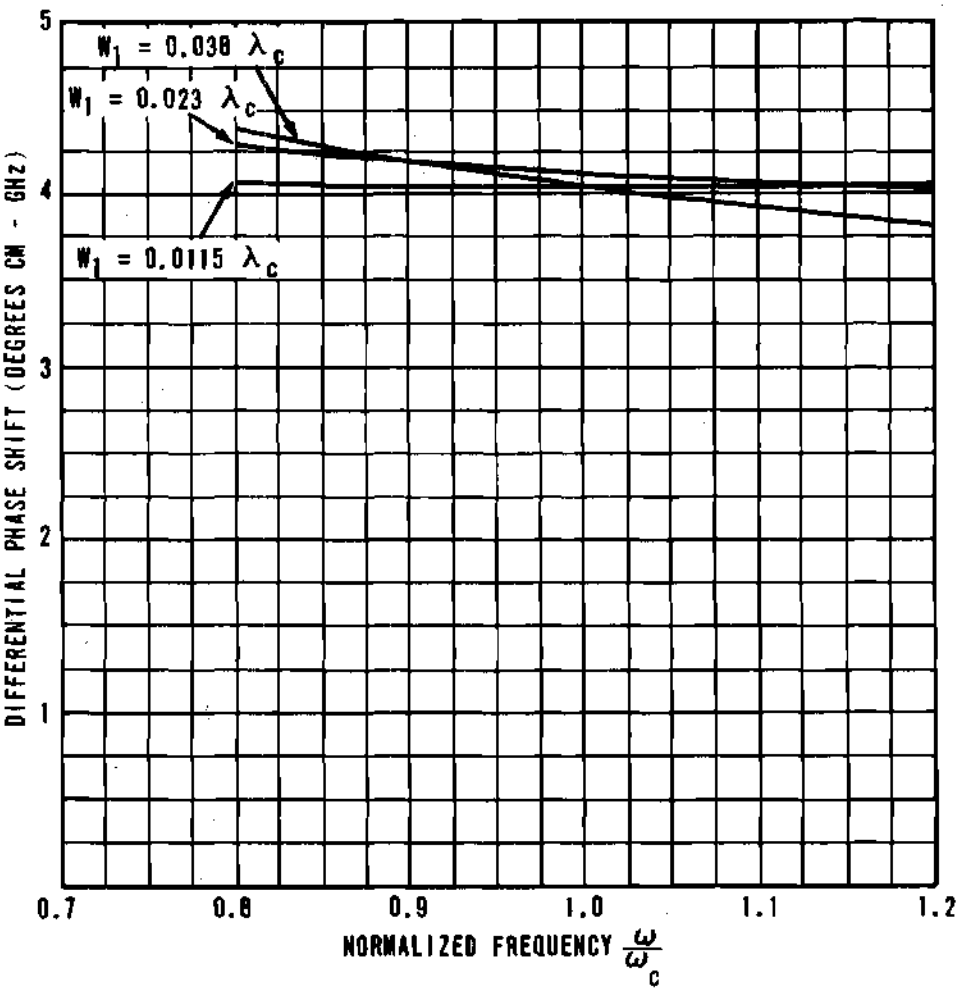

Figure 42. Differential Phase Shift vs Normalized Frequency With Dielectric Load Thickness As A Parameter

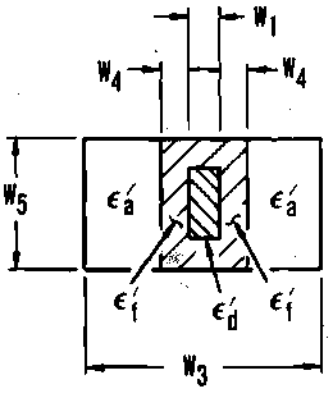

$m_s = \frac{\gamma 4\pi M_s}{\omega_c} = 0.38$

$f_c = 9$ Gc

$m = \frac{\gamma 4\pi M_r}{\omega_c} = 0.19$

W_1 = PARAMETER
W_3 = VARIABLE
$W_4 = 0.04\ \lambda_c$
$W_5 = 0.294\ \lambda_c$

$R_r = 0.5$

$\epsilon'_a = 1.0$
$\epsilon'_d = 16.0$
$\epsilon'_f = 16.0$
$\tan \delta_a = 0$
$\tan \delta_d = 0.0005$
$\tan \delta_f = 0.0007$
$\lambda_c = 3.33$ Cm
HF = 0
$\Delta H = 65$ Oe.

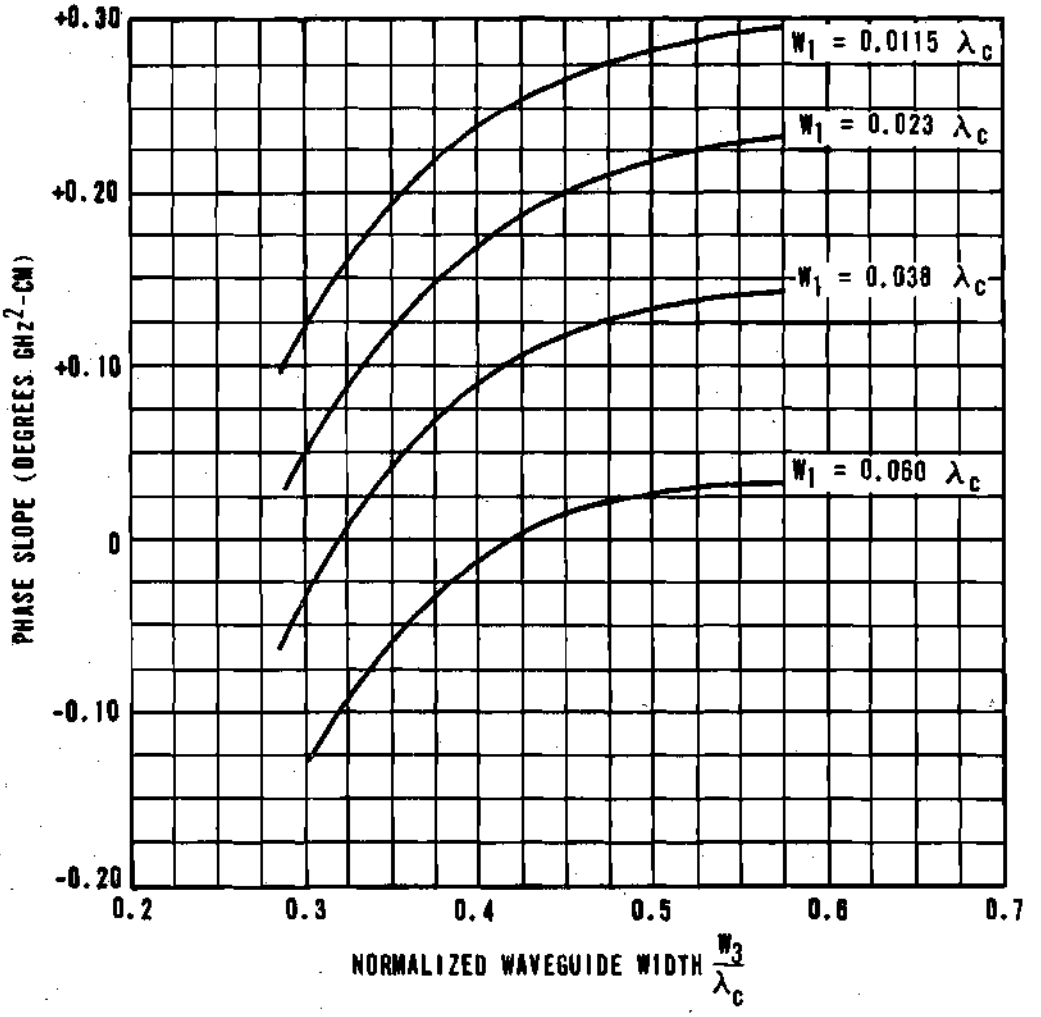

Figure 43. Phase Slope vs Normalized Waveguide Width With Dielectric Load Thickness As A Parameter

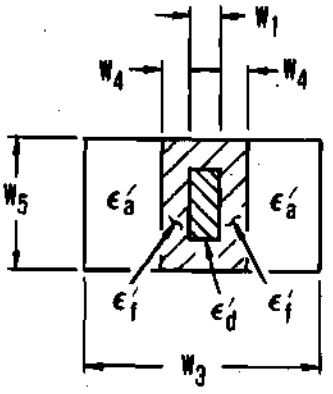

$m_s = \frac{\gamma 4\pi M_s}{\omega_c} = 0.8$

$f_c = 9$ Gc

$m = \frac{\gamma 4\pi M_f}{\omega_c} = 0.4$

FR = 1.0

W_1 = VARIABLE

$W_3 = 0.5\ \lambda_c$

$W_4 = 0.04\ \lambda_c$

$W_5 = 0.294\ \lambda_c$

$R_r = 0.5$

$\epsilon'_a = 1.0$

ϵ'_d = PARAMETER

$\epsilon'_f = 16.0$

$\tan \delta_a = 0$

$\tan \delta_d = 0.0005$

$\tan \delta_f = 0.0007$

$\lambda_c = 3.33$ Cm

HF = 0

$\Delta H = 65$ Oe.

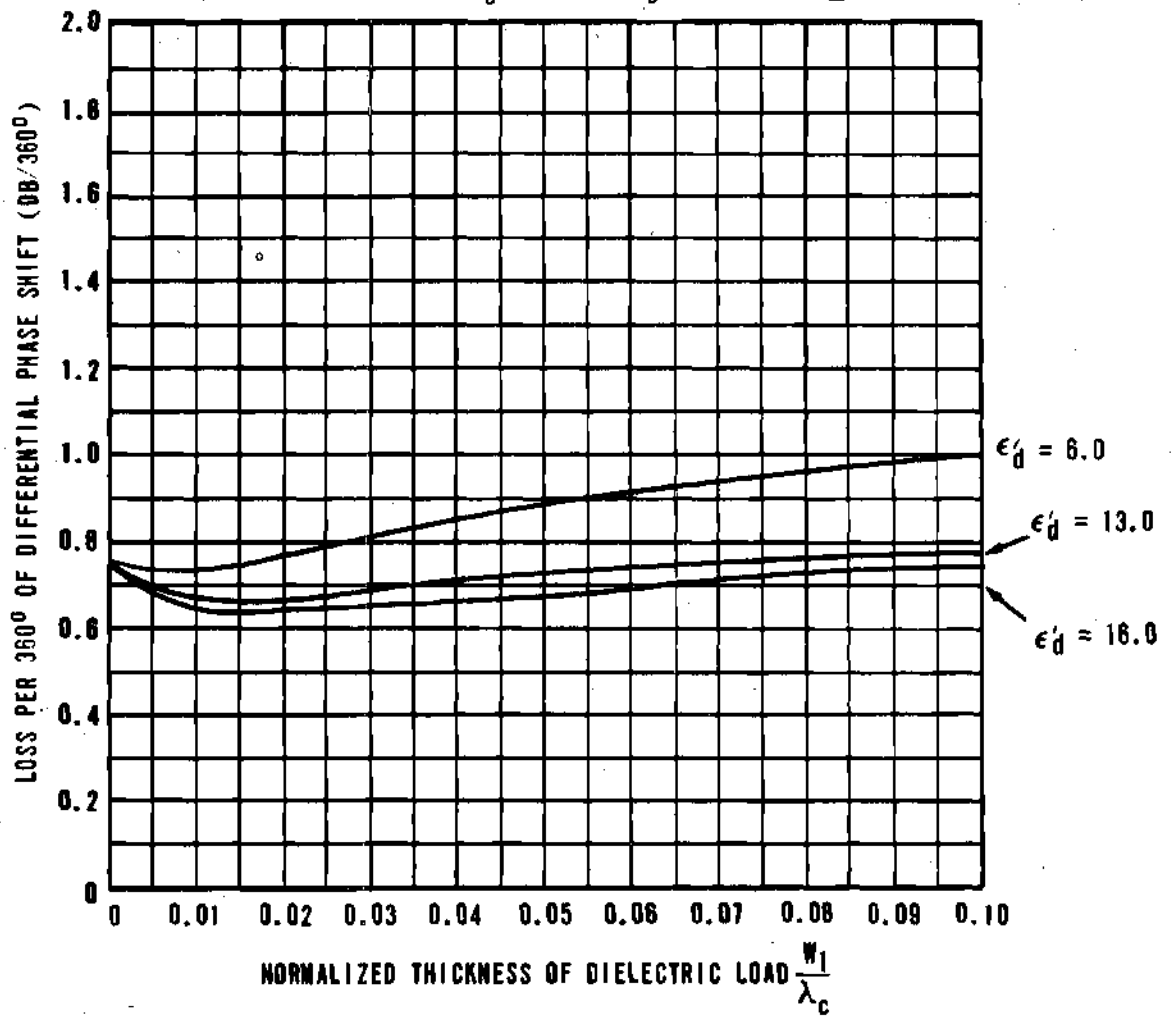

Figure 44. Loss Per 360° Of Differential Phase Shift vs Normalized Dielectric Load Thickness With Load Dielectric Constant As A Parameter

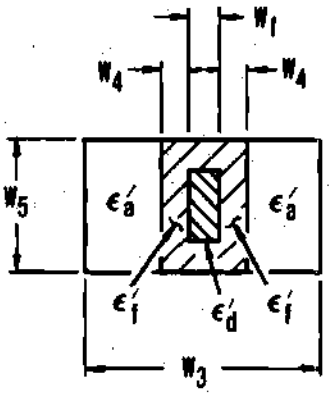

$m_s = \frac{\gamma 4\pi M_s}{\omega_c} = 0.8$

$f_c = 9$ Gc

$m = \frac{\gamma 4\pi M_r}{\omega_c} = 0.4$

FR = 1.0

W_1 = PARAMETER

$W_3 = 0.5\ \lambda_c$

W_4 = VARIABLE

$W_5 = 0.294\ \lambda_c$

$R_r = 0.5$

$\epsilon'_a = 1.0$

$\epsilon'_d = 16.0$

$\epsilon'_f = 16.0$

$\tan \delta_a = 0$

$\tan \delta_d = 0.0005$

$\tan \delta_f = 0.0007$

$\lambda_c = 3.33$ Cm

MF = 0

$\Delta H = 65$ Oe.

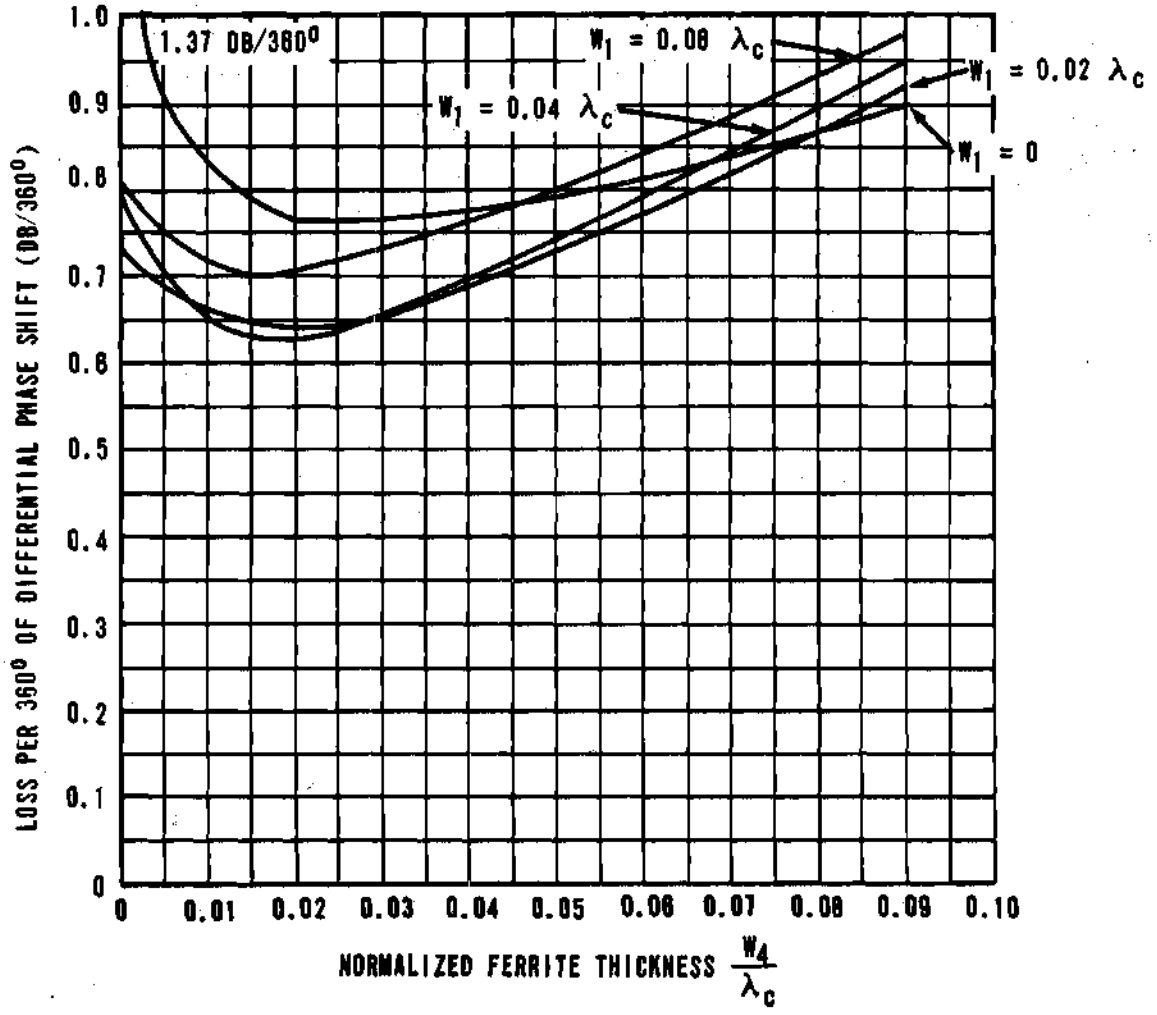

Figure 45. Loss Per 360° Of Differential Phase Shift vs Normalized Ferrite Thickness With Dielectric Load Thickness As A Parameter

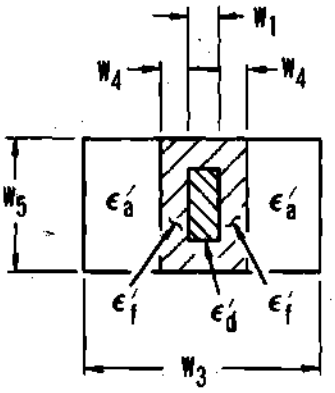

$m_s = \dfrac{\gamma 4\pi M_s}{\omega_c} = 0.38$

$f_c = 9$ Gc

$m = \dfrac{\gamma 4\pi M_f}{\omega_c} = 0.19$

FR = VARIABLE

$W_1 = 0.023\ \lambda_c$

W_3 = PARAMETER

$W_4 = 0.04\ \lambda_c$

$W_5 = 0.294\ \lambda_c$

$R_f = 0.5$

$\epsilon'_a = 1.0$

$\epsilon'_d = 16.0$

$\epsilon'_f = 16.0$

$\tan \delta_a = 0$

$\tan \delta_d = 0.0005$

$\tan \delta_f = 0.0007$

$\lambda_c = 3.33$ Cm

$HF = 0.137 = \gamma \left| \vec{H_i} \right| / \omega_c$

$\Delta H = 65$ Oe.

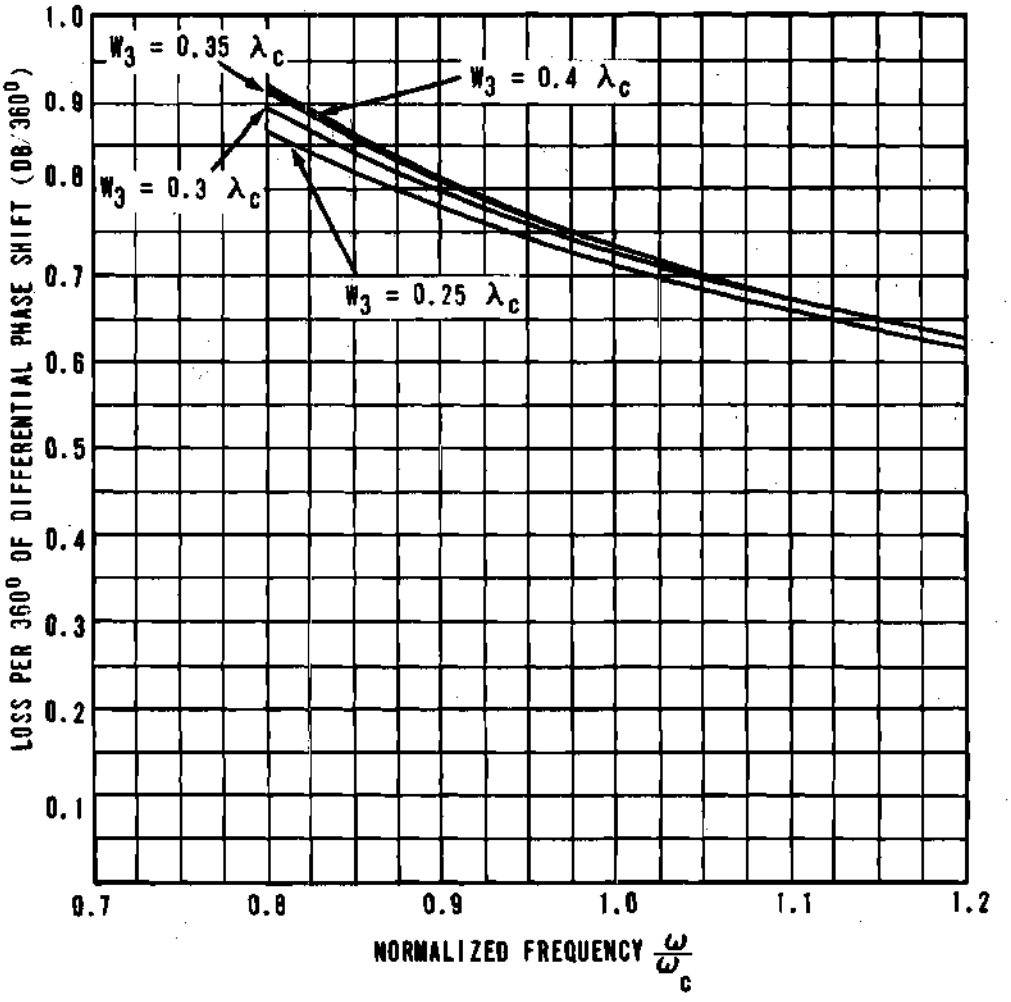

Figure 46. Loss Per 360° Of Differential Phase Shift vs Normalized Frequency With Waveguide Width As A Parameter

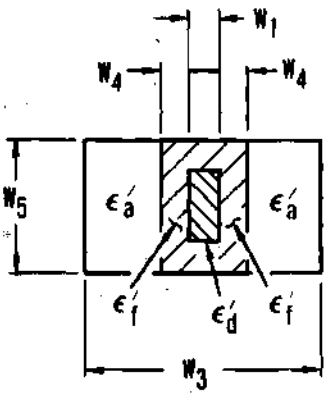

$m_s = \frac{\gamma 4\pi M_s}{\omega_c} = 0.38$

$f_c = 9$ Gc

$m = \frac{\gamma 4\pi M_r}{\omega_c} = 0.19$

FR = VARIABLE

W_1 = PARAMETER

$W_3 = 0.25\ \lambda_c$

$W_4 = 0.04\ \lambda_c$

$W_5 = 0.294\ \lambda_c$

$R_r = 0.5$

$\epsilon'_a = 1.0$

$\epsilon'_d = 16.0$

$\epsilon'_f = 16.0$

$\tan \delta_a = 0$

$\tan \delta_d = 0.0005$

$\tan \delta_f = 0.0007$

$\lambda_c = 3.33$ Cm

HF = 0

$\Delta H = 65$ Oe.

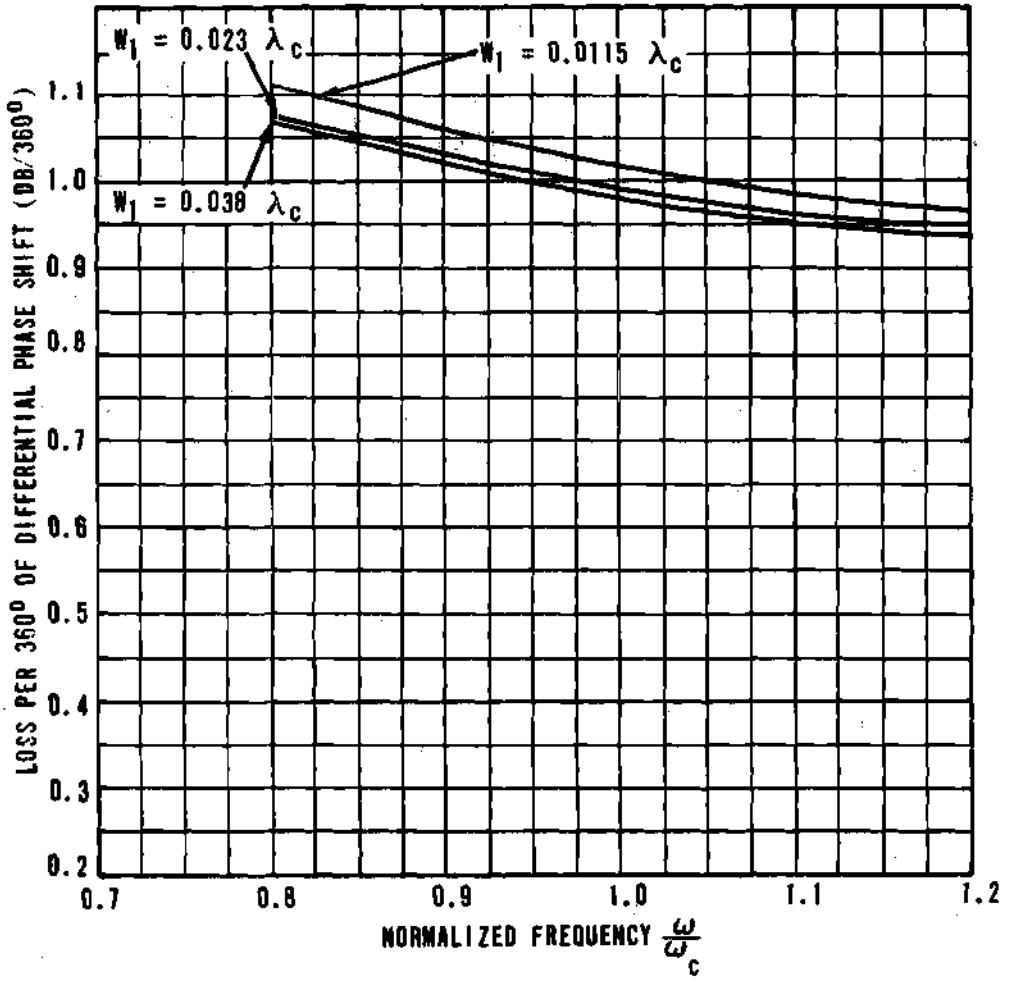

Figure 47. Loss Per 360° Of Differential Phase Shift vs Normalized Frequency With Dielectric Load Thickness As A Parameter

LP360 is found to be a linear function of resonance linewidth as shown in Figure 48. For the larger linewidths (> 100 oe.), the nonreciprocal loss component is excessive for many applications. Figure 49 illustrates the variation of LP360 with saturation magnetization for fixed remanence ratio. Note that the internal effective field is taken to be zero. An effective field could be computed for each value of saturation magnetization as shown in Chapter IV. In that case, the LP360 would be appreciably larger for the high magnetization values. If the saturation magnetization is fixed in value and the remanence ratio is varied, LP360 is found to increase sharply for low remanence ratios as shown in Figure 50. This behavior is largely due to the small differential phase shift for low remanence ratios.

High Power Effects. At high rf peak power levels insertion loss will increase appreciably if the internal rf magnetic field of the ferrite exceeds the threshold value for the onset of nonlinear effects. The actual rf field strength in the ferrite, and hence the input power level at which nonlinear effects set in, is a function of the dimensional and material parameters of the device structure. Figures 51 and 52 illustrate the variation of the maximum of field intensity in the ferrite for one watt of incident power as a function of dielectric load thickness. It can be seen that some improvement in peak power capability is possible for large spacing between the ferrite slabs.

Performance characteristics of ferrite phase shifters normally deteriorate as the rf average power level is increased. This degradation of performance is due primarily to heating effects. Removal of heat from the ferrite is considerably improved by placing slabs of dielectric material having a high thermal conductivity (such as boron nitride) in contact with the ferrite and the waveguide as shown in Figure 14. The model for this structure is shown in Figure 19. The principal effect of adding the cooling slabs is to decrease the differential phase shift as shown in Figure 53. From Figure 54 it can be seen that even though the differential phase shift decreases with the addition of the cooling slabs, the figure of merit, LP360, is changed very little. This is due

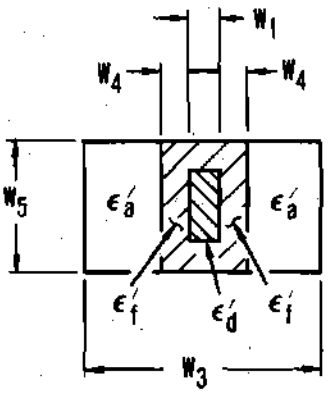

$m_s = \dfrac{\gamma 4\pi M_s}{\omega_c} = 0.38$

$f_c = 9$ Gc

$m = \dfrac{\gamma 4\pi M_r}{\omega_c} = 0.19$

FR = 1.0

$W_1 = 0.06\ \lambda_c$

$W_3 = 0.382\ \lambda_c$

$W_4 = 0.04\ \lambda_c$

$W_5 = 0.294\ \lambda_c$

$R_r = 0.5$

$\epsilon'_a = 1.0$

$\epsilon'_d = 16.0$

$\epsilon'_f = 16.0$

$\tan \delta_a = 0$

$\tan \delta_d = 0.0005$

$\tan \delta_f = 0.0007$

$\lambda_c = 3.33$ Cm

HF = 0.1

ΔH = VARIABLE

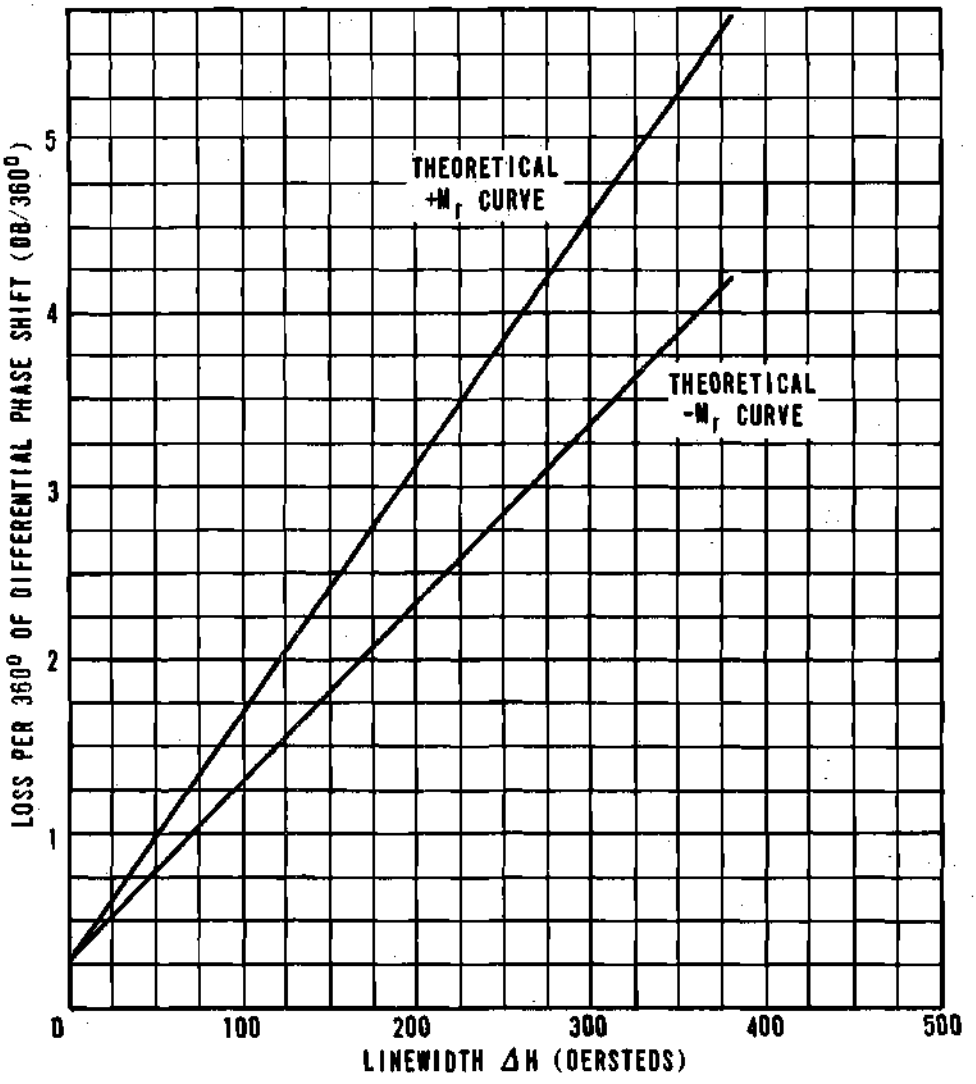

Figure 48. Loss Per 360° Of Differential Phase Shift vs Linewidth

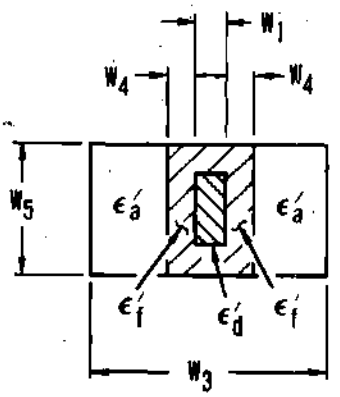

$m_s = \frac{\gamma 4\pi M_s}{\omega_c}$ = VARIABLE

f_c = 9 Gc

$m = \frac{\gamma 4\pi M_r}{\omega_c} = R_r M_s$

FR = 1.0

W_1 = 0.04

W_3 = 0.761 λ_c

W_4 = 0.05 λ_c

W_5 = 0.294 λ_c

R_r = 0.5

ϵ'_a = 1.0

ϵ'_d = 13.0

ϵ'_f = 12.0

tan δ_a = 0

tan δ_d = 0.00005

tan δ_f = 0.0001

λ_c = 3.33 Cm

MF = 0

ΔH = 65 Oe.

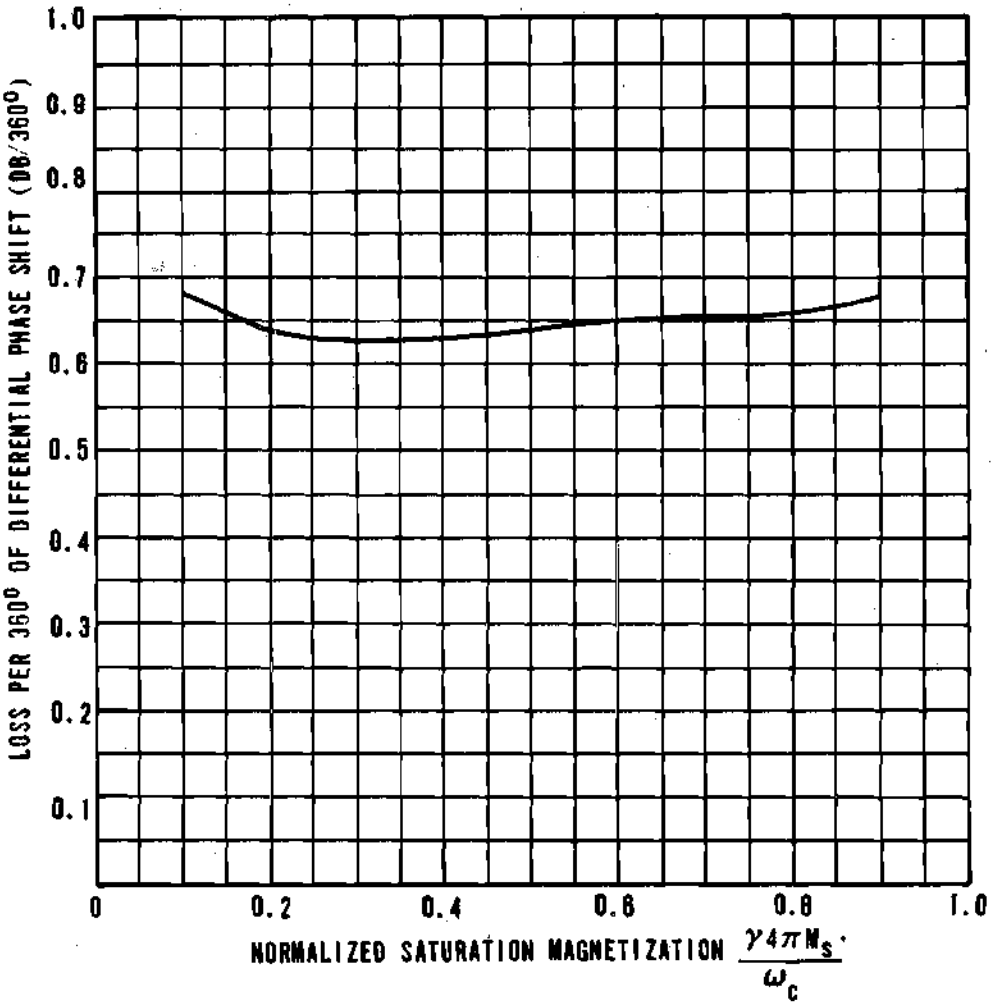

Figure 49. Loss Per 360° Of Differential Phase Shift vs Normalized Saturation Magnetization For Constant Remanence Ratio

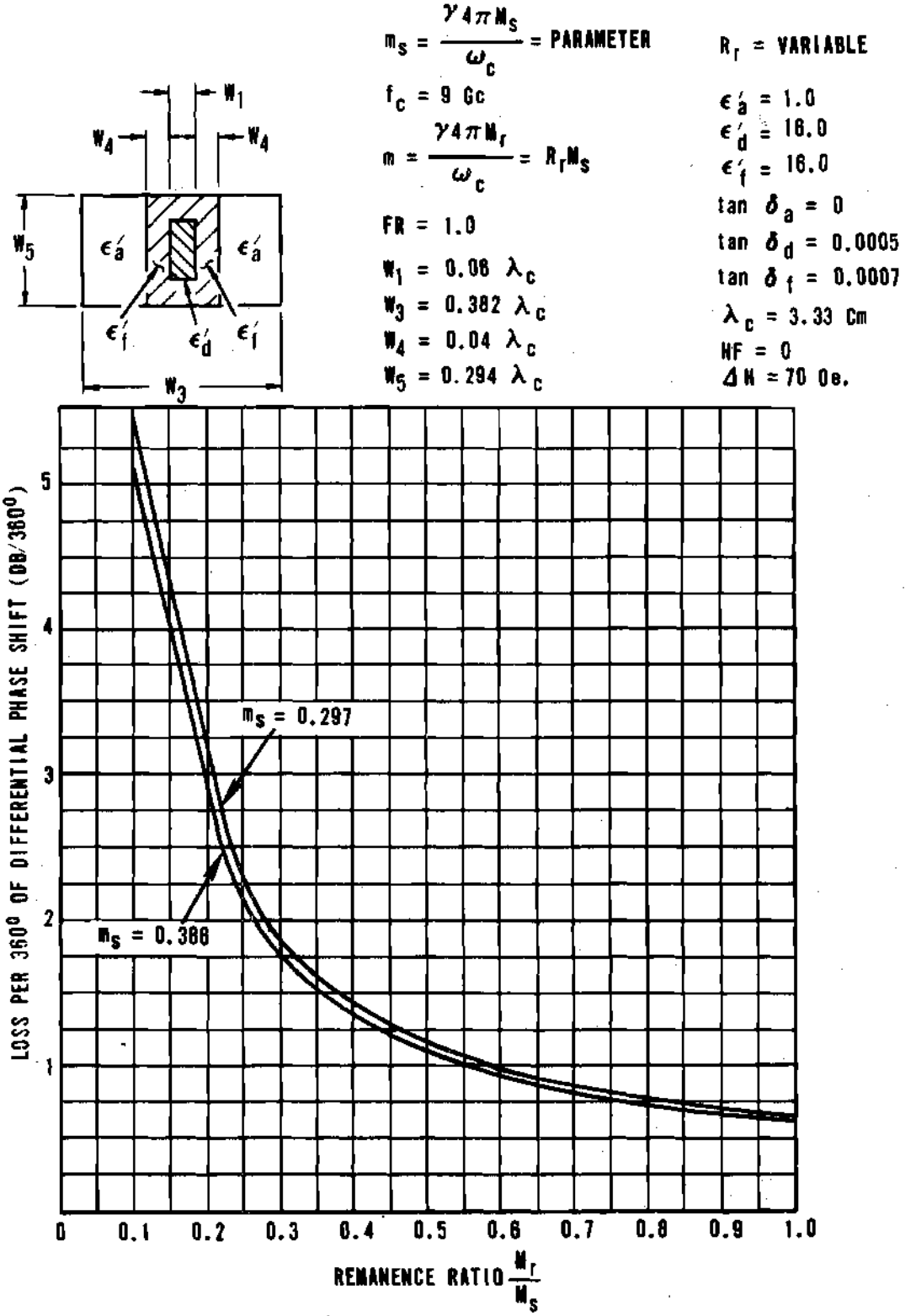

Figure 50. Loss Per 360° Of Differential Phase Shift vs Remanence Ratio For Two Values Of Saturation Magnetization

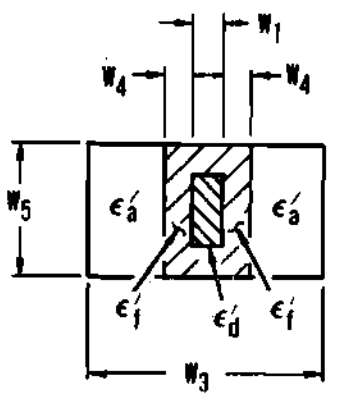

$m_s = \frac{\gamma 4\pi M_s}{\omega_c} = 1.6$

$f_c = 9$ Gc

$m = \frac{\gamma 4\pi M_f}{\omega_c} = 0.8$

FR = 1.0

W_1 = VARIABLE

$W_3 = 0.761\ \lambda_c$

$W_4 = 0.04\ \lambda_c$

$W_5 = 0.2\ \lambda_c$

$R_f = 0.5$

$\epsilon'_a = 1.0$

ϵ'_d = PARAMETER

ϵ'_f = PARAMETER

$\tan \delta_a = 0$

$\tan \delta_d = 0.0005$

$\tan \delta_f = 0.0007$

$\lambda_c = 3.33$ Cm

HF = 0

$\Delta H = 65$ Oe.

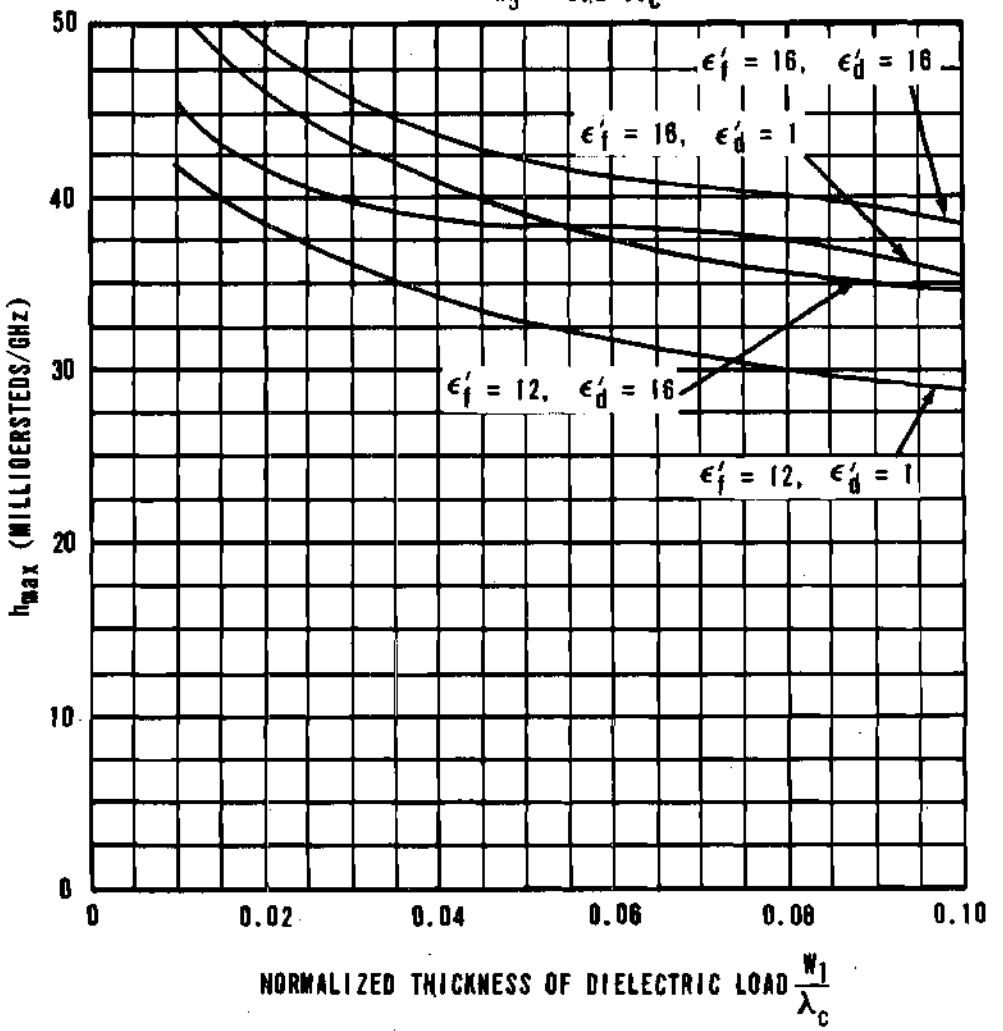

Figure 51. Maximum Magnetic Field Intensity In Ferrite vs Normalized Dielectric Load Thickness With Load And Ferrite Dielectric Constants As Parameters For One Watt Of Incident Power

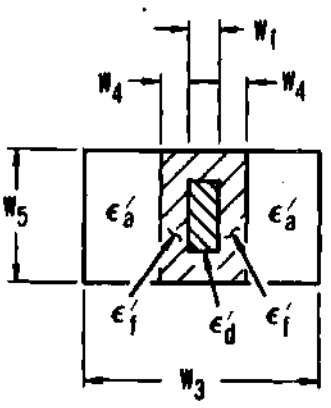

$m_s = \frac{\gamma 4\pi M_s}{\omega_c} = 0.8$

$f_c = 9$ Gc

$m = \frac{\gamma 4\pi M_f}{\omega_c} = 0.4$

FR = 1.0

W_1 = VARIABLE

$W_3 = 0.3\ \lambda_c$

W_4 = PARAMETER

$W_5 = 0.2\ \lambda_c$

$R_f = 0.5$

$\epsilon'_a = 1.0$

$\epsilon'_d = 16.0$

$\epsilon'_f = 16.0$

$\tan \delta_a = 0$

$\tan \delta_d = 0.0005$

$\tan \delta_f = 0.0007$

$\lambda_c = 3.33$ Cm

HF = 0

$\Delta H = 65$ Oe.

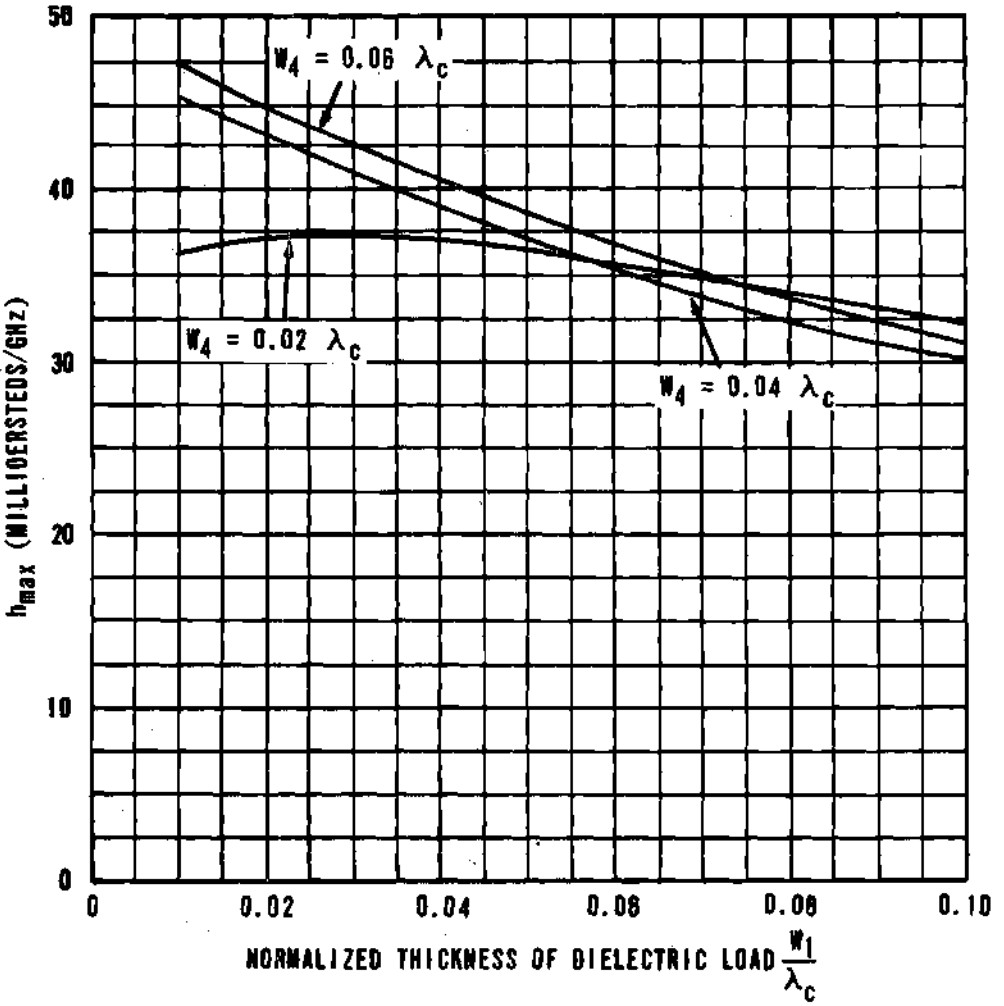

Figure 52. Maximum Magnetic Field Intensity In Ferrite vs Normalized Dielectric Load Thickness With Ferrite Thickness As A Parameter For One Watt Of Incident Power

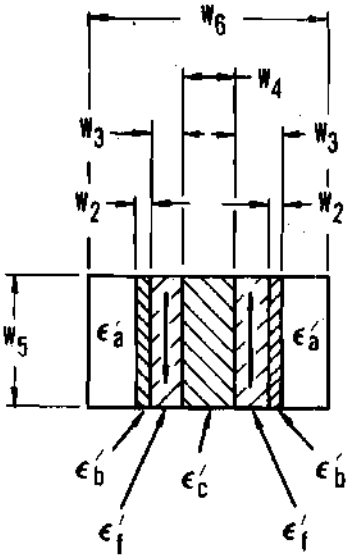

$m_s = \frac{\gamma 4\pi M_s}{\omega_c} = 0.38$

$R_f = 0.5$

$m = \frac{\gamma 4\pi M_f}{\omega_c} = 0.19$

$f_c = 9$ Gc

$\Delta H = 65$ Oe.

W_2 = PARAMETER

$W_3 = 0.04\ \lambda_c$

$W_4 = 0.023\ \lambda_c$

$W_5 = 0.294\ \lambda_c$

W_6 = VARIABLE

FR = 1.0

$\epsilon'_a = 1.0$

$\epsilon'_b = 4.5$

$\epsilon'_c = 16.0$

$\epsilon'_f = 16.0$

$\tan \delta_a = 0$

$\tan \delta_b = 0.0001$

$\tan \delta_c = 0.00005$

$\tan \delta_f = 0.0001$

$\lambda_c = 3.33$ Cm

NF = 0

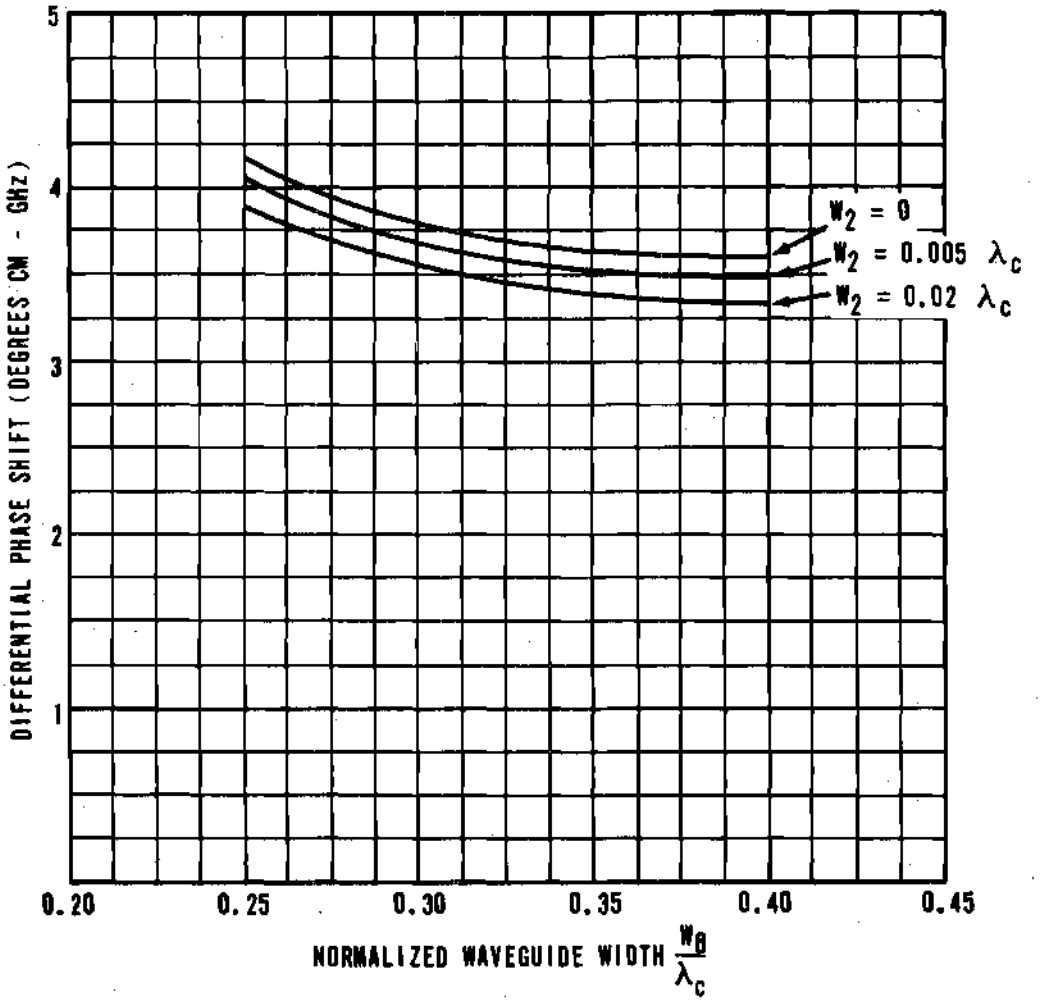

Figure 53. Differential Phase Shift vs Normalized Waveguide Width With Cooling Slab Thickness As A Parameter

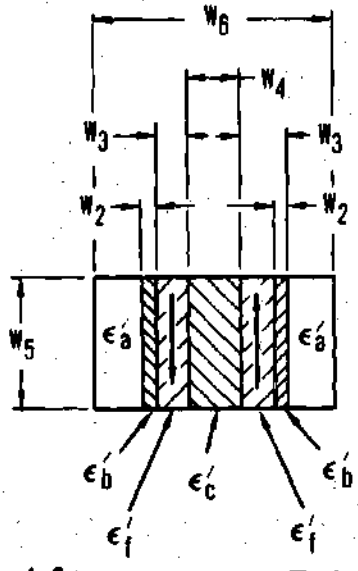

$m_s = \frac{\gamma 4\pi M_s}{\omega_c} = 0.38$

$R_r = 0.5$

$m = \frac{\gamma 4\pi M_r}{\omega_c} = 0.19$

$f_c = 9$ Gc

$\Delta H = 65$ Oe.

W_2 = PARAMETER

$W_3 = 0.04\ \lambda_c$

$W_4 = 0.023\ \lambda_c$

$W_5 = 0.294\ \lambda_c$

W_6 = VARIABLE

FR = 1.0

$\epsilon'_a = 1.0$

$\epsilon'_b = 4.5$

$\epsilon'_c = 16.0$

$\epsilon'_f = 16.0$

$\tan \delta_a = 0$

$\tan \delta_b = 0.0001$

$\tan \delta_c = 0.00005$

$\tan \delta_f = 0.0001$

$\lambda_c = 3.33$ Cm

HF = 0

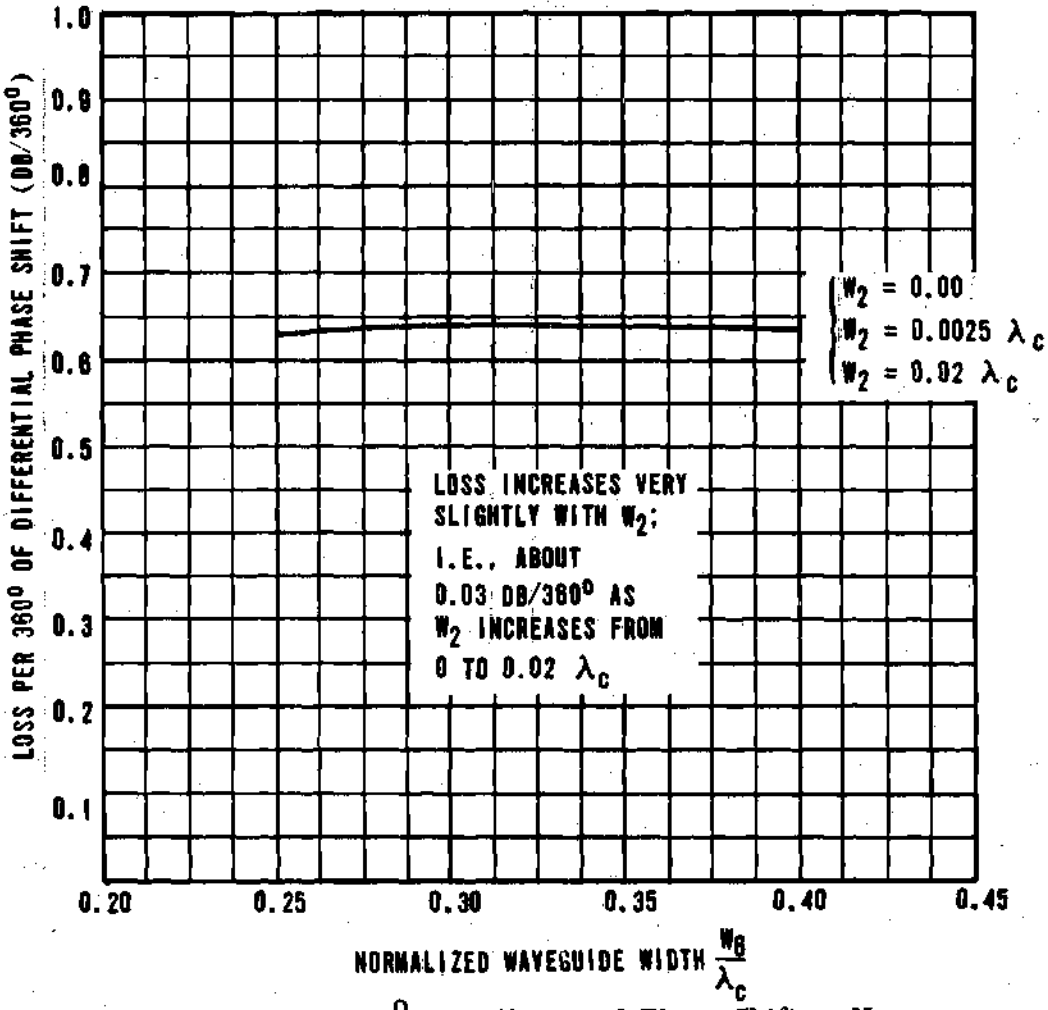

Figure 54. Loss Per 360° Of Differential Phase Shift vs Normalized Waveguide Width With Cooling Slab Thickness As A Parameter

to the redistribution of rf energy with a portion of the energy previously in the ferrite now in the lower loss cooling slabs. Thus, the overall loss is decreased, and the ratio of differential phase shift to loss is essentially unchanged.

Applied Field Phase Shifters

The basic models analyzed are the dielectric loaded twin slab structure shown in Figure 18 and the dielectric loaded single slab structure shown in Figure 22. For most purposes, at a fixed value of bias field, an applied field phase shifter can be considered to be a remanent device with a remanence ratio of unity. That is, the same general trends in loss and differential phase shift variations with dimensional and material parameters are found for both latching and applied field phase shifters. The applied field devices, of course, have the bias field as an additional degree of freedom. The variation of differential phase shift and LP360 for the twin slab structure as a function of bias field are shown in Figures 55 and 56. Both loss and differential phase shift are almost linear functions of the normalized internal magnetic field for a small range of values near zero. Differential phase shift and LP360 for the single slab structure as a function of bias field are illustrated in Figures 23 and 24.

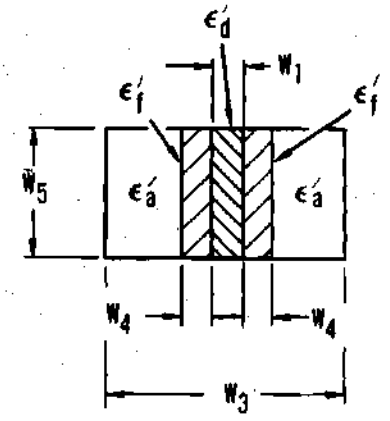

$$m_s = \frac{\gamma 4\pi M_s}{\omega_c} = 0.38$$

f_c = 9 Gc

HF = VARIABLE

ΔH = 65 Oe.

FR = 1.0

$W_1 = 0.08\ \lambda_c$
$W_3 = 0.4\ \lambda_c$
$W_4 = 0.04\ \lambda_c$
$W_5 = 0.294\ \lambda_c$

$\epsilon'_a = 1.0$
ϵ'_d = PARAMETER
$\epsilon'_f = 16.0$
$\tan \delta_a = 0$
$\tan \delta_d = 0.0005$
$\tan \delta_f = 0.0007$

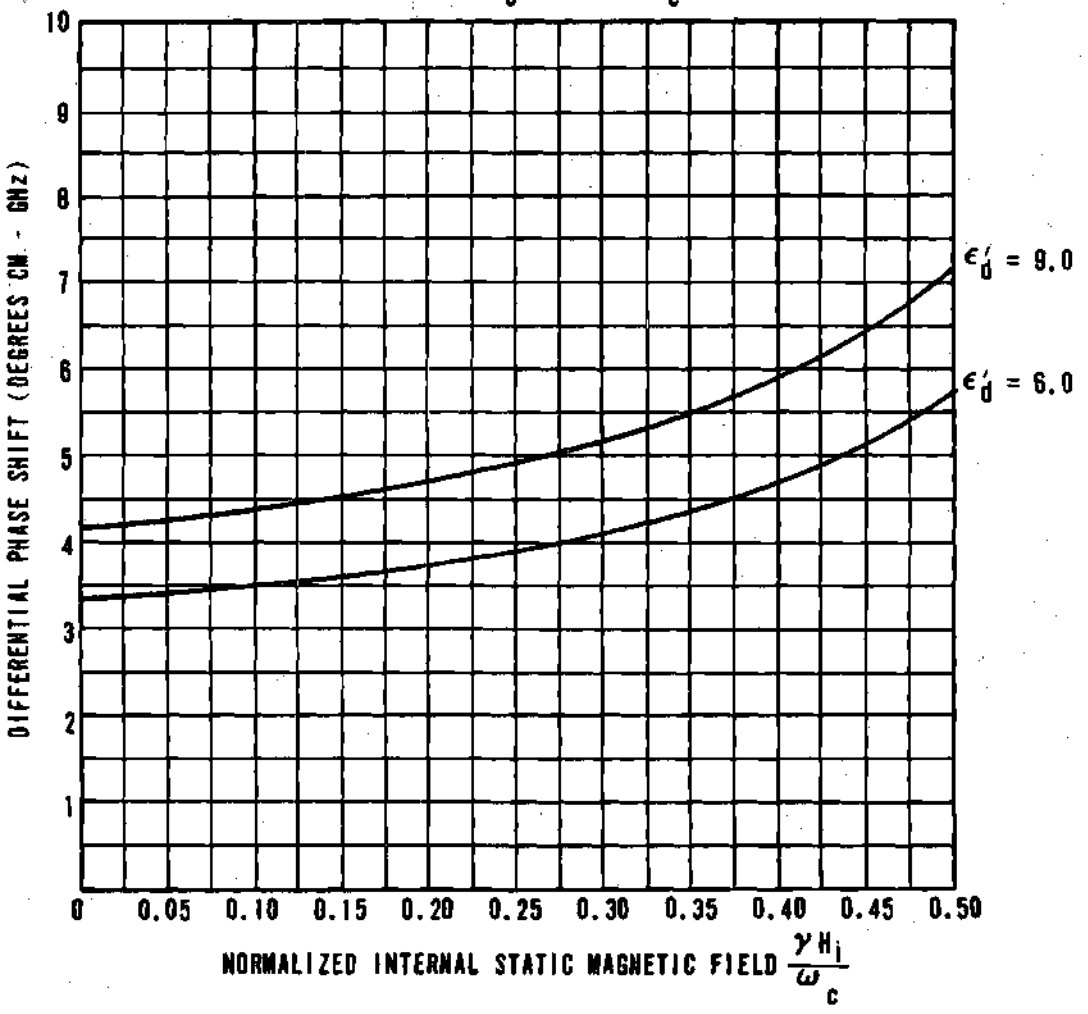

Figure 55. Differential Phase Shift vs Bias Field For An Applied Field Phase Shifter

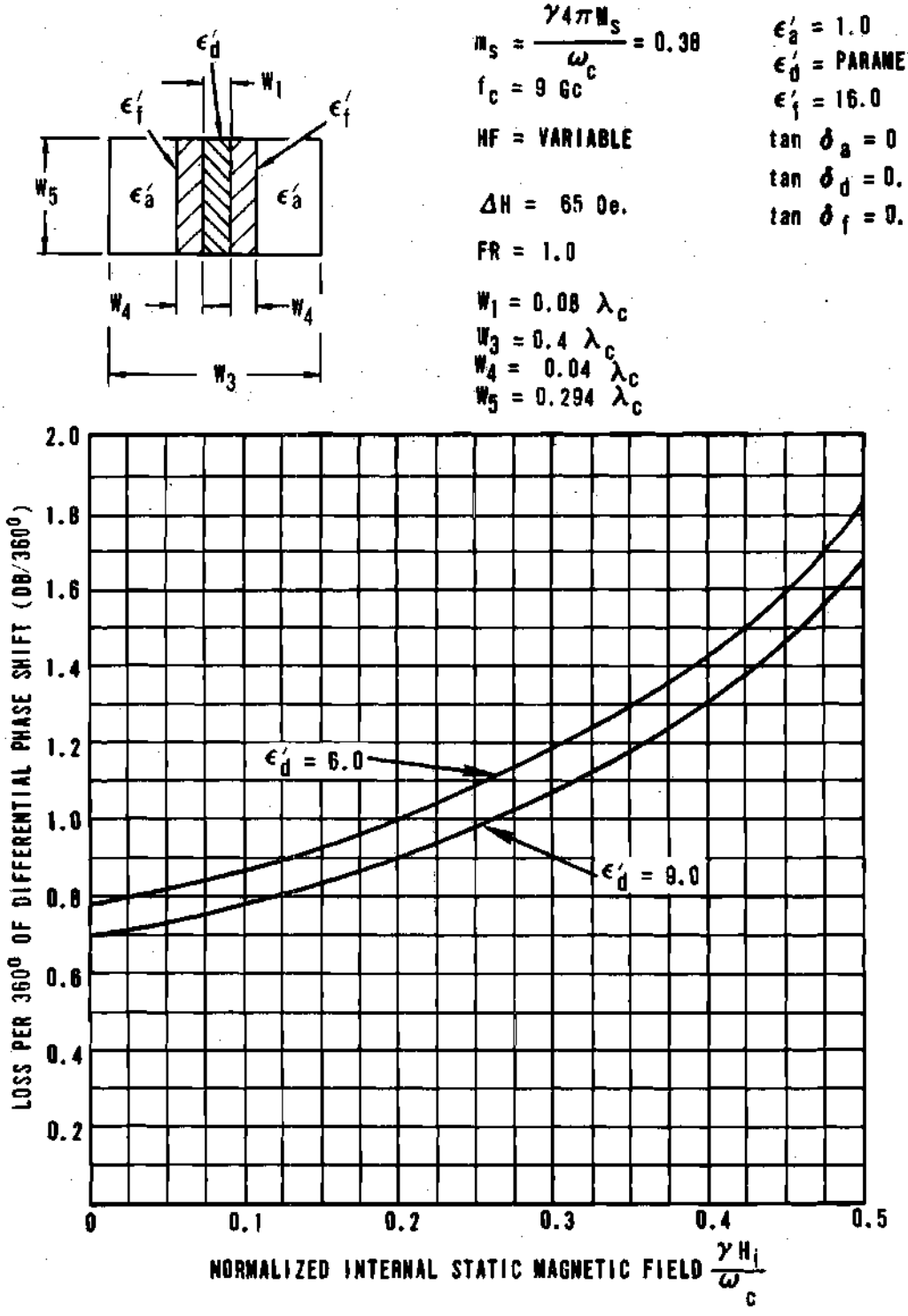

Figure 56. Loss Per 360° Of Differential Phase Shift vs Bias Field For An Applied Field Phase Shifter

CHAPTER VI

RESULTS AND CONCLUSIONS

The analytical and experimental results presented in this thesis demonstrate conclusively the practicability of precise quantitative prediction of losses in practical ferrite devices. The central issue dealt with is the problem of magnetic loss representation, both in magnetically saturated and in partially magnetized ferrites. In both cases a loss representation is desired which is simple in physical concept, quantitatively accurate, and for which the parameters involved are measurable intrinsic properties of the material. For magnetically saturated ferrites the traditional Landau-Lifshitz phenomenological loss representation certainly satisfies the first and third of the desired conditions. The question of its quantitative accuracy has been less clear. For polycrystalline ferrites common belief has been that the Landau-Lifshitz representation is quantitatively valid only at resonance. However, the theoretical and experimental results presented in this thesis have demonstrated that the Landau-Lifshitz loss representation can in fact be used with confidence for the prediction of magnetic losses in saturated polycrystalline ferrites even in the region far from resonance. This conclusion was reached by comparing the theoretical operating characteristics of an analog phase shifter, whose phase shift element was a single magnetically saturated ferrite slab, with the measured characteristics of an experimental model of the device. The theoretical characteristics were obtained by solving the exact boundary value problem for the structure.

The representation of losses in partially magnetized ferrites is complicated by the existence of a multiplicity of magnetic domains of various shapes and orientations. The only technique available in the literature for representing magnetic losses in such materials is the "bulk" loss representation normally

associated with totally unmagnetized samples. This type of loss representation is undesirable for partially magnetized materials for several reasons. The principal two being (a) its failure to provide an explicit relationship between the losses and fundamental material parameters such as saturation magnetization and resonance linewdith, and (b) the apparent failure of "bulk" magnetic loss tangents, obtained by existing measurement procedures, to account for magnetic losses observed in ferrite devices.

Because of the inherent disadvantages of the "bulk" representation of magnetic losses, an alternate way of representing losses in partially magnetized ferrites was developed in this thesis. The new representation has the desired features of conceptual simplicity, quantitative accuracy, and explicit relationship to measurable intrinsic material parameters. It is based on an extension of the Landau-Lifshitz tensor representation of losses in saturated samples (or single domains) to multi-domain (partially magnetized) samples. Analytical expressions for the components of the new "lossy" small signal permeability tensor for partially magnetized ferrites were derived using a spatial averaging technique on the permeability tensors for combinations of "single" domains whose effective fields and saturation magnetizations are oriented at different angles. The real (phase shift) part of the average permeability components is found to be proportional to the net magnetization of the sample. On the other hand, the imaginary (loss) part of the permeability components is related to an effective magnetization which is always greater than the net magnetization but less than the saturation magnetization of the material. This simply implies that domains must be favorably oriented to yield positive phase shift, while even domains unfavorably oriented so far as phase shift is concerned contribute to the loss. For remanence devices this means that phase shift will be directly related to remanence magnetization, but loss will be more intimately related to saturation magnetization. The validity of the derived "average" permeability tensor for the prediction of losses in partially magnetized ferrites was demonstrated by a comparison of the theoretically predicted

characteristics of several devices with experimental results. The devices examined were remanence ("latching") phase shifters, whose phase shift elements were ferrite toroids. Theoretical characteristics were obtained by solving the exact boundary value problem for each structure.

One of the more interesting results of the theoretical analysis of latching phase shifters was the prediction of an unexpected strong dependence of loss in the partially magnetized material on resonance linewidth. This surprising prediction was subsequently verified experimentally, convincingly demonstrating the validity of the "average" tensor representation of losses in partially magnetized ferrites.

Resonance linewidth has, thus, been shown to be of great importance in determining losses in partially magnetized ferrites as well as in magnetically saturated materials. The measured polycrystalline linewidth has been exclusively used in the computations in this thesis. Theoretical device characteristics predicted on this basis are, in general, in excellent agreement with experimentally determined characteristics. There is some experimental data available, however, which indicates that for some materials of types not examined in detail in this thesis, the appropriate linewidth to use in theoretical calculations may be something other than the polycrystalline linewidth. Any conclusion drawn at this time must of necessity be somewhat vague, because of the sparcity of experimental evidence. Tentatively, however, it appears that for many materials, such as the rare earth doped garnets, in which intrinsic damping is the dominant line broadening mechanism the polycrystalline linewidth is indeed the appropriate linewidth to use. On the other hand, for materials, such as magnesium manganese ferrite, in which anisotropy and porosity are the dominant line broadening mechanisms the appropriate linewidth to use in theoretical calculations in the region far from resonance may be the linewidth due to intrinsic damping only. This linewidth would, of course, be appreciably smaller than the polycrystalline linewidth. Additional work is required to clarify this issue.

The "small loss" computational technique has been used extensively in the past to predict losses in dielectrics and more recently in ferrites. This technique assumes that the rf field distributions in the presence of losses are the same as those that would exist if the material were lossless. Losses are then computed using a loss tangent and the lossless energy densities. A comparison of losses predicted using this technique with those obtained from the solution of the exact boundary value problem and with experimental results indicates that "small loss" solutions are unsatisfactory for quantitative prediction of dielectric and magnetic losses. Losses predicted by the "small loss" technique are typically 40 to 50 per cent of the losses predicted by the solution of the exact boundary value problem. Losses predicted by the exact solution are in excellent agreement with experimental results. Conductor losses in waveguide walls predicted by the "small loss" procedure appear to be in better agreement with experimental data. However, these losses are typically so small that measurement inaccuracies cloud the issue.

As a prelude to the derivation of the "average" permeability tensor for partially magnetized ferrites, the various equations of motion for the magnetization in magnetically saturated ferrites were examined. All of the equations examined (including phenomenological damping terms) were shown to be obtainable from a single equation. The various forms of the single phenomenological equation simply highlight specific aspects of the general problem.

The practicability of precise analytical design of latching and applied field ferrite devices including the prediction of insertion loss, was demonstrated by theoretical and experimental results presented in this thesis. Quantitative relationships were provided relating device transfer characteristics to the intrinsic material and dimensional parameters for a number of phase shifter configurations. These relationships, when programmed for a digital computer, allow a very wide variety of parameter combinations to be examined in a short time (typically more than one hundred configurations per minute). Extensive design data for waveguide latching and analog phase shifters were presented in the form of families of normalized curves.

APPENDIX A

TENSOR PERMEABILITY FOR UNSATURATED FERRITES

The small signal permeability $\langle \mu_{j\kappa} \rangle$ relating the effective rf fields $\langle \vec{b} \rangle$ and $\langle \vec{h} \rangle$ in an unsaturated ferrite can be obtained from the "point" small signal permeability $\mu_{j\kappa}$ which relates the "point" rf fields $\vec{b}$ and $\vec{h}$ of an appropriate saturated media problem by performing a spatial averaging as follows. Consider a ferrite sample consisting of a single domain magnetized by an effective static magnetic field. The saturation magnetization $\vec{M}_s$ of the domain and the net effective static magnetic field $\vec{H}_i$ are assumed to be oriented in different directions as shown in Figure 10. The equation of motion for the macroscopic magnetization, including losses via the Landau-Lifshitz damping term, is

$$\frac{d\vec{M}}{dt} = \gamma_e (\vec{M} \times \vec{H}) - \frac{\alpha}{|\vec{M}|} \vec{M} \times \frac{d\vec{M}}{dt} \tag{51}$$

where

$$\vec{M} = \vec{M}_s + \vec{m}_e^{\,j\omega t} \qquad \vec{H} = \vec{H}_i + \vec{h}_e^{\,j\omega t}$$

$\vec{M}_s = |\vec{M}_s| \{\vec{i} \sin\theta \cos\phi + \vec{j} \sin\theta \sin\phi + \vec{k} \cos\theta\}$ = saturation magnetization

$\vec{H}_i = |\vec{H}_i| \{\vec{i} \sin B \cos A + \vec{j} \sin B \sin A + \vec{k} \cos B\}$ = net effective static magnetic field

$\vec{h} = \vec{i} h_x + \vec{j} h_y + \vec{k} h_z$ = rf magnetic field

$\vec{m} = \vec{i} m_x + \vec{j} m_y + \vec{k} m_z$ = rf magnetization

$\gamma_e = \gamma(1 + \alpha^2)$, $\alpha = \frac{1}{\omega t}$, τ = damping time constant

By expanding Equation 51 and equating coefficients of $e^{j\omega t}$, the following equation is obtained.

$$j\omega\vec{m} = \gamma_e (\vec{M} \times \vec{h}) - \gamma_e (\vec{H}_i \times \vec{m}) - j \frac{\omega\alpha}{|M|} (M \times \vec{m}) \tag{52}$$

where

$$\vec{M} \times \vec{h} = \vec{i}\,(M_y h_z - M_z h_y) + \vec{j}\,(M_z h_x - M_x h_z) + \vec{k}\,(M_x h_y - M_y h_x)$$

$$\vec{H}_i \times \vec{m} = \vec{i}\,(H_y m_z - H_z m_y) + \vec{j}\,(H_z m_x - H_x m_z) + \vec{k}\,(H_x m_y - H_y m_x)$$

$$\vec{M} \times \vec{m} = \vec{i}\,(M_y m_z - M_z m_y) + \vec{j}\,(M_z m_x - M_x m_z) + \vec{k}\,(M_x m_y - M_y m_x)$$

Writing out the equations for the components and rearranging terms for convenience yields a system of equations which can be written as

$$\begin{aligned} a_{11} m_x + a_{12} m_y + a_{13} m_z &= f_1 \\ a_{21} m_x + a_{22} m_y + a_{23} m_z &= f_2 \\ a_{31} m_x + a_{32} m_y + a_{33} m_z &= f_3 \end{aligned} \tag{53}$$

where

$$a_{11} = a_{22} = a_{33} = j\omega$$

$$a_{21} = a_{12} = \gamma_e H_z + j \frac{\omega\alpha}{|\vec{M}_s|} M_z$$

$$a_{13} = -a_{31} = \gamma_e H_y + j \frac{\omega\alpha}{|\vec{M}_s|} M_y$$

$$a_{32} = -a_{23} = \gamma_e H_x + j \frac{\omega\alpha}{|\vec{M}_s|} M_x$$

$$f_1 = \gamma_e M_z h_x + \gamma_e M_y h_z$$

$$f_2 = \gamma_e M_z h_x - \gamma_e M_x h_z$$

$$f_3 = -\gamma_e M_y h_x + \gamma_e M_x h_y$$

Solving for m_x, m_y, and m_z in terms of h_x, h_y, and h_z yields

$$m_x = \frac{1}{\Delta}\Big\{h_x\Big[\gamma_e M_z(a_{13}a_{32} - a_{12}a_{11}) + \gamma_e M_y(a_{12}a_{32} + a_{13}a_{11})\Big] \qquad (54)$$

$$+ h_y\Big[-\gamma_e M_z(a_{11}^2 + a_{32}^2) - \gamma_e M_x(a_{12}a_{32} + a_{13}a_{11})\Big]$$

$$+ h_z\Big[\gamma_e M_y(a_{11}^2 + a_{32}^2) - \gamma_e M_x(a_{13}a_{32} - a_{12}a_{11})\Big]\Big\}$$

$$m_y = \frac{1}{\Delta}\Big\{h_x\Big[\gamma_e M_x(a_{11}^2 + a_{13}^2) - \gamma_e M_y(a_{11}a_{32} - a_{13}a_{12})\Big]$$

$$+ h_y\Big[-\gamma_e M_z(a_{13}a_{32} + a_{12}a_{11}) + \gamma_e M_x(a_{11}a_{32} - a_{13}a_{12})\Big]$$

$$+ h_z\Big[\gamma_e M_y(a_{13}a_{32} + a_{12}a_{11}) - \gamma_e M_x(a_{11}^2 + a_{13}^2)\Big]\Big\}$$

$$m_z = \frac{1}{\Delta}\Big\{h_x\Big[\gamma_e M_z(-a_{12}a_{13} - a_{11}a_{32}) - \gamma_e M_y(a_{11}^2 + a_{12}^2)\Big]$$

$$+ h_y\Big[-\gamma_e M_z(-a_{12}a_{32} + a_{13}\,a_{11}) + \gamma_e M_x(a_{11}^2 + a_{12}^2)\Big]$$

$$+ h_z\Big[\gamma_e M_y(-a_{12}a_{32} + a_{13}a_{11}) - \gamma_e M_x(-a_{12}a_{13} - a_{11}a_{32})\Big]\Big\}$$

where

$$\Delta = j\omega\Big|-\omega^2 - (\omega\alpha)^2 + (\gamma_e|\vec{H_i}|)^2 + 2j\omega\alpha\gamma_e H_z\cos\theta$$

$$+ 2j\omega\alpha\gamma_e(H_x\sin\theta\cos\phi + H_y\sin\theta\sin\phi + H_z\cos\theta)\Big|$$

$$H_x = |\vec{H_i}|\sin B\cos A$$

$$H_y = |\vec{H_i}|\sin B\sin A$$

$$H_z = |\vec{H_i}|\cos A$$

Equation 54 is of the form

$$\begin{bmatrix} m_x \\ m_y \\ m_z \end{bmatrix} = \begin{bmatrix} x_{11} & x_{12} & x_{13} \\ x_{21} & x_{22} & x_{23} \\ x_{31} & x_{32} & x_{33} \end{bmatrix} \begin{bmatrix} h_x \\ h_y \\ h_z \end{bmatrix} \tag{55}$$

Substituting for the a_{ij}'s into Equation 54 to evaluate the susceptibilities x_{ij} of Equation 55 leads to

$$x_{11} = \frac{j\omega\alpha\gamma_e|\vec{M}_s|}{\Delta}\left\{\left[\gamma_e H_z(\cos\theta - \alpha\sin^2\theta\sin\phi\cos\phi) + \gamma_e H_y(\sin\theta\sin\phi + \alpha\sin\theta\cos\theta\cos\phi)\right] + j\left[\omega\alpha(\cos^2\theta + \sin^2\phi\sin^2\theta) - \frac{1}{\omega}\gamma_e H_x(\gamma_e H_y\cos\theta - \gamma_e H_z\sin\theta\sin\phi)\right]\right\} \tag{56}$$

$$x_{12} = \frac{\omega\gamma_e|\vec{M}_s|}{\Delta}\left\{\omega\cos\theta + \alpha\sin^2\theta\cos\phi(\omega\sin\phi + j\gamma_e H_z\cos\phi) + j(\alpha\gamma_e H_x\cos\theta - \gamma_e H_y)\sin\theta\cos\phi - \frac{1}{\omega}(\gamma_e H_x)(\gamma_e H_x\cos\theta + \gamma_e H_z\sin\theta\cos\phi)\right\}$$

$$x_{13} = \frac{\omega\gamma_e|\vec{M}_s|}{\Delta}\left\{-\omega\sin\theta\sin\phi + \omega\alpha\cos\theta\sin\theta\cos\phi - j\gamma_e H_z\sin\theta\cos\phi + j\alpha\sin^2\theta\cos\phi(2\gamma_e H_x\sin\phi - \gamma_e H_y\cos\phi) + \frac{1}{\omega}\sin\theta\gamma_e H_x(\gamma_e H_x\sin\phi - \gamma_e H_y\cos\phi)\right\}$$

$$x_{21} = \frac{\omega\gamma_e|\vec{M}_s|}{\Delta}\left\{-\omega\cos\theta + \omega\alpha\sin^2\theta\sin\phi\cos\phi + \frac{1}{\omega}\gamma_e H_y(\gamma_e H_y\cos\theta - \gamma_e H_z\sin\theta\sin\phi) + j(\sin\theta\sin\phi)(\alpha\gamma_e H_y\cos\theta - \gamma_e H_x - \alpha\gamma_e H_z\sin\theta\sin\phi)\right\}$$

$$x_{22} = \frac{j\omega\gamma_e|\vec{M}_s|}{\Delta}\Big\{\gamma_e H_z(\cos\theta + \alpha\sin^2\theta\sin\phi\cos\phi) + \gamma_e H_z\sin\theta(\cos\phi - \alpha\cos\theta\sin\phi) + j\omega\alpha(\cos^2\theta + \cos^2\phi\sin^2\phi) + \frac{1}{\omega}\gamma_e H_y(\gamma_e H_x\cos\theta - \gamma_e H_z\sin\theta\cos\phi)\Big\}$$

$$x_{23} = \frac{\omega\gamma_e|\vec{M}_s|}{\Delta}\Big\{\omega\sin\theta\cos\phi + \omega\alpha\cos\theta\sin\theta\sin\phi + \frac{1}{\omega}\gamma_e H_y(\gamma_e H_x\sin\theta\sin\phi - \gamma_e H_y\sin\theta\cos\phi) + j\alpha\gamma_e H_x\sin^2\theta\sin^2\phi - j\gamma_e H_z\sin\theta\sin\phi - j\alpha\gamma_e H_y\sin^2\theta\sin\phi\cos\phi\Big\}$$

$$x_{31} = \frac{\omega\gamma_e|\vec{M}_s|}{\Delta}\Big\{\omega\sin\theta\sin\phi + \omega\alpha\sin\theta\cos\theta\cos\phi + \frac{1}{\omega}\gamma_e H_z(\gamma_e H_y\cos\theta - \gamma_e H_z\sin\theta\sin\phi) + j\alpha\gamma_e H_y\cos^2\theta - j\gamma_e H_x\cos\theta - j\alpha\gamma_e H_z\sin\theta\cos\theta\sin\phi\Big\}$$

$$x_{32} = \frac{\omega\gamma_e|\vec{M}_s|}{\Delta}\Big\{-\omega\sin\theta\cos\phi + \omega\alpha\sin\theta\cos\theta\sin\phi + \frac{1}{\omega}\gamma_e H_z(\gamma_e H_z\sin\theta\cos\phi - \gamma_e H_x\cos\theta) - j\alpha\gamma_e H_x\cos^2\theta - j\gamma_e H_y\cos\theta + j\alpha\gamma_e H_z\cos\theta\sin\theta\cos\phi\Big\}$$

$$x_{33} = \frac{j\omega\gamma_e|\vec{M}_s|}{\Delta}\Big\{\alpha\gamma_e H_x\sin\theta\cos\theta\sin\phi + \gamma_e H_y\sin\theta\sin\phi - \alpha\gamma_e H_y\sin\theta\cos\theta\cos\phi + \gamma_e H_x\sin\theta\cos\phi - j\frac{1}{\omega}\gamma_e H_z(\gamma_e H_x\sin\theta\sin\phi + \gamma_e H_y\sin\theta\cos\phi) + j\omega\alpha\sin^2\theta\Big\}$$

where $$\Delta = j\omega\Big\{-\omega^2 - (\omega\alpha)^2 + (\gamma_e|\vec{H}_i|)^2 + j2\,\omega\alpha\gamma_e\left[H_x\sin\theta\cos\phi + H_y\sin\theta\sin\phi + H_z\cos\theta\right]\Big\}$$

From the domain theory of magnetization it is known that unsaturated magnetic media are made up of large numbers of "saturated domains." Thus, the individual domain behavior is described by Equation 56. This suggests that the result of Equation 56 can be extended so that it applies in unsaturated media by performing spatial averages with respect to ϕ, θ, A, and B. If it is assumed that the +z direction is a physically preferred direction for the magnetization $\vec{M}_s$ and the effective static magnetic field $\vec{H}_i$, all values of ϕ and of A between 0 and 2π are equally likely. Provided that $|\vec{M}_s|$ and $|\vec{H}_i|$ have the same value for all of the "several domains" over which the averaging process is to be performed, the following results is obtained when the averaging with respect to ϕ and A is carried out.

$$\langle x_{11} \rangle_{\phi, A} = \langle x_{22} \rangle_{\phi, A} = j\omega \left\{ \frac{k_1}{k_4} + k_3 \left[\frac{-k_4 + \sqrt{k_4^2 - k_5^2}}{2k_5 \sqrt{k_4^2 - k_5^2}} \right] \right\} \tag{57}$$

$$\langle x_{12} \rangle_{\phi, A} = -\langle x_{21} \rangle_{\phi, A} = j\omega \left\{ \frac{k_8}{\sqrt{k_4^2 - k_5^2}} + k_{10} \left[\frac{-k_4 + \sqrt{k_4^2 - k_5^2}}{2k_5 \sqrt{k_4^2 - k_5^2}} \right] \right\}$$

$$\langle x_{33} \rangle_{\phi, A} = j\omega \left\{ \frac{k_{11}}{\sqrt{k_4^2 - k_5^2}} + k_{12} \left[\frac{-k_4 + \sqrt{k_4^2 - k_5^2}}{2k_5 \sqrt{k_4^2 - k_5^2}} \right] \right\}$$

$$\langle x_{13} \rangle_{\phi, A} = \langle x_{31} \rangle_{\phi, A} = \langle x_{23} \rangle_{\phi, A} = \langle x_{32} \rangle_{\phi, A} = 0$$

where

$$k_1 = \gamma_e |\vec{M}_s| \left\{ \gamma_e H_z \cos\theta + j\omega\alpha(\cos^2\theta + \frac{1}{2}\sin^2\theta) \right\}$$

$$k_3 = \gamma_e |\vec{M}_s| \left\{ \gamma_e |\vec{H}_i| \sin\theta \frac{\sin B}{2} \right\}$$

$$k_4 = -\omega^2 - (\omega\alpha)^2 + (\gamma_e |\vec{H}_i|)^2 + 2j\omega\alpha\gamma_e H_z \cos\theta$$

$$k_5 = 2j\omega\alpha\gamma_e |\vec{H}_i| \sin\theta \sin B$$

$$k_8 = -j\gamma_e |\vec{M}_s| \left\{ \omega\cos\theta + j\alpha\gamma_e H_z \frac{\sin^2\theta}{2} - \frac{1}{\omega}(\gamma_e |\vec{H}_i|)^2 \cos\theta \frac{\sin^2 B}{2} \right\}$$

$$k_{10} = j\gamma_e |\vec{M}_s| \left\{ -j\alpha\gamma_e |\vec{H}_i| \sin\theta\cos\theta \frac{\sin B}{2} + \left(\frac{\gamma_e H_z}{\omega}\right)(\gamma_e \vec{H}_i) \sin\theta \frac{\sin B}{2} \right\}$$

$$k_{11} = \gamma_e |\vec{M}_s| \{ j\omega\alpha\sin^2\theta \}$$

$$k_{12} = \gamma_e |\vec{M}_s| \{ \gamma_e |H_i| \sin\theta \sin B \}$$

$$H_z = |\vec{H}_i| \cos B$$

If the angles between the $\vec{H}_i$'s and the z-axis are small, the tensor permeability $\langle \overleftrightarrow{\mu} \rangle_{\phi, A} = \mu_o \{ \langle \overleftrightarrow{x} \rangle_{\phi, A} + 1 \}$ becomes Equation 21 of Chapter II. The average with respect to θ can then be performed resulting in a tensor permeability $\langle \overleftrightarrow{\mu} \rangle_{\phi, A, \theta}$ which contains various average quantities. These average quantities can be related to experimentally measurable parameters. The interpretation of the average parameters and their relation to quantities obtainable experimentally are given in Chapter II in the pages following Equation 21.

APPENDIX B

A "SMALL LOSS" TECHNIQUE FOR COMPUTING LOSSES

The attenuation in a ferrite device due to small losses can sometimes be computed using a small loss technique (67) (68) which assumes the rf fields in the presence of losses to be identical to those in the absence of the losses. The attenuation per unit length can be written as

$$\alpha = \frac{P_L}{2P_t} \quad \text{nepers per unit length}$$

where P_t = Power transferred in the absence of loss

P_L = Power lost assuming fields are unchanged by the addition of loss

The calculations required for evaluating α are indicated below.

Power Transferred

P_t = Power transferred in the direction of propagation in the absence of losses

$$= \frac{1}{2} \iint_{\substack{\text{Waveguide} \\ \text{Cross Section}}} (\vec{E} \times \vec{h}^*) \cdot \vec{da}$$

Waveguide Losses

$$\alpha_w = \frac{P_w}{2P_t} \quad \text{nepers per unit length}$$

P_w = Power dissipated per unit length due to resistive losses in the waveguide walls assuming the currents flowing in the walls to be the same as those which would flow if the walls were perfect conductors

$$= R_s \iint_{\text{walls}} \frac{|\vec{K}_{\text{walls}}|}{2} \, da$$

where $\vec{K}$ = surface current = $\vec{n} \times \vec{h}\Big|_{\text{walls}}$

$\vec{n}$ = inward normal to wall

R_s = surface resistivity

Based on a comparison of theoretical and experimental results, this appears to be a satisfactory method for computing waveguide conductor losses and has been used for that purpose in this thesis.

Dielectric Losses

$$\alpha_d = \frac{P_d}{2P_t} \text{ nepers per unit length}$$

P_d = Power dissipated per unit length due to dielectric losses assuming the fields in the dielectric to be the same as those in the absence of losses

$$= \frac{1}{2} \iint_{\substack{\text{Cross Section} \\ \text{of Dielectric}}} \vec{E} \cdot \sigma \, \vec{E}^* \, da$$

where $\sigma = \omega \epsilon'' \epsilon_o$

ϵ'' = imaginary part of the dielectric constant

A comparison of results obtained using this procedure with results of the "exact" method and with experimental data indicate that the small loss technique is unsatisfactory for quantitative prediction of dielectric losses in ferrite phase shifters.

"Bulk" Magnetic Losses

$$\alpha_m = \frac{P_m}{2P_t} \text{ nepers per unit length}$$

P_m = Power dissipated per unit length due to magnetic losses assuming the fields in the ferrite to be the same as those in the absence of losses

$$= \iint_{\text{Cross Section of Ferrite}} \frac{\tan \delta_m}{2} \, (\vec{h} \cdot \vec{b}^*) \, da$$

where $\tan \delta_m$ = bulk magnetic loss tangent

A comparison of results obtained using this procedure with results of the "exact" method (using the tensor permeability) and with experimental data indicate that the representation of magnetic losses in remanent phase shifters as small bulk losses is unsatisfactory.

APPENDIX C

TRANSVERSE OPERATOR PARAMETERS

Consider a TE mode waveguide structure such as that shown in Figure 57. The ferrite slab is of width δ and is assumed to be infinitely long in the y direction. The preferred direction for the effective internal static magnetic field H_i and the saturation magnetization $\vec{M}_s$ is assumed to be in the +z direction. The intrinsic permeability tensor then has the general form

$$\langle \vec{\mu} \rangle_{avg} = \mu_o \begin{bmatrix} \langle \mu \rangle_{avg} & -j\langle \kappa \rangle_{avg} & 0 \\ j\langle \kappa \rangle_{avg} & \langle \mu \rangle_{avg} & 0 \\ 0 & 0 & \langle \mu_z \rangle_{avg} \end{bmatrix} \tag{58}$$

where $\langle \mu \rangle_{avg} = \langle \mu' \rangle_{avg} - j\langle \mu'' \rangle_{avg}$

$\langle \kappa \rangle_{avg} = \langle \kappa' \rangle_{avg} - j\langle \kappa''' \rangle_{avg}$

$\langle \mu_z \rangle_{avg} = \langle \mu_z' \rangle_{avg} - j\langle \mu_z'' \rangle_{avg}$

and $\langle \mu' \rangle_{avg}, \langle \mu'' \rangle_{avg}, \langle \kappa' \rangle_{avg}, \langle \kappa'' \rangle_{avg}, \langle \mu_z' \rangle_{avg}$, and $\langle \mu_z'' \rangle_{avg}$ are given by Equation 24 of Chapter II.

Assume a general form for the electric field inside the ferrite, say

$$E_z = \left[Be^{jk_m x} + Ce^{-jk_m x} \right] e^{-\gamma y} e^{j\omega t} \tag{59}$$

where

$$k_m^2 = \gamma^2 + \frac{\omega^2 \mu_o \epsilon_o \epsilon_f}{\rho} = \text{square of the wave number in the ferrite}$$

$$\rho = \frac{<\mu>_{avg}}{\left[<\mu>_{avg}\right]^2 - \left[<\kappa>_{avg}\right]^2}$$

γ = propagation constant

Using Equation 30 (Chapter 3), the magnetic field intensity in the y direction is found to be

$$h_y = \frac{\rho}{j\omega\mu_o}\left[\left(jk_m + \frac{\gamma}{\theta}\right) Be^{jk_m x} + \left(-jk_m + \frac{\gamma}{\theta}\right) Ce^{-jk_m x}\right] e^{-\gamma y} e^{j\omega t} \qquad (60)$$

where

$$\theta = \frac{-<\mu>_{avg}}{j<\kappa>_{avg}}$$

Using Equations 59 and 60, the fields at point one ($x = x_1$) and at point two ($x = x_1 + \delta$) can be written as

$$E_{z1} = \left[Be^{jk_m x_1} + Ce^{-jk_m x_1}\right] e^{-\gamma y} e^{j\omega t} \qquad (61)$$

$$E_{z2} = \left[Be^{jk_m (x_1 + \delta)} + Ce^{-jk_m (x_1 + \delta)}\right] e^{-\gamma y} e^{j\omega t} \qquad (62)$$

$$h_{y1} = \frac{\rho}{j\omega\mu_o}\left[\left(jk_m + \frac{\gamma}{\theta}\right) Be^{jk_m x_1} + \left(-jk_m + \frac{\gamma}{\theta}\right) Ce^{-jk_m x_1}\right] e^{-\gamma y} e^{j\omega t} \qquad (63)$$

$$h_{y2} = \frac{\rho}{j\omega\mu_o}\left[\left(jk_m + \frac{\gamma}{\theta}\right)Be^{jk_m(x_1+\delta)} + \left(-jk_m + \frac{\gamma}{\theta}\right)Ce^{-jk_m(x_1+\delta)}\right]e^{-\gamma y}e^{j\omega t} \tag{64}$$

Referring to Figure 57, the electric field in the z-direction and the magnetic field in the y-direction at point one can be related to the corresponding fields at point two by the transverse operator equation

$$\begin{bmatrix} E_{z1} \\ h_{y1} \end{bmatrix} = \begin{bmatrix} A & B \\ C & D \end{bmatrix} \begin{bmatrix} E_{z2} \\ h_{y2} \end{bmatrix} \tag{65}$$

Expanding Equation 65 yields the following two equations.

$$E_{z1} = AE_{z2} + Bh_{y2} \tag{66}$$

$$h_{y1} = CE_{z2} + Dh_{y2} \tag{67}$$

Substituting Equations 61 through 64 into Equations 66 and 67 allows the parameters A B C D to be evaluated. These parameters for a ferrite region are given in Equation 44 of Chapter III. If the internal effective static magnetic field and the magnetization reverse in direction, the only change necessary in Equation 44 is to reverse the sign of θ.

For a dielectric region $\rho \rightarrow 1$ and $\theta \rightarrow \infty$, so that the parameters for a dielectric region can be written in the form given in Equation 45 of Chapter III.

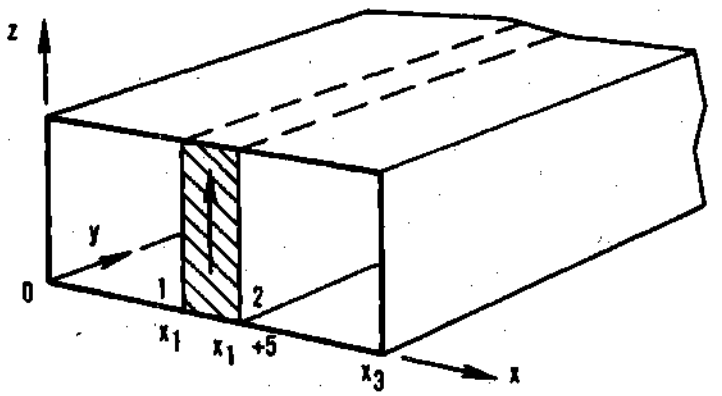

Figure 57. A Ferrite Loaded Rectangular Waveguide

APPENDIX D

SUPPLEMENTARY COMPARISONS OF THEORETICAL AND EXPERIMENTAL RESULTS

A number of curves are presented in this appendix which further illustrate the accuracy of the procedures developed for the prediction of performance characteristics of practical phase shifters. The experimental structure was a single dielectric loaded internal toroid latching phase shifter. All theoretical data were computed using appropriate effective values of dielectric constant and loss tangent as discussed in Chapter V.

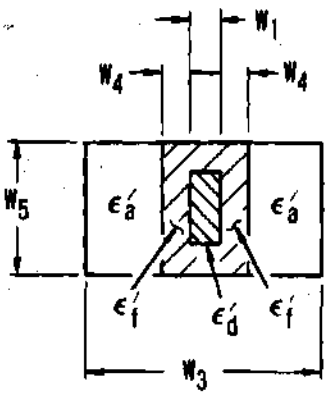

$m_s = \frac{\gamma 4\pi M_s}{\omega_c} = 0.366$

$f_c = 9$ Gc

$m = \frac{\gamma 4\pi M_r}{\omega_c} = 0.193$

FR = 1.0

W_1 = VARIABLE

$W_3 = 0.382\ \lambda_c$

$W_4 = 0.04\ \lambda_c$

$W_5 = 0.294\ \lambda_c$

$R_r = 0.5$

$\epsilon'_a = 1.0$

ϵ'_d = PARAMETER

$\epsilon'_f = 16.0$

$\tan \delta_a = 0.0007$

$\tan \delta_d = 0$

$\tan \delta_f = 0.0005$

$\lambda_c = 3.33$ Cm

HF = 0.1

$\Delta H = 65$ Oe.

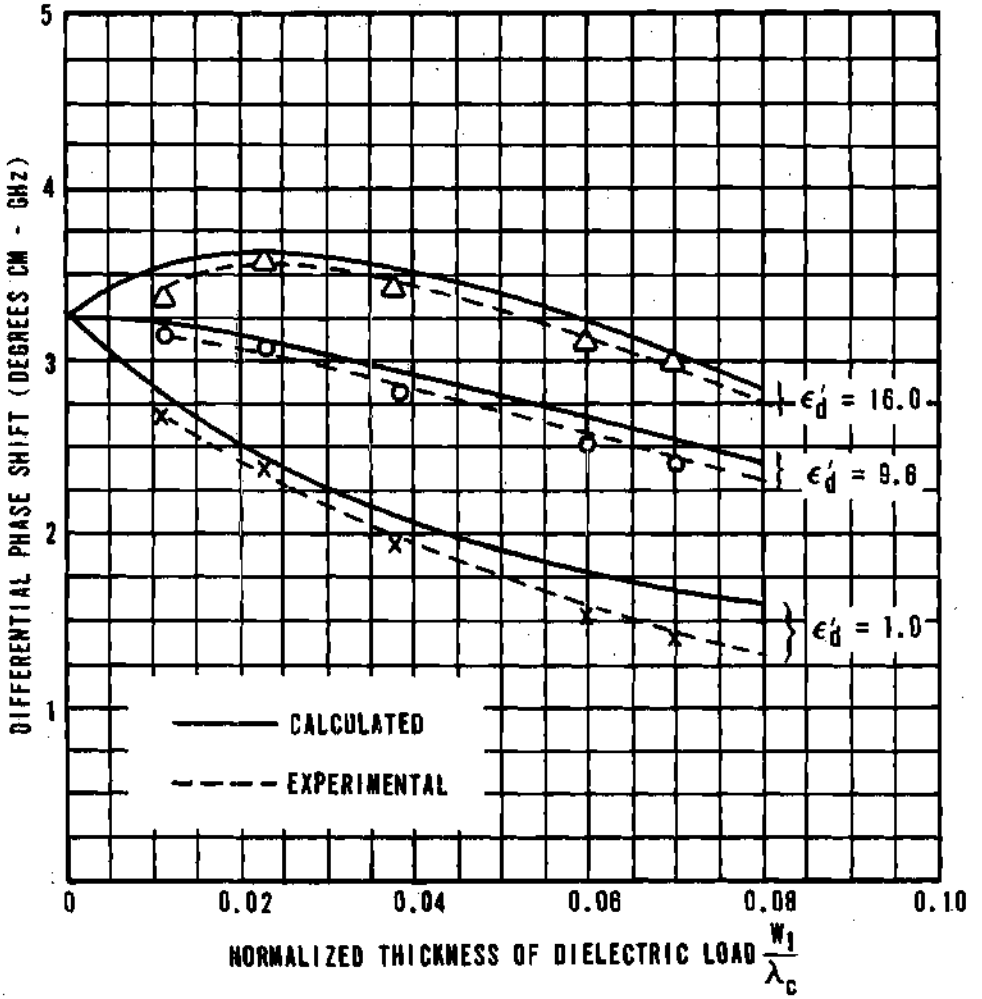

Figure 58. Differential Phase Shift vs Normalized Thickness Of Dielectric Load With Load Dielectric Constant As A Parameter

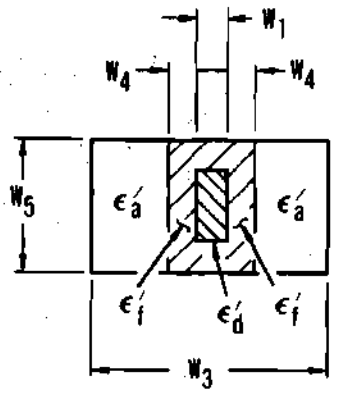

$m_s = \frac{\gamma 4\pi M_s}{\omega_c} = 0.386$

f_c = 9 Gc

$m = \frac{\gamma 4\pi M_r}{\omega_c} = 0.193$

FR = VARIABLE

W_1 = PARAMETER

$W_3 = 0.382\ \lambda_c$

$W_4 = 0.04\ \lambda_c$

$W_5 = 0.294\ \lambda_c$

$R_r = 0.5$

$\epsilon'_a = 1.0$

$\epsilon'_d = 16.0$

$\epsilon'_f = 16.0$

$\tan \delta_a = 0$

$\tan \delta_d = 0.0005$

$\tan \delta_f = 0.0007$

$\lambda_c = 3.33$ Cm

HF = 0.1

ΔH = 65 Oe.

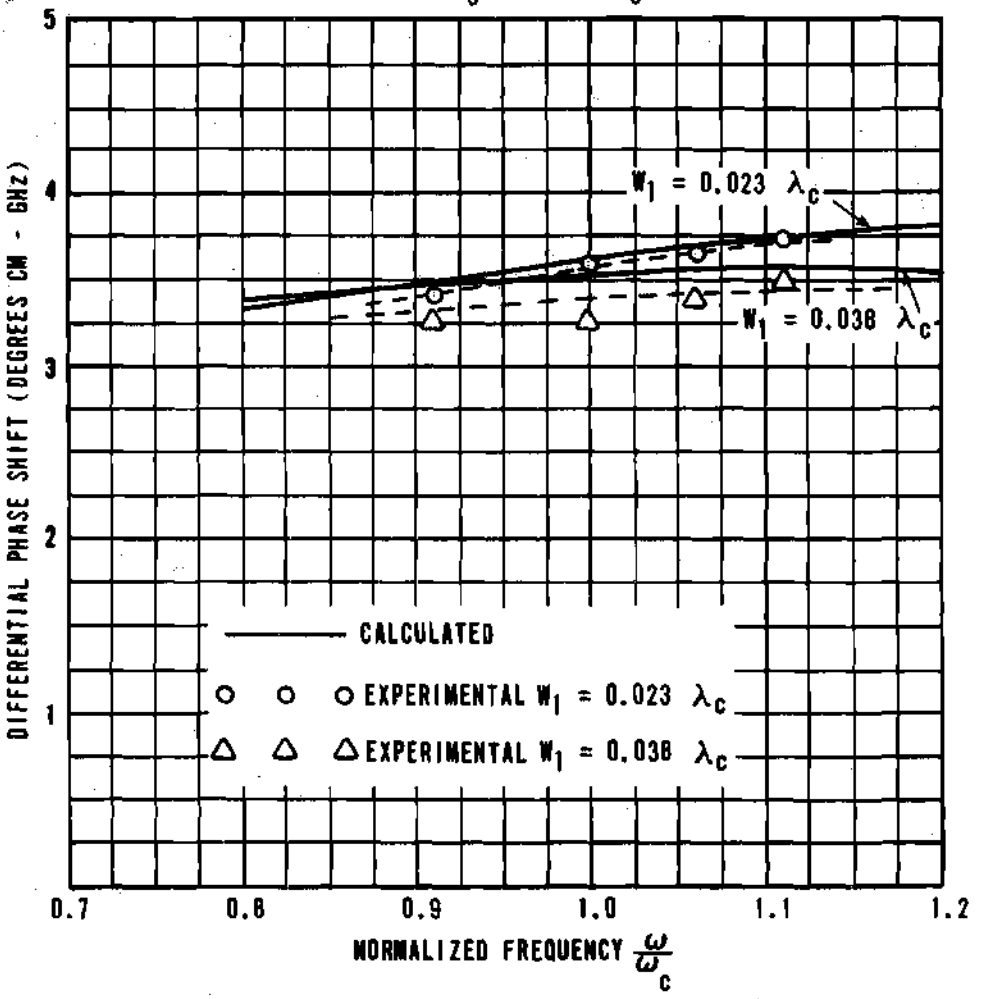

Figure 59. Differential Phase Shift vs Normalized Frequency With Dielectric Load Thickness As A Parameter

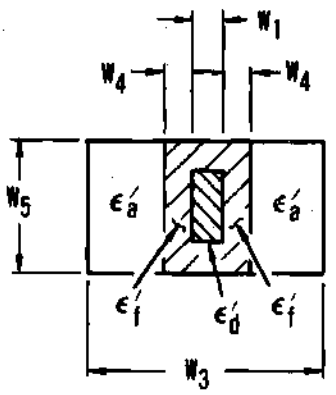

$m_s = \frac{\gamma 4\pi M_s}{\omega_c} = 0.386$

$f_c = 9$ Gc

$m = \frac{\gamma 4\pi M_f}{\omega_c} = 0.193$

FR = VARIABLE

W_1 = PARAMETER

$W_3 = 0.382\ \lambda_c$

$W_4 = 0.04\ \lambda_c$

$W_5 = 0.294\ \lambda_c$

$R_f = 0.5$

$\epsilon'_a = 1.0$

$\epsilon'_d = 1.0$

$\epsilon'_f = 16.0$

$\tan \delta_a = 0$

$\tan \delta_d = 0.0005$

$\tan \delta_f = 0.0007$

$\lambda_c = 3.33$ Cm

HF = 0.1

$\Delta H = 65$ Oe.

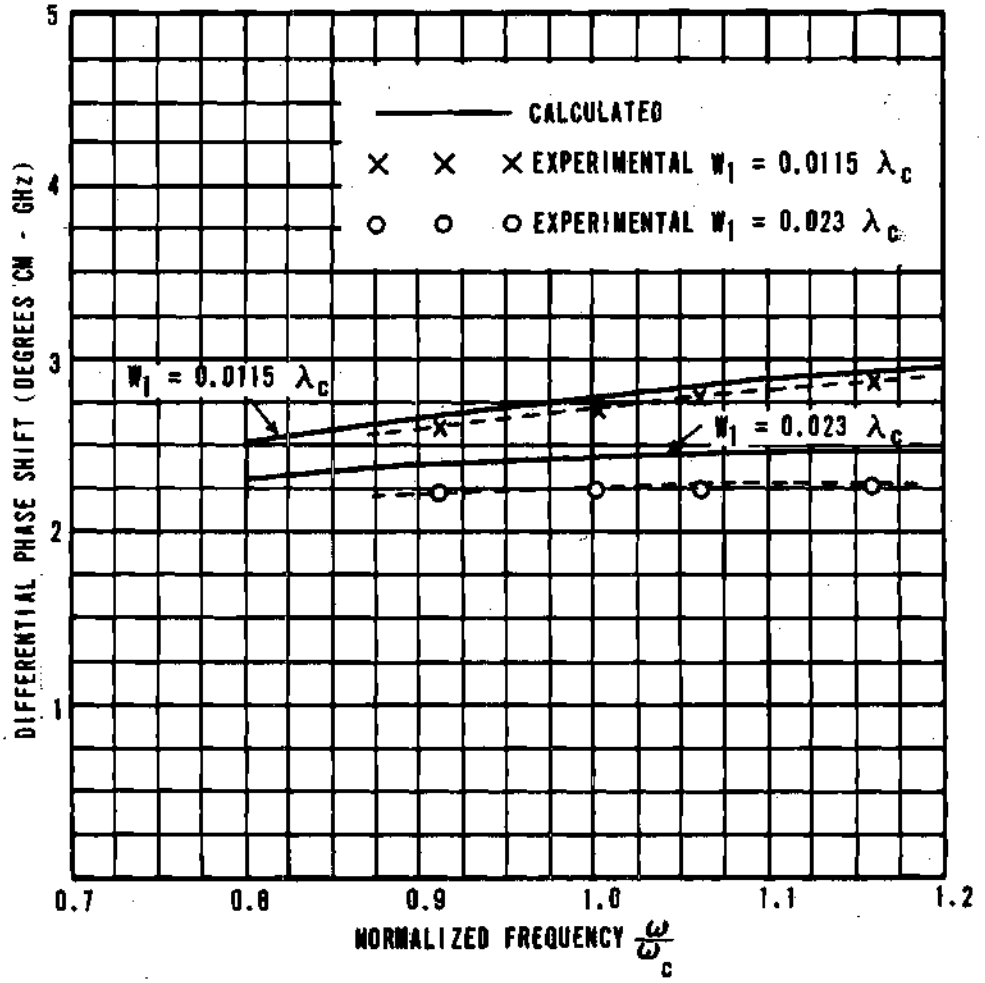

Figure 60. Differential Phase Shift vs Normalized Frequency With Dielectric Load Thickness As A Parameter

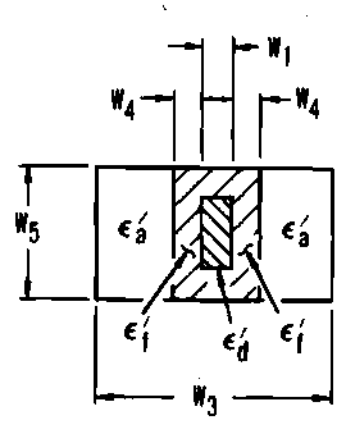

$m_s = \frac{\gamma 4\pi M_s}{\omega_c} = 0.386$

$f_c = 9$ Gc

$m = \frac{\gamma 4\pi M_r}{\omega_c} = 0.193$

W_1 = PARAMETER
W_3 = VARIABLE
$W_4 = 0.04\ \lambda_c$
$W_5 = 0.294\ \lambda_c$

$R_r = 0.5$

$\epsilon'_a = 1.0$
$\epsilon'_d = 1.0$
$\epsilon'_f = 16.0$
$\tan \delta_a = 0$
$\tan \delta_d = 0.0005$
$\tan \delta_f = 0.0007$
$\lambda_c = 3.33$ Cm
HF = 0
$\Delta H = 65$ Oe.

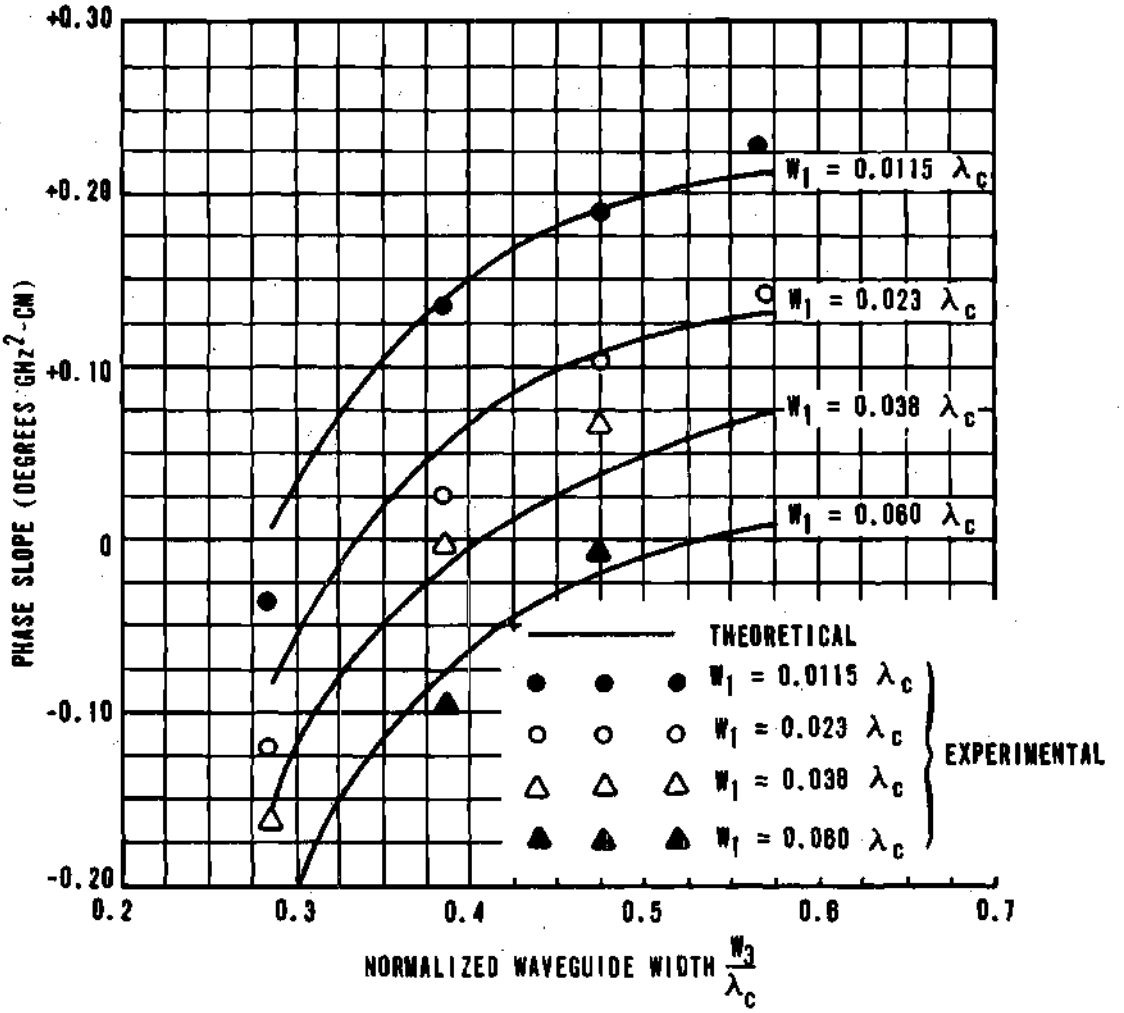

Figure 61. Phase Slope vs Normalized Waveguide Width With Dielectric Load Thickness As A Parameter

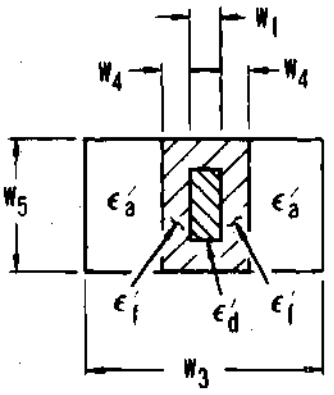

$m_s = \frac{\gamma 4\pi M_s}{\omega_c} = 0.386$

$f_c = 9$ Gc

$m = \frac{\gamma 4\pi M_r}{\omega_c} = 0.193$

W_1 = PARAMETER
W_3 = VARIABLE
$W_4 = 0.04\ \lambda_c$
$W_5 = 0.294\ \lambda_c$

$R_r = 0.5$

$\epsilon'_a = 1.0$
$\epsilon'_d = 16.0$
$\epsilon'_f = 16.0$
$\tan \delta_a = 0$
$\tan \delta_d = 0.0005$
$\tan \delta_f = 0.0007$
$\lambda_c = 3.33$ Cm
HF = 0
$\Delta H = 65$ Oe.

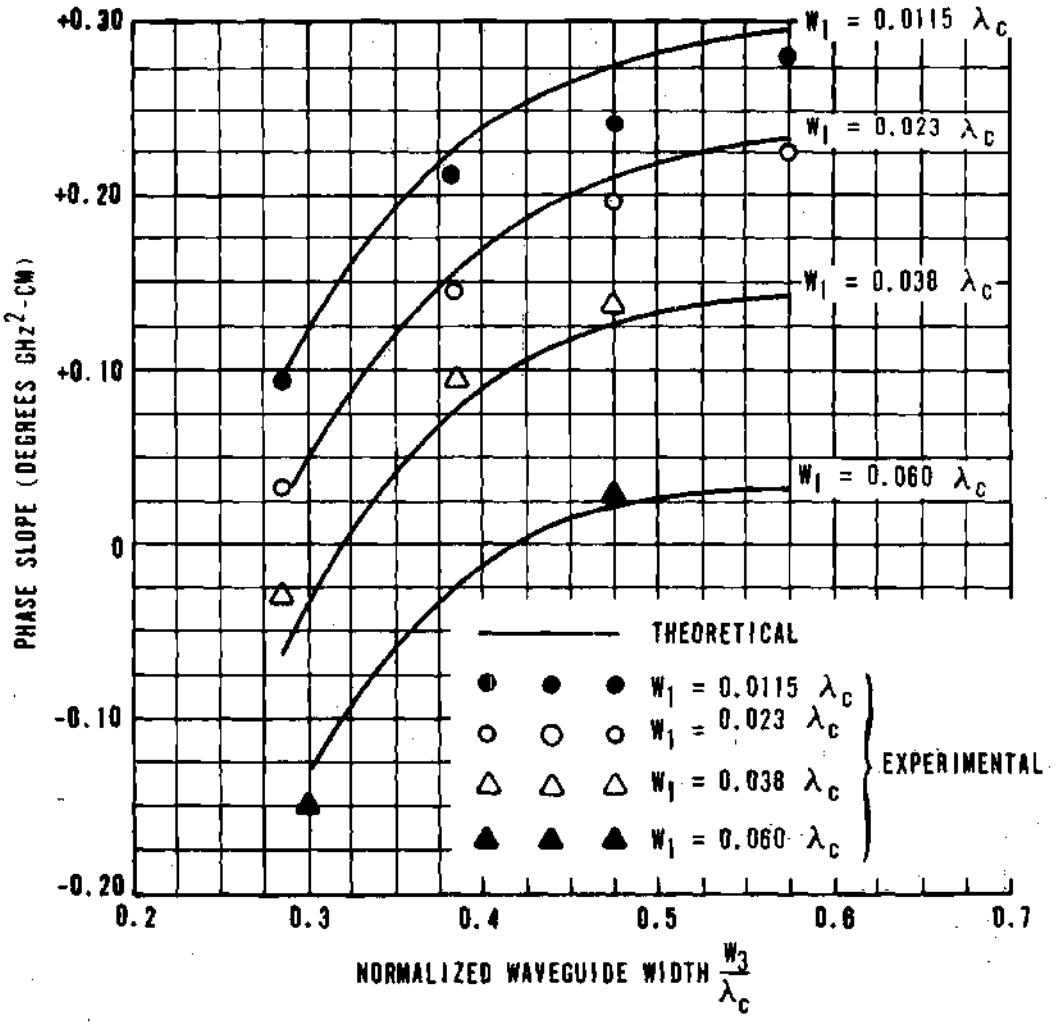

Figure 62. Phase Slope vs Normalized Waveguide Width With Dielectric Load Thickness As A Parameter

LITERATURE CITED

1. D. Polder, "On the Theory of Ferromagnetic Resonance," Philosophical Magazine, vol. 40, pp. 99-115, 1949.
2. H. G. Beljers, "Measurements on Gyromagnetic Resonance of a Ferrite Using a Cavity Resonator," Physica, vol. 14, p. 629, 1949.
3. F. F. Roberts, "A Note on the Ferromagnetic Faraday Effect at Centimeter Wavelength," Journal de Physique et le Radium, vol. 12, p. 305, 1951.
4. C. L. Hogan, "The Ferromagnetic Faraday Effect of Microwave Frequencies and Its Applications," Bell System Technical Journal, vol. 31, p. 1, June 1952.
5. A. G. Fox, S. E. Miller, and M. T. Weiss, "Behavior and Applications of Ferrites in the Microwave Region," Bell System Technical Journal, vol. 34, pp. 5 - 103, January 1955.
6. B. Lax and K. J. Button, Microwave Ferrites and Ferrimagnetics, McGraw-Hill Book Company, Inc., 1962.
7. Ibid., pp. 590 - 597.
8. D. H. Landry and W. C. Passaro, "A Four-Bit Latching Ferrite Switch," Presented at the 1965 G-MTT Symposium.
9. M. L. Kales, H. N. Chait, and N. G. Sakiotis, "A Non-reciprocal Micro-Microwave Component," Journal of Applied Physics, vol. 24, p. 816, 1953.
10. J. H. Rowen, "Ferrites in Microwave Applications," Bell System Technical Journal, vol. 32, p. 1333, 1953.
11. B. Lax, K. J. Button, and L. M. Roth, "Ferrite Phase Shifters in Rectangular Waveguide," Journal of Applied Physics, vol. 25, p. 1413, 1954.
12. W. J. Crowe, "Behavior of the TE Modes in Ferrite Loaded Rectangular Waveguide in the Region of Ferrimagnetic Resonance," Journal of Applied Physics, vol. 29, pp. 397 - 398, March 1958.
13. D. Bush, "Discussion on Microwave Apparatus," Proceedings of the Institute Electrical Engineers, (London), vol. 104B, suppl. 6, p. 368, 1956.
14. F. Reggia and E. G. Spencer, "A New Technique in Ferrite Phase Shifting for Beam Scanning of Microwave Antennas," Proceedings of Radio Engineers, vol. 45, p. 1510, 1957.

15. P. A. Rizzi and B. Gatlin, "Rectangular Guide Ferrite Phase Shifters Employing Longitudinal Magnetic Fields," Proc. IRE, vol. 47, p. 446, 1959.

16. A. C. Brown, R. S. Cole, and W. N. Honeyman, "Some Applications of Ferrites to Microwave Switches, Phasers, and Isolators," Proc. IRE, vol. 46, p. 722, 1958.

17. J. A. Weiss, "The Reggia-Spencer Microwave Phase Shifter," J. Appl. Phys., vol. 30, 1. 1535, 1959.

18. K. J. Button and B. Lax, "Perturbation Theory of the Reciprocal Ferrite Phase Shifter," Proc. Inst. Elec. Engrs. (London), vol. 109B, suppl. 21, 1962.

19. M. A. Treuhaft and L. M. Silber, "Use of Microwave Ferrite Toroids to Eliminate External Magnets and Reduce Switching Power," Proc. IRE, vol. 46, p. 8, 1958.

20. G. R. Harrison, L. R. Hodges, D. R. Taft, and R. E. Greenwood, "Microwave 'Square Loop' Ferrimagnetic Materials for Application in Fast Switching Phased Array Components," RADC Symposium on Electronically Scanned Array Radars, May 1965.

21. L. R. Whicker and R. R. Jones, "A Digital Latching Ferrite Strip Transmission Line Phase Shifter," Presented at 1965 G-MTT Symposium.

22. D. R. Taft, J. W. Simon, and J. D. Sweeney, "Ferrite Digital Phase Shifters," Presented at 1965 G-MTT Symposium.

23. R. Seckelmann, "Microwave Digital Phase Shifters," Intermagnetics Conference, Washington, D. C., 1965.

24. C. L. Heiter, "A Latching Type Ferrite Coaxial S-Band Phase Shifter," Intermag. Conf., Washington, D. C., 1965.

25. J. A. Kempic and R. R. Jones, "A Temperature Stable High Power C-Band Digital Phase Shifter," Presented at 1965 NEREM Symposium.

26. L. Dubrowsky, G. Kern, and G. Kern, and G. Klein, "A High Power X-Band Latching Digital Ferrite Phase Shifter for Phased Array Application," Presented at 1965 NEREM Symposium.

27. E. Schloemann, "Theoretical Analysis of Twin Slab Phase Shifters in Rectangular Waveguide," IEEE Transactions on Microwave Theory and Techniques, January 1966.

28. W. J. Ince and E. Stern, "Waveguide Non-Reciprocal Remanence Phase Shifter," Proc. Int. Conf. on Microwave Behavior of Ferrimagnetics and Plasmas, IEE, London, England (September 1965).

29. W. J. Ince and E. Stern, "Non-Reciprocal Remanence Phase Shifters in Rectangular Waveguide," IEEE International Convention Record, Part 5, p. 33, 1966.

30. Lax and Button, Microwave Ferrites ..., p. 146.

31. J.M. Luttinger and C. Kittel, Helvetica Physica Acta, 21, p. 480 (1948).

32. J.M. Richardson, Physical Review, 75, p. 1630, (1949).

33. D. Polder, Philosophical Magazine, 40, p. 99, 1949.

34. J.H. Van Vleck, Physical Review, 78, p. 266, 1950.

35. L. Landau and E. Lifshitz, "On the Theory of Dispersion of Magnetic Permeability in Ferromagnetic Bodies," Physik Z. Sowjetunion, vol. 8, p. 153, 1935, (in English).

36. N. Bloembergen, "On the Ferromagnetic Resonance in Nickel and Supermalloy," Phys. Rev., vol. 78, p. 572, 1950.

37. N. Bloembergen, "Magnetic Resonance in Ferrites," Proc. IRE, vol. 44, p. 1259, 1956.

38. T.L. Gilbert, Phys. Rev., 100, p. 1243, 1955.

39. S. IIDA, "The Difference Between Gilbert's and Landau-Lifshitz's Equations," Journal of Physics and Chemistry Solids, vol. 24, p. 625, 1963.

40. Lax and Button, Microwave Ferrites ..., p. 151.

41. M.A. Garstens, "Paramagnetic Resonance in Gases at Low Fields," Phys. Rev., vol. 93, p. 1228, 1954.

42. M.A. Garstens and R.K. Wangness, "Magnetic Resonance for Arbitrary Field Strengths," Phys. Rev., vol. 98, p. 927, 1955.

43. P.J.B. Clarricoats, Microwave Ferrites, John Wiley and Sons (1961), p. 39.

44. Rado and Suhl, Magnetism, Academic Press (1963), "Ferromagnetic Relaxation and Resonance Linewidths," C.W. Haas and H.B. Callen, p. 466.

45. H.B. Callen, "A Ferromagnetic Dynamical Equation," J. Phys. Chem. Solids, vol. 4, p. 256, 1958.

46. Clarricoats, p. 110.

47. A.H. Morrish, The Physical Principles of Magnetism, John Wiley and Sons (1965), p. 549.

48. Lax and Button, Microwave Ferrites ..., p. 169.

49. Clarricoats, p. 61.

50. G.T. Rado, "Theory of the Microwave Permeability Tensor and Faraday Effect in Nonsaturated Ferromagnetic Materials," Phys. Rev., vol. 89, p. 529, 1953.

51. G. T. Rado, "On the Electromagnetic Characterization of Ferromagnetic Media: Permeability Tensors and Spin Wave Equations," IRE Trans. on Ant. and Prop., vol. AP-4, p. 512 (1956).

52. Lax and Button, Microwave Ferrites ... , p. 159.

53. Ibid., p. 446.

54. Ibid., p. 541.

55. E. Stern and W. J. Ince, "Temperature Stabilization of Unsaturated Microwave Ferrite Devices," 11th Annual Conf. on Magnetism and Magnetic Materials, San Francisco (November 1965).

56. G. Harrison and L. R. Hodges, Jr., "Temperature Stable Microwave Hybrid Garnets," J. Appl. Phys., vol. 33, p. 1375, March 1962.

57. H. Seidel, "Ferrite Slabs in Transverse Electric Mode Wave Guide," J. Appl. Phys., 28, February 1957.

58. N. H. Frank, Radiation Lab Report No. T-9, 1942.

59. S. Ramo and J. R. Whinnery, Fields and Waves in Modern Radio, John Wiley & Sons, Inc., 2nd Edition, 1953, p. 333 ff.

60. Lax and Button, Microwave Ferrites ... , p. 108 ff.

61. G. R. Harrison and L. R. Hodges, Jr. , "Microwave Properties of Polycrystalline Hybrid Garnets," Journal of American Ceramic Society, vol. 44, May 1961.

62. H. Suhl, "Theory of Ferromagnetic Resonance at High Signal Powers," J. of Phys. and Chem. of Solids, vol. 1, p. 209, April 1957.

63. E. Schloemann, "Ferromagnetic Resonance at High Power Levels," Raytheon Technical Report No. R-48, October 1959.

64. J. Brown, "Ferrimagnetic Limiters," Microwave Journal, November 1961.

65. Foner, "Versatile and Sensitive Vibrating Sample Magnetometer," Rev. of Scientific Instruments, 30, p. 549, 1959.

66. J. K. Hunton and E. Lorence, "Improved Sweep Frequency Techniques for Broadband Microwave Test," Hewlett-Packard Journal, vol. 12, No. 4, December 1960.

67. Ramo and Whinnery, 2nd Edition, p. 336.

68. P. H. Vartanian, W. P. Ayres, and A. L. Helgesson, "Propagation in a Dielectric Slab Loaded Rectangular Waveguide," IRE Trans. on Microwave Theory and Techniques, vol. 6, p. 215, 1958.

VITA

James Lamar Allen was born in Graceville, Florida on September 25, 1936. He is the son of Victor C. and Shirley J. Allen. In October, 1959, he was married to Lou Ann Allmon of Lafayette, Georgia.

He was graduated from high school in Bonifay, Florida in June, 1954. He received the degrees of Bachelor of Electrical Engineering and Master of Science in Electrical Engineering from the Georgia Institute of Technology in June, 1959 and June, 1961, respectively.

His experience includes two and one-half years with the Engineering Experiment Station of the Georgia Institute of Technology, Atlanta, Georgia, two years with the Sperry Microwave Electronics Company, Clearwater, Florida, and two and one-half years as an Instructor of Electrical Engineering at the Georgia Institute of Technology.